

Copyright

by

Malgorzata Chwatko

2019

**THE DISSERTATION COMMITTEE FOR MALGORZATA  
CHWATKO CERTIFIES THAT THIS IS THE APPROVED  
VERSION OF THE FOLLOWING DISSERTATION:**

**Sustainable polymers for the next generation technologies**

**Committee:**

Nathaniel A. Lynd, Supervisor

Benny D. Freeman

Adrianne M. Rosales

Eric V. Anslyn

**Sustainable Polymers for The Next Generation Technologies**

**by**

**Malgorzata Chwatko**

**Dissertation**

Presented to the Faculty of the Graduate School of

The University of Texas at Austin

in Partial Fulfillment

of the Requirements

for the Degree of

**Doctor of Philosophy**

**The University of Texas at Austin**

**August 2019**

## **Acknowledgements**

It is impossible to express how grateful I am to everyone who has supported me through the years. Getting this far in my education and life would not have been possible if not for you. My family, friends, teachers and coaches have offered many words of encouragement and the sometimes-needed push to excel, and I am beyond grateful.

I'm grateful to my advisor, Professor Lynd for the opportunity to have been a part of his research group. I am also extremely grateful for my other mentors who have helped me throughout my academic career: Professor Aoshima, Professor Cosgriff-Hernandez, Professor Freeman, Professor Kanazawa, Professor Katz, Professor McCutcheon, Professor Rosales, and Professor Segalman, and I can't express how much they have all helped me grow as a researcher and as a person.

Similarly, I am thankful to all my colleagues; it's been an unforgettable experience to work with so many talented people. Beginning in my undergraduate education, I had the great pleasure to work with Dr. Jason Arena, Dr. Daniel Anastasio and many others that gave me my first glimpses of research. Without their patience and mentorship, I would not have ended up where I am today. Special thanks to Aaron Burkey, Christina Rodriguez, and Bill Wheatle for being such a great team; we all did great learning new techniques and setting up the Lynd lab together. I'd also like to thank Caitlin Bentley, Alysha Helenic, Michelle Dose, Melanie Merrick, Alon Kirschner, Lauren Cordova, Kelly Markham, Matt Minus, Xiaolong Sun for being amazing collaborators that helped spark ideas and produce new research. A special thanks to the entire MWET crew, you are all amazing and I am extremely glad to have gotten a chance to work with so many of you. Thanks to Carol Huang, Austin Boudreaux, Youngjin Lee, Shinsuke Segawa, Bailey Rhodes, the incredibly

talented undergrads I have worked with, for all the excellent work. I also want to give a special thanks to all of the other students and post-docs I've had the opportunity to work with the last few years: Natalie Czarnecki, Chola Dandamud, Gang Fan, Rob Ferrier Jr., Freddy Rivers, Jennifer Imbrogno, Ji-Yeon Kim, Jay Koh, Paul Meyer, Benjamin Pedretti, Rahul Sujamani, Diana Zhang and Qingjun Zhu. You all have made UT a wonderful place to work.

This dissertation would not have been possible if not for the funding sources. I would like to acknowledge The University of Texas at Austin for their financial support. I would also like to acknowledge the National Science Foundation, Eastman Chemical, Welch Foundation, Department of Energy Office of Basic Energy Sciences and Center for the Materials for Water and Energy Systems (MWET). I would also like to thank the international joint research promotion program at Osaka University, which allowed me to travel to Japan and learn so much both in and out of the laboratory.

Graduate school has many ups and downs. In going through this process, I have leaned on so many people. Thank you to my parents, Agnieszka and Waldemar Chwatko, for being always there for me. My siblings, Krzysztof and Elzbieta, for many late-night calls just to check in on each other. My fiancée, Dr. Kevin Baldrige for all the amazing things you have done and continue doing to support me through the years. I couldn't have done this without you. I am grateful to the entire Baldrige, Balcor and Chwatko families. To my furry family members, Bella and Maggie, thank you for all our games of fetch and cuddles on the couch. An additional thank you to Jake and Linh, who are some of my favorite people in the world, for our many weekly dinners and rock-climbing adventures. Thank you to Mary Ann, who is one of the sweetest people I know, for all your support. A special shoutout to Abby, Alysha, Andre, Bill, Caitlin, Jeff, Jodie, Kevin and Tommy, aka

the Cherrywood crew, for our many fun evenings together. You were all there through all the good times and hard times, and you always found a way to make me laugh.

## **Abstract**

### **Sustainable polymers for the next generation processes**

Malgorzata Chwatko, PhD

The University of Texas at Austin, 2019

Supervisor: Nathaniel A. Lynd

Many polymers synthesized today suffer from two major faults: non-degradability and lack of sustainability. While some of these polymers are recyclable, the consumer application may not align easily with recycling processes. For example, food contamination makes recycling very difficult, reducing sustainability for many polymer products.

Creating degradable polymers is another strategy to improve sustainability. Degradability can be invoked in the material via an introduction of degradable functionalities. One way to accomplish this can be through copolymerization; however, copolymerization is typically limited to structurally similar monomers. In these studies, copolymerization of structurally distinct lactones and epoxides utilizing the classical Vandenberg catalyst was explored. Similarly, copolymerization of carbonates and lactones, epoxides and anhydrides were also explored utilizing the bis( $\mu$ -alkoxo)bis(alkylaluminum) catalysts.

Sustainability can also be improved by obtaining monomers from sources other than petroleum, such as biological systems. Cells can be engineered to produce various products or to increase production of existing products that are relevant as polymer feedstocks. Another angle to achieve sustainability is through the use of the polymer. For

example, utilizing polymers as barrier materials to extend produce shelf-life would be a great benefit. Lastly, sustainability can be achieved through the education of young scholars to be aware of the issues and opportunities in polymer engineering.

This dissertation explores the aforementioned topics and provides support for the development of more sustainable polymers with collected data. Through the studies described herein, new polymerization methodologies were established for both sustainable and degradable polymers, and newly designed polymers were applied to the field of polymer electrolytes and plastic packaging.

## Table of Contents

<b>ABSTRACT</b> .....	<b>VII</b>
<b>LIST OF TABLES</b> .....	<b>XV</b>
<b>LIST OF FIGURES</b> .....	<b>XVII</b>
<b>LIST OF SCHEMES</b> .....	<b>XXVI</b>
<b>CHAPTER 1: INTRODUCTION</b> .....	<b>1</b>
Sustainability.....	2
Polymerization strategies .....	3
Applications to batteries .....	4
Dissertation Outline .....	5
<b>CHAPTER 2: STATISTICAL COPOLYMERIZATION OF EPOXIDES AND LACTONES TO HIGH MOLECULAR WEIGHT</b> .....	<b>7</b>
Introduction.....	7
Results and Discussion .....	9
Homopolymerization of DL-Lactide and Propylene Oxide .....	9
Copolymerization of Epoxides and Lactones .....	12
Conclusions.....	24
Experimental Section .....	25
Materials .....	25
Measurements and Characterization.....	25
Synthesis of the Aluminum Chelate (Vandenberg) Catalyst.....	26
Synthesis of Poly[(dl-lactide)].....	26
Synthesis of Poly[(dl-lactide)-co-(ethylene oxide)] (P(LA-co-EO)).....	27
Synthesis of Poly[(dl-lactide)-co-(epichlorohydrin)] (P(LA-co-ECH)) .....	27

Synthesis of Poly[(dl-lactide)-co-(butylene oxide)] (P(LA-co-BO)) .....	28
Synthesis of Poly[(dl-lactide)-co-(propylene oxide)] (P(LA-co-PO)).....	28
Synthesis of Poly[( $\epsilon$ -caprolactone)-co-(epichlorohydrin)] (P(CL-co-ECH)).....	29
Synthesis of Poly[( $\epsilon$ -caprolactone)-co-(butylene oxide)] (P(CL-co-BO)) ...	29
Synthesis of Poly[( $\epsilon$ -caprolactone)-co-(propylene oxide)] (P(CL-co-PO)).....	30
Kinetic Experiments .....	30
Degradation Experiments .....	31
Acknowledgment .....	31
<b>CHAPTER 3: SIMPLE BIS(<math>\mu</math>-ALKOXO-DIALKYLALUMINUM) INITIATORS FOR RING-OPENING POLYMERIZATION OF LACTONE AND MIXED MONOMER FEEDS.....</b>	<b>32</b>
Introduction.....	32
Experimental Section .....	34
Materials .....	34
Measurements and characterization.....	34
Synthesis of Bis( $\mu$ -alkoxo-dialkylaluminum)s (BODs) .....	35
General procedure for synthesis of polymers .....	35
[DL-lactide] <sub>0</sub> /[Al] <sub>0</sub> sweep .....	35
[ $\epsilon$ -caprolactone] <sub>0</sub> /[Al] <sub>0</sub> sweep .....	36
Results and Discussion .....	37
Initiator characterization .....	37
Copolymerization.....	39
Copolymerization of carbonates and lactones. ....	40
Copolymerization of anhydrides and epoxides.....	42

Comparison to mono- $\mu$ -oxo- dialuminium initiator (MOB). .....	44
Conclusion .....	46
Acknowledgments.....	46
<b>CHAPTER 4: SYNTHESIS OF BARRIER MATERIALS FROM BIOLOGICALLY DERIVED MONOMERS .....</b>	<b>47</b>
Introduction.....	47
Materials .....	48
Measurements and characterization.....	48
Polymer Characterization .....	48
General Procedure for Synthesis of linear Polyethers .....	49
General Procedure for Synthesis of Crosslinked Block Copolymer Membranes.....	49
General Procedure for Synthesis of Crosslinked Alternating Copolymer Membranes.....	50
Density Measurement .....	50
Thermal Characterization .....	51
Pure Gas Permeation Measurements .....	51
Results.....	52
Synthesis of linear liquid crystalline polyethers (PLE) .....	52
Film synthesis .....	53
Transport Characterization .....	55
Conclusion .....	57
Acknowledgment .....	57

<b>CHAPTER 5: IMPACT OF POLYETHER POLARITY ON IONIC CONDUCTIVITY.....</b>	<b>58</b>
Introduction.....	58
Materials and methods .....	60
Polymer synthesis and characterization.....	60
Electrolyte preparation.....	60
Differential scanning calorimetry .....	60
Electrochemical measurements.....	61
Results and discussion .....	61
Conclusion .....	64
Acknowledgment .....	64
<b>CHAPTER 6: HYDROPHOBIC OR HYDROPHILIC: POLYMERIZATION OF DOPAMINE ON SURFACES .....</b>	<b>65</b>
Introduction.....	65
Background.....	65
Hazards .....	67
Experiment.....	67
Results.....	67
Discussion.....	68
Extensions .....	70
Conclusions.....	70
Acknowledgments.....	71
<b>CHAPTER 7: CONCLUSIONS AND RECOMMENDATIONS .....</b>	<b>72</b>

<b>APPENDIX A .....</b>	<b>74</b>
SUPPORTING INFORMATION FOR CHAPTER 2: STATISTICAL COPOLYMERIZATION OF EPOXIDES AND LACTONES TO HIGH MOLECULAR WEIGHT .....	74
<b>APPENDIX B .....</b>	<b>101</b>
SUPPORTING INFORMATION FOR CHAPTER 3: SIMPLE BIS( $\mu$ -ALKOXO- DIALKYLALUMINUM) INITIATORS FOR HETERO-COPOLYMER SYNTHESIS VIA RING- OPENING.....	101
Methods.....	102
Synthesis of a Bis( $\mu$ -alkoxo alkyl aluminum) species 2.....	102
Synthesis of a Bis- $\mu$ -alkoxo alkyl aluminum species 3 .....	102
Synthesis of a Bis- $\mu$ -alkoxo alkyl aluminum species 4 .....	102
Synthesis of a Bis- $\mu$ -alkoxo alkyl aluminum species 5 .....	102
<b>APPENDIX C .....</b>	<b>138</b>
SUPPORTING INFORMATION FOR CHAPTER 4: BIOLOGICALLY DERIVED MONOMERS FOR SYNTHESIS OF FUNCTIONABLE MATERIAL .....	138
<b>APPENDIX D .....</b>	<b>143</b>
SUPPORTING INFORMATION FOR CHAPTER 5: IMPACT OF POLYETHER POLARITY ON IONIC CONDUCTIVITY .....	143
Methods.....	144
Polymer 1 synthesis .....	144
Polymer synthesis 2 .....	145
Polymer synthesis 3 .....	146
Polymer synthesis 4 .....	147

<b>APPENDIX E .....</b>	<b>154</b>
SUPPORTING INFORMATION FOR CHAPTER 5: HYDROPHOBIC OR HYDROPHILIC: FORMATION OF POLYDOPAMINE ON SURFACES .....	<b>154</b>
Teacher Handout.....	156
Student Handout.....	157
Pre-Assessment .....	158
Post Assessment:.....	159
<b>REFERENCES.....</b>	<b>161</b>

## List of Tables

Table 2-1. Characteristics of Poly(ester-co-ether)s .....	14
Table 3-1 Selected bond lengths and angles for BOD initiators.....	37
Table 3-2 Properties of lactone carbonate copolymers.....	42
Table 3-3 Properties of anhydride epoxide copolymers .....	43
Table 4-1 Properties of the long alkyl chain polyethers (PLEs).....	52
Table 4-2 Properties of the synthesized thin films.....	55
Table 4-3 Gas transport properties of thin films .....	56
Table 5-1 Polymer electrolyte properties.....	61
Table 6-1 Survey results post laboratory experiments. The survey used a 4-point Likert scale where Strongly Disagree = 1, Disagree = 2, Agree = 3, Strongly Agree = 4.....	69
Table B1 Crystal data and structure refinement for Ethyl-EtGlycol BOD (species 2)....	104
Table B2 Atomic coordinates ( x 10 <sup>4</sup> ) and equivalent isotropic displacement parameters (Å <sup>2</sup> x 10 <sup>3</sup> ) for Ethyl-EtGlycol BOD (species 2). U(eq) is defined as one third of the trace of the orthogonalized U <sup>ij</sup> tensor.....	105
Table B3 Bond lengths [Å] and angles [°] for Ethyl-EtGlycol BOD (species 2).....	105
Table B4 Anisotropic displacement parameters (Å <sup>2</sup> x 10 <sup>3</sup> ) for Ethyl-EtGlycol BOD (species 2).The anisotropic displacement factor exponent takes the form: $-2\pi^2[h^2 a^2 U^{11} + \dots + 2 h k a^* b^* U^{12}]$ .....	107
Table B5 Hydrogen coordinates ( x 10 <sup>4</sup> ) and isotropic displacement parameters (Å <sup>2</sup> x 10 <sup>3</sup> ) for Ethyl-EtGlycol BOD (species 2). .....	107
Table B6 Torsion angles [°] for Ethyl-EtGlycol BOD (species 2).....	109
Table B7 Crystal data and structure refinement for Ethyl-EtGlycol BOD (species 2)....	111

Table B8 Atomic coordinates ( $\times 10^4$ ) and equivalent isotropic displacement parameters ( $\text{\AA}^2 \times 10^3$ ) for Ethyl-EtGlycol BOD (species 2). $U(\text{eq})$ is defined as one third of the trace of the orthogonalized $U^{ij}$ tensor.....	112
Table B9 Bond lengths [ $\text{\AA}$ ] and angles [ $^\circ$ ] for Ethyl-EtGlycol BOD (species 2).....	112
Table B10 Anisotropic displacement parameters ( $\text{\AA}^2 \times 10^3$ ) for Ethyl-EtGlycol BOD (species 2). The anisotropic displacement factor exponent takes the form: $-2\pi^2 [h^2 a^{*2} U^{11} + \dots + 2 h k a^* b^* U^{12}]$ .....	115
Table B11 Hydrogen coordinates ( $\times 10^4$ ) and isotropic displacement parameters ( $\text{\AA}^2 \times 10^3$ ) for Ethyl-EtGlycol BOD (species 2).....	116
Table B12 Torsion angles [ $^\circ$ ] for Ethyl-EtGlycol BOD (species 2).....	117
Table B13 Crystal data and structure refinement for Ethyl-THP BOD (species 5).....	119
Table B14 Atomic coordinates ( $\times 10^4$ ) and equivalent isotropic displacement parameters ( $\text{\AA}^2 \times 10^3$ ) for Ethyl-THP BOD (species 5). $U(\text{eq})$ is defined as one third of the trace of the orthogonalized $U^{ij}$ tensor.....	120
Table B15 Bond lengths [ $\text{\AA}$ ] and angles [ $^\circ$ ] for Ethyl-THP BOD (species 5).....	121
Table B16 <i>Anisotropic displacement parameters (<math>\text{\AA}^2 \times 10^3</math>) for Ethyl-THP BOD (species 5). The anisotropic displacement factor exponent takes the form: <math>-2\pi^2 [h^2 a^{*2} U^{11} + \dots + 2 h k a^* b^* U^{12}]</math>.....</i>	123
Table B17 Hydrogen coordinates ( $\times 10^4$ ) and isotropic displacement parameters ( $\text{\AA}^2 \times 10^3$ ) for Ethyl-THP BOD (species 5).....	124
Table B18 Torsion angles [ $^\circ$ ] for Ethyl-THP BOD (species 5).....	124

## List of Figures

- Figure 1-1. Global production, use, and fate of polymer resins, synthetic fibers, and additives from 1950 to 2015 in million metric tons. From R. Geyer, J. R. Jambeck and K. L. Law, *Sci. Adv.*, 2017, 3, e1700782. Reprinted with permission from AAAS. ....2
- Figure 1-2 Schematic of the lithium-ion battery. Reproduced from Ref. 34 with permission from the Royal Society of Chemistry.....4
- Figure 2-1. Comparison of size exclusion chromatograms (light scattering intensity) of poly(propylene oxide) (PPO) and poly(DL-lactide) (PLA) synthesized using the same monomer-to-aluminum ratio of the Vandenberg catalyst. The polymerization of lactones appears to be more controlled than those of the epoxides. ....11
- Figure 2-2 Relationship between  $[LA]_0/[Al]_0$  and degree of polymerization indicates that approximately four aluminum atoms are involved in the creation of a single poly(DL-lactide) chain. Degrees of polymerization were determined by size exclusion chromatography with a multiangle light scattering detector in chloroform, and dispersities were calculated from the RI signal. Each data point represents a separate experiment. ....12
- Figure 2-3 Representative  $^1H$  NMR spectra (400 MHz,  $CDCl_3$ ) of (a) P(LA-co-PO) and (b) P(CL-co-BO). The spectra can be viewed as a superposition of the two homopolymer spectra with the addition of distinct signals consistent with dyad formation. Signals were assigned based on COSY NMR spectra shown in Appendix A.....15

Figure 2-4  $^1\text{H}$  NMR spectroscopy (600 MHz,  $\text{CD}_2\text{Cl}_2$ ) of the copolymerization of LA and PO over 65 h at room temperature. LA resonances at  $\delta$  5.15 (2H) and 1.62 (6H) are shaded in blue, and PO resonances at  $\delta$  2.4–3.0 (3H) are shaded in red. Resonances associated with the copolymer are shaded in purple: (a)  $\delta$  5.2 2H, (a')  $\delta$  4.2 1H, (c', d, c)  $\delta$  3.4–3.7 3H, (b, b')  $\delta$  1.58 6H.....18

Figure 2-5.  $^1\text{H}$  NMR spectroscopy (600 MHz,  $\text{CD}_2\text{Cl}_2$ ) of the copolymerization of CL and PO over 65 h at room temperature. CL resonances at  $\delta$  4.20 (2H),  $\delta$  2.59 (2H),  $\delta$  1.81 (2H), and  $\delta$  1.71 (4H) are shaded in blue, and PO resonances at  $\delta$  2.39,  $\delta$  2.9–2.6 (3H), and  $\delta$  1.26 (3H) are shaded in red. Resonances associated with the copolymer are shaded in purple: (a)  $\delta$  4.03 (2H), (e, f)  $\delta$  3.3–3.6 (3H), (b)  $\delta$  2.3 (2H), (c)  $\delta$  1.63 (4H), (d)  $\delta$  1.37 (2H), (g)  $\delta$  1.10 (3H).....19

Figure 2-6 Reactivity ratios could be estimated from the raw <sup>1</sup>H NMR spectroscopy data shown in Figure 2-4 and Figure 2-5 by two methods: (a) The nonterminal model of copolymerization kinetics reported by Beckingham et al. was used to produce an estimate of the reactivity ratios:  $r_{PO} = 4.50 \pm 0.47$  and  $r_{LA} = 0.37 \pm 0.02$ . (b) The Meyer–Lowry equation for the traditional terminal model of copolymerization produced similar values:  $r_{PO} = 2.81 \pm 0.27$  and  $r_{LA} = 0.36 \pm 0.02$ . The results of fitting by both methodologies were consistent with a gradient copolymer. (c)  $\epsilon$ -Caprolactone and propylene oxide reactivity ratios could not be accurately described by the model of Beckingham et al. Curves are drawn to guide the eye. (d) The Meyer–Lowry equation produced a fit that was consistent with a strong gradient copolymer with generally isolated CL repeat units  $r_{PO} = 2.17 \pm 0.04$  and  $r_{CL} = 0.08 \pm 0.01$ .....21

Figure 2-7 A pressed film of poly[(DL-lactide)-co-(butylene oxide)] (Table 2-1, entry 7) was optically clear and homogeneous. ....23

Figure 2-8 Degradation of poly[(DL-lactide)-co-(ethylene oxide)] cubes was conducted under standard aqueous and basic conditions. Experiments were conducted in triplicate, and error bars represent the standard deviation among the three samples. ....24

Figure 3-1 Structures obtained by X-ray crystallography contain variation in alkyl groups on aluminum, and in the initiator moiety. Thermal ellipsoids are drawn at 50% probability.....36

Figure 3-3 Control of molecular weight was demonstrated in homopolymerization of lactones a)  $\epsilon$ -caprolactone b) DL-lactide. ....39

Figure 3-4 Copolymerization of carbonates and lactones gives a lower than theoretical incorporation of carbonates as seen by the presence of peak e in the case of formation of poly[(D,L-lactide)-(ethylene carbonate)].	41
Figure 3-5 Copolymerization of anhydrides and epoxides provides new polymeric structures.	44
Figure 3-6 Comparison of polymerization rates of MOB 1 vs BODs with heterocyclic monomers (a) copolymerization of EGE and MA at 60°C at [M]/[Al]=25 (b) polymerization of PLA at 90°C at [M]/[Al]=50.	45
Figure 4-1 Representative <sup>1</sup> H NMR spectra (400 MHz, CDCl <sub>3</sub> ) of poly(dodecane ether).	53
Figure 4-2 Picture of thin films A) P(LE-CHO) film to show transparency, B) folded P(LE-CHO) film shows flexibility C) P(LE-MA) to show color and flexibility of thin films.	54
Figure 5-1 Structures of synthesized polyethers.	59
Figure 5-2 Ionic conductivity of the polymers vs A) temperature at 13 wt% LiTFSI and B) salt concentration at 90°C. Segmental dynamics and polarity play an important role in the final ionic conductivity.	62
Figure 5-3 Ionic conductivity measured 60 °C below T <sub>g</sub> of each polymer versus dielectric constant. Data without error bars is based off single data points to be remeasured in future.	63
Figure 6-1 A) The proposed chemical structure of a poly(dopamine) B) chemical structure of dopamine.	66
Figure 6-2 Picture of the droplet test on the modified and unmodified Teflon sheet. A) pure water B) methylene blue dyed droplet. The droplet retains shape on the unmodified Teflon, and smears on the PDA modified sample.	68

Figure 6-3 Sample of kinetic data of polydopamine formation at different pHs obtained from RGB smartphone method. ....	70
Figure A1 $^1\text{H}$ and $^{13}\text{C}$ NMR spectra for poly[(DL-lactide) $_{0.45}$ -co-(ethylene oxide) $_{0.55}$ ] in 2:1 $\text{CD}_2\text{Cl}_2$ : $\text{CDCl}_3$ .....	75
Figure A2 COSY(HH) NMR spectra for poly[(DL-lactide) $_{0.45}$ -co-(ethylene oxide) $_{0.55}$ ] in 2:1 $\text{CD}_2\text{Cl}_2$ : $\text{CDCl}_3$ .....	76
Figure A3 $^1\text{H}$ and $^{13}\text{C}$ NMR spectra for poly[(DL-lactide) $_{0.45}$ -co-(epichlorohydrin) $_{0.55}$ ] in 1:2 $\text{CD}_2\text{Cl}_2$ : $\text{CDCl}_3$ .....	77
Figure A4 COSY(HH) NMR spectra for poly[(DL-lactide) $_{0.45}$ -co- (epichlorohydrin) $_{0.55}$ ] in 1:2 $\text{CD}_2\text{Cl}_2$ : $\text{CDCl}_3$ .....	78
Figure A5 $^1\text{H}$ and $^{13}\text{C}$ NMR spectra for poly[(DL-lactide) $_{0.08}$ -co-(epichlorohydrin) $_{0.92}$ ] in 1:2 $\text{CD}_2\text{Cl}_2$ : $\text{CDCl}_3$ .....	79
Figure A6 $^1\text{H}$ and $^{13}\text{C}$ NMR spectra for poly[(DL-lactide) $_{0.22}$ -co- (epichlorohydrin) $_{0.78}$ ] in 1:2 $\text{CD}_2\text{Cl}_2$ : $\text{CDCl}_3$ .....	80
Figure A7 $^1\text{H}$ and $^{13}\text{C}$ NMR spectra for poly[(DL-lactide) $_{0.25}$ -co-(butylene oxide) $_{0.75}$ ] in $\text{CDCl}_3$ .....	81
Figure A8 COSY(HH) NMR spectra for poly[(DL-lactide) $_{0.25}$ -co-(butylene oxide) $_{0.75}$ ] in $\text{CDCl}_3$ .....	82
Figure A9 $^1\text{H}$ and $^{13}\text{C}$ NMR spectra for poly[(DL-lactide) $_{0.40}$ -co-(butylene oxide) $_{0.60}$ ] in $\text{CDCl}_3$ .....	83
Figure A10 $^1\text{H}$ and $^{13}\text{C}$ NMR spectra for poly[(DL-lactide) $_{0.24}$ -co-(butylene oxide) $_{0.76}$ ] in $\text{CDCl}_3$ .....	84
Figure A11 $^1\text{H}$ and $^{13}\text{C}$ NMR spectra for poly[(DL-lactide) $_{0.20}$ -co-(propylene oxide) $_{0.80}$ ] in $\text{CDCl}_3$ .....	85

Figure A12 COSY(HH) NMR spectra for poly[(DL-lactide) <sub>0.20</sub> -co-(propylene oxide) <sub>0.80</sub> ] in CDCl <sub>3</sub> .....	86
Figure A13 <sup>1</sup> H and <sup>13</sup> C NMR spectra for poly[(DL-lactide) <sub>0.40</sub> -co-(propylene oxide) <sub>0.60</sub> ] in CDCl <sub>3</sub> .....	87
Figure A14 <sup>1</sup> H and <sup>13</sup> C NMR spectra for poly[(DL-lactide) <sub>0.24</sub> -co-(propylene oxide) <sub>0.76</sub> ] in CDCl <sub>3</sub> .....	88
Figure A15 <sup>1</sup> H and <sup>13</sup> C NMR spectra for poly[(ε-caprolactone) <sub>0.48</sub> -co-(epichlorohydrin) <sub>0.52</sub> ] in CDCl <sub>3</sub> .....	89
Figure A16 COSY(HH) NMR spectra for poly[(ε-caprolactone) <sub>0.48</sub> -co-(epichlorohydrin) <sub>0.52</sub> ] in CDCl <sub>3</sub> .....	90
Figure A17 <sup>1</sup> H and <sup>13</sup> C NMR spectra for poly[(ε-caprolactone) <sub>0.67</sub> -co-(epichlorohydrin) <sub>0.33</sub> ] in CDCl <sub>3</sub> .....	91
Figure A18 <sup>1</sup> H and <sup>13</sup> C NMR spectra for poly[(ε-caprolactone) <sub>0.93</sub> -co-(epichlorohydrin) <sub>0.07</sub> ] in CDCl <sub>3</sub> .....	92
Figure A19 <sup>1</sup> H and <sup>13</sup> C NMR spectra for poly[(ε-caprolactone) <sub>0.29</sub> -co-(butylene oxide) <sub>0.71</sub> ] in CDCl <sub>3</sub> .....	93
Figure A20 COSY(HH) NMR spectra for poly[(ε-caprolactone) <sub>0.29</sub> -co-(butylene oxide) <sub>0.71</sub> ] in CDCl <sub>3</sub> .....	94
Figure A21 <sup>1</sup> H and <sup>13</sup> C NMR spectra for poly[(ε-caprolactone) <sub>0.32</sub> -co-(butylene oxide) <sub>0.68</sub> ] in CDCl <sub>3</sub> .....	95
Figure A22 <sup>1</sup> H and <sup>13</sup> C NMR spectra for poly[(ε-caprolactone) <sub>0.59</sub> -co-(butylene oxide) <sub>0.41</sub> ] in CDCl <sub>3</sub> .....	96
Figure A23 <sup>1</sup> H and <sup>13</sup> C NMR spectra for poly[(ε-caprolactone) <sub>0.28</sub> -co-(propylene oxide) <sub>0.72</sub> ] in CDCl <sub>3</sub> .....	97

Figure A24 COSY(HH) NMR spectra for poly[( $\epsilon$ -caprolactone) <sub>0.28</sub> -co-(propylene oxide) <sub>0.72</sub> ] in CDCl <sub>3</sub> .....	98
Figure A25 <sup>1</sup> H and <sup>13</sup> C NMR spectra for poly[( $\epsilon$ -caprolactone) <sub>0.20</sub> -co-(propylene oxide) <sub>0.80</sub> ] in CDCl <sub>3</sub> .....	99
Figure A26 <sup>1</sup> H and <sup>13</sup> C NMR spectra for poly[( $\epsilon$ -caprolactone) <sub>0.51</sub> -co-(propylene oxide) <sub>0.49</sub> ] in CDCl <sub>3</sub> .....	100
Figure B2 View of Ethyl-EtGlycol BOD (species 2). showing the atom labeling scheme. Displacement ellipsoids are scaled to the 50% probability level. The complex resides around a crystallographic inversion center at $\frac{1}{2}$ , $\frac{1}{2}$ , $\frac{1}{2}$ . Atoms with labels appended by a ‘ are related by 1-x, 1-y, 1-z. ....	110
Figure B3 View of Ethyl-THP BOD (species 5) showing the heteroatom labeling scheme. Displacement ellipsoids are scaled to the 50% probability level. The complex sits around a crystallographic inversion center at $\frac{1}{2}$ , $\frac{1}{2}$ , $\frac{1}{2}$ . Atoms with labels appended by a ‘ are related by 1-x, 1-y, 1-z. ....	118
Figure B4 <sup>1</sup> H NMR spectrum Methyl-EtGlycol BOD (species 1) initiator (benzene, 400 MHz).....	126
Figure B5 <sup>1</sup> H NMR spectrum Ethyl-EtGlycol BOD (species 2) initiator (benzene, 400 MHz) .....	127
Figure B6 <sup>1</sup> H NMR spectrum Isobutyl-EtGlycol BOD (species 3) initiator (benzene, 400 MHz).....	128
Figure B7 <sup>1</sup> H NMR spectrum Ethyl-PropGlycol BOD (species 4) initiator (benzene, 400 MHz).....	129
Figure B8 <sup>1</sup> H NMR spectrum Ethyl-THP BOD (species 5) initiator (CDCl <sub>3</sub> , 400 MHz) .....	130

Figure B9 Kinetic study on the performance on initiators on the rate of lactide polymerization. ....	131
Figure B10 <sup>1</sup> H NMR spectrum of poly(maleic anhydride-co-epichlorohydrin) created with BOD initiator (CD <sub>1</sub> Cl <sub>3</sub> , 400 MHz) .....	132
Figure B11 <sup>1</sup> H NMR spectrum of poly(maleic anhydride-co-propylene oxide) created with BOD initiator (CD <sub>1</sub> Cl <sub>3</sub> , 400 MHz). This polymerization had excess propylene oxide leading to some homopolymerization. ....	133
Figure B12 <sup>1</sup> H NMR spectrum of poly(DL-lactide) created with MOD initiator(CD <sub>1</sub> Cl <sub>3</sub> , 400 MHz).....	134
Figure B13 <sup>1</sup> H NMR spectrum of poly(DL-lactide) created with MOD initiator from an attempted copolymerization involving propylene carbonate and lactide (CD <sub>1</sub> Cl <sub>3</sub> , 400 MHz).....	135
Figure B14 <sup>1</sup> H NMR spectrum of poly(succinic anhydride-co-ethyl glycidyl ether) created with MOD initiator (CD <sub>1</sub> Cl <sub>3</sub> , 400 MHz).....	136
Figure B15 Control of molecular weight with the MOD via homopolymerization of DL-lactide .....	137
Figure C1 DSC characterization of linear homopolymer and the crosslinked polymer created after. The crystalline peak width shifts in location and shape upon further polymerization. ....	139
Figure C2 DSC characterization of linear homopolymer and the crosslinked alternating copolymer created. The crystalline peak width shifts in location and shape upon further polymerization. ....	140
Figure C3 Pure gas permeability as a function of upstream pressure at 35 °C in crosslinked P(MA-co-DE) .....	141

Figure C4 Pure gas permeability as a function of upstream pressure at 35 °C in crosslinked P(DE- <i>b</i> -CHO).....	141
Figure C5 Pure gas permeability as a function of temperature at 2 atm in crosslinked P(DE- <i>b</i> -CHO) film. The deviation from the fit showcases the deviation from Arrhenius behavior due to crystallization. ....	142
Figure D1 <sup>1</sup> H NMR characterization of synthesis steps in creation of polymer <b>2</b> .....	148
Figure D2 GPC characterization of polymers used in the creation of polymer <b>2</b> to show oxidation related molecular weight increase. ....	149
Figure D3 <sup>1</sup> H NMR of the modified poly allyl glycidyl ether created in the first step of synthesized of polymer <b>3</b> .....	150
Figure D4 <sup>1</sup> H NMR of the oxidation of to produce polymer <b>3</b> .....	151
Figure D5 GPC characterization of polymers used in the creation of polymer <b>3</b> .....	151
Figure D6 <sup>1</sup> H NMR of the modified poly allyl glycidyl ether created in the first step of synthesized of polymer <b>4</b> .....	152
Figure D7 GPC characterization of polymers used in the creation of polymer <b>4</b> .....	152
Figure D8 <sup>1</sup> H NMR of the synthesized of polymer <b>4</b> .....	153
Figure E1 IRB reviewal of the experimental protocol used in the study.....	155
Figure E2 Complete post assessment results from the study.....	160

## List of Schemes

Scheme 2-1. Statistical Copolymerization of Lactones and Epoxides. ....	8
Scheme 2-2 (a) Originally Proposed Structure for the Vandenberg Catalyst and (b) a Renewed Stoichiometrically Representative Structure.....	10
Scheme 2-3 General Statistical Copolymerization of Lactones and Epoxides.....	13
Scheme 3-1 Copolymerization of lactones and carbonates. ....	40
Scheme 3-2 Copolymerization of anhydrides and epoxides.....	42
Scheme 4-1 Scheme of sustainable synthesis of crosslinked liquid crystalline films .....	48
Scheme D1 Synthesis scheme of polymer <b>1</b> .....	145
Scheme D2 Synthesis scheme of polymer <b>2</b> .....	146
Scheme D3 Synthetic scheme of polymer <b>3</b> .....	146
Scheme D4 Synthetic scheme of polymer <b>4</b> .....	147

## Chapter 1: **Introduction**

Plastic and rubber-based materials have enhanced quality of life. Something as simple as a pen, which originated from the use of feathers with external ink supply has become an all-in-one package. The ink is encapsulated by a plastic tube taking form as a variety of shapes and colors. It is almost too easy to forget how much the world has changed due to the synthetic capabilities of chemists and design of engineers.

Polymers' low cost, and tunability have made them an vital part in any design.<sup>1-4</sup> In many cases the designer can pick a polymer out of a catalog and design the part around the polymer's processability. The polymer is only modified by the addition of additives such as plasticizers or dyes if the part does not meet specifications. This process is not the best option in the long term as it can lead to leaching of these additives, which may be harmful to humans or the environment.<sup>5-8</sup> An example of this circumstance can be seen with bisphenol-A in recent years.<sup>9,10</sup>

To avoid the problems associated with potential small molecule toxicity, polymers can be synthesized with a variety of properties for a specific application. The designs of polymer structure can incorporate the necessary design parameters in addition to considering sustainability of monomer feedstock or polymer product.

## SUSTAINABILITY

Sustainability has become a key issue for consumers.<sup>6,11-14</sup> Many consumer products such as detergents or soaps have sustainably sourced alternatives. This trend is also seen in the plastics used for packaging which can highlight recycling or degradability.<sup>15,16</sup>

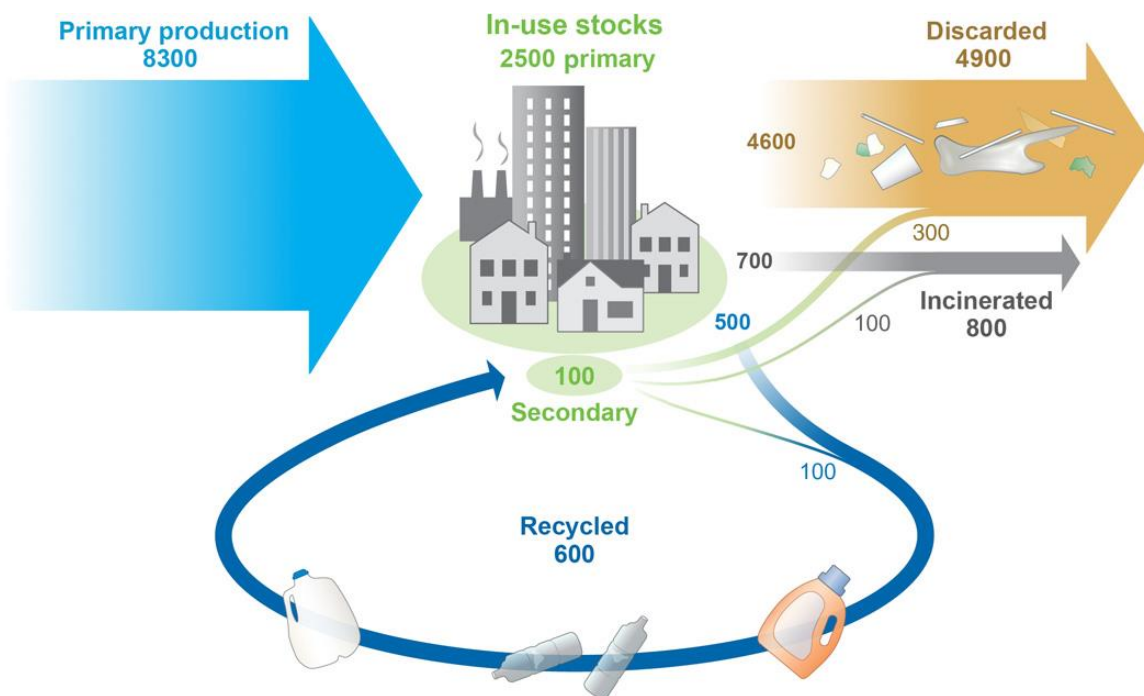


Figure 1-1. Global production, use, and fate of polymer resins, synthetic fibers, and additives from 1950 to 2015 in million metric tons. From R. Geyer, J. R. Jambeck and K. L. Law, *Sci. Adv.*, 2017, 3, e1700782. Reprinted with permission from AAAS.

Most commercially used polymers are derived from petroleum.<sup>17,18</sup> This fact ties polymer supply to non-renewable resources associated with damaging side effects to our planet. While there has been a push for utilizing gentler, less harmful chemistry to create the same molecules, there is still room for improvement.<sup>19-21</sup> In recent years, there has been an additional push to utilize biologically derived resources.<sup>17-19,22</sup> Biologically derived resources can come from plants, trees,

engineered bacteria or yeast strains. These approaches attempt to match existing polymer feedstock requirements or be a source of new polymer structures.

When considering the currently used commercial polymers, only ~9% end up commonly recycled at the consumer scale.<sup>23</sup> Recycling of polymers (when done properly) is a great tool to avoid accumulation of plastics. However, it is clear that even if recycling was possible for all commercial polymers, this would not solve the problem completely. To achieve a sustainable world, plastic end of life must also be considered. Even though very few industries require their products withstand more than 15 years of use, most plastic components are not even partially degraded on this time scale, resulting in accumulation of plastic waste (Figure 1-1).<sup>19,23,24</sup>

One way of closing the sustainability loop is by considering polymer degradation. Degradability of polymers can be engineered to match the lifespan of products, such that there is no major change in properties during use. This trend has begun with degradable polymers such as poly(lactide) becoming a part of the market, however they can still suffer from their poor mechanical properties and slow degradation in the ocean.<sup>25</sup>

## **POLYMERIZATION STRATEGIES**

There are many different polymerization approaches undertaken in the literature depending on the feedstock.<sup>18,26-29</sup> In this dissertation, the focus is specifically on ring opening polymerization (ROP). ROP allows for the polymer backbone to contain a variety of functionalities such as esters or ethers. These functionalities can change the polymer's polarity, segmental dynamics, and mechanical properties.

To create a polymer, as in other chemical reactions, we are concerned with thermodynamics and kinetics. Thermodynamically, the polymerization can be described via Gibbs free energy, if  $\Delta G < 0$  the polymerization is favored, whereas if  $\Delta G > 0$  the polymerization is not favored. The equation below describes the polymerization equilibrium behavior. Practically, thermodynamics determine if a monomer can be polymerized.

$$\Delta G_p = \Delta H_p - T\Delta S_p$$

The kinetics or rate of polymerization is not determined thermodynamically. Depending on the polymerization conditions such as temperature or the catalytic system used, different degrees of activation with either the monomer or propagating chain end are obtained.<sup>30</sup> By tuning these parameters, we can tune the polymerization rate.

Catalyst development is a crucial part of polymer design as it is an independent tool to help push the reaction to completion. The use of catalysts typically allows for achievement of larger molecular weights, and milder conditions such that lower thermal energy input required.<sup>31-33</sup>

## APPLICATIONS TO BATTERIES



Figure 1-2 Schematic of the lithium-ion battery. Reproduced from Ref. 34 with permission from the Royal Society of Chemistry.

As the world moves to more portable electronics, high density energy storage devices will be necessary. A schematic of a lithium polymer battery can be seen in Figure 1-2. For applications such as electric cars polymer electrolytes offer several advantages over liquid electrolytes typically used, such as improved safety features, excellent flexibility and processability.<sup>34</sup> They can also behave as separators by providing the necessary mechanical strength necessary in the device.<sup>35,36</sup>

While research into polymer electrolytes has been ongoing for over 50 years, not a lot of polymers have surpassed the state of the art, poly(ethylene oxide). A generally accepted perspective is that a low glass transition temperature ( $T_g$ ), low molecular weight, and low viscosity

are essential for high ionic conductivity. However a quantitative establishment of robust structure-property relationships for conductivity in amorphous polymer electrolytes has not yet been achieved.<sup>35,37-39</sup>

A less commonly studied parameter in polyelectrolyte performance is polymer polarity. Two major studies have identified that polymer polarity, as typically measured by the dielectric constant, can be the dominant influence over ionic transport in polymer electrolytes.<sup>40,41</sup> These findings suggested that reducing ionic aggregation by increasing the host dielectric constant may serve as a means to improve ionic transport.

## **DISSERTATION OUTLINE**

This dissertation is comprised of 7 chapters with several appendices provided as a reference for Chapters 2-6.

The first section focuses on the synthesis of degradable polymers. Chapter 2 focuses on the use of a classical aluminum-based catalyst for the copolymerization of lactones and epoxides. The system can achieve high molecular weights and works with numerous monomers. Chapter 3 focuses on the design of a new set of aluminum initiators. These initiators are applied to polymerizations involving a large set of cyclic monomers.

The second section focuses on applications of various polymers, specifically polyethers. Chapter 4 focuses on the use of sustainable feedstocks in the creation of polymers. Sustainable monomers can come from a variety of sources and this section, will focus on the utilization of feedstocks derived from microbes to create polymers. Chapter 5 focuses on the use of polyethers as polymer electrolytes, specifically investigating the impact of polymer polarity on properties such as conductivity.

The third section (Chapter 6) focuses on polymer education. Polymers are commonly overlooked in a formal education setting even though students encounter them numerous times in everyday life. The main introduction to polymers that most students receive is in biology classes through the discussion of proteins, and polynucleotides such as DNA. Chapter 6 discusses an activity which can be used to introduce students to synthetic polymers in the context of already commonly discussed topics such as pH.

Finally, chapter 7 presents the conclusions for this dissertation from both a synthetic and applications perspective. Recommendations for future work are offered based on the knowledge obtained from these studies.

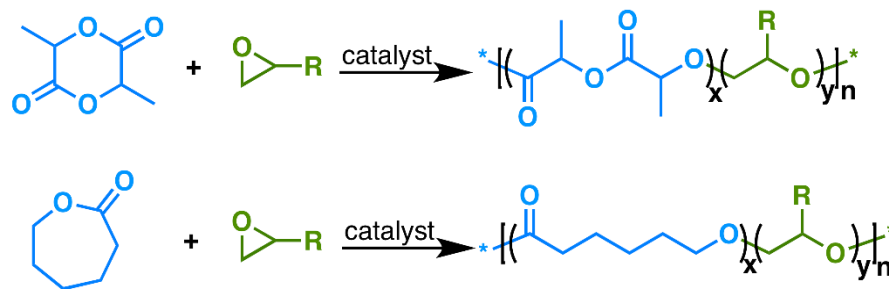
## Chapter 2: Statistical Copolymerization of Epoxides and Lactones to High Molecular Weight<sup>1</sup>

### INTRODUCTION

Copolymerization is a classically versatile and commonly employed strategy to exert compositional control over structure–property relationships in polymeric materials. The scope of copolymerization typically encompasses strictly homologous monomer classes such as pure (meth)acrylate<sup>42</sup> or epoxide-based systems.<sup>43–51</sup> There are specific reports of the copolymerization of disparate classes of monomers such as epoxides and carbon dioxide<sup>52–61</sup> and/or cyclic anhydrides,<sup>62–66</sup> and examples of alternating copolymerization between epoxides and lactones have been reported for lactones incapable of homopolymerization.<sup>67,68</sup> Significantly, Chen et al. conducted copolymerizations of ethylene oxide and lactide using a variety of organometallic species and concluded that multiblock architectures resulted based on spectroscopic and thermal evidence.<sup>69</sup> Pitet et al. successfully synthesized branched poly(lactide) via copolymerization of glycidol with lactide.<sup>70</sup> Others have reported sequential block and statistical copolymers of specific epoxide/lactones pairs.<sup>71–74</sup> Multicomponent copolymerizations of an array of heterocyclic monomer species have also been reported with the specificity of a zinc-based catalyst resulting in block polymers formed from feed mixtures encompassing epoxide, lactone, anhydride, and carbon dioxide comonomers.<sup>75</sup> A general synthetic strategy that would enable the direct copolymerization of epoxides and lactones into single, high molecular weight statistical copolymers would provide a versatile material design platform as shown in Scheme 2-1.

---

<sup>1</sup> Reprinted with permission from Malgorzata Chwatko, Nathaniel A. Lynd *Macromolecules* 2017 50, 7, 2714-2723. Copyright 2017 American Chemical Society.



Scheme 2-1. Statistical Copolymerization of Lactones and Epoxides.

Relative reactivity toward polymerization between multiple monomers is a central concern for the synthesis of multifunctional materials from disparate monomers.<sup>76,77</sup> For heterocyclic monomers, the thermodynamic driving force for polymerization is ring strain which varies from ca.  $-110$  to  $-130$  kJ/mol for epoxides<sup>78</sup> and from  $-15$  to  $-30$  kJ/mol for lactones.<sup>79</sup> The disparity in ring strain suggests that copolymer composition would be dictated by a proportional incorporation of heterocyclic comonomers based on ring strain alone. However, additional kinetic factors contribute to the reactivity ratios of a given system, notably, the affinity of the monomer for the propagating center. During an active copolymerization of disparate heterocycles, monomer incorporation statistics (i.e., reactivity ratios) would be strongly affected by the relative Lewis basicity of the monomers, which, in part, would dictate their coordination equilibria for the propagation center of the polymerization the first step to monomer enchainment.<sup>75,80</sup>

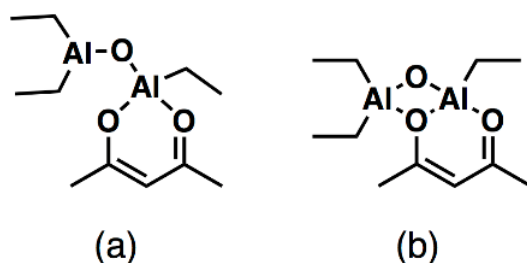
Given the importance of polyesters such as polylactide as the basis for renewable-resource derived thermoplastics and degradable and/or biocompatible scaffolds, significant research effort has focused on developing methods to modify and improve properties.<sup>81</sup> In this report, we present a synthetic approach that enables the facile combination of properties from disparate polymers into a single material with little synthetic overhead. We focused our investigation on the copolymerization between common lactones such as DL-lactide and  $\epsilon$ -caprolactone with alkylene

oxides such as ethylene oxide, propylene oxide, butylene oxide, and epichlorohydrin into single heterocopolymer architectures.

## RESULTS AND DISCUSSION

### Homopolymerization of DL-Lactide and Propylene Oxide

To statistically copolymerize lactones and epoxides, a catalyst or initiator must be capable of separate homopropagation of each species. The classical Vandenberg catalyst (Scheme 2-2) was selected for its unique ability to polymerize a broad range of heterocyclic monomers to high molecular weight. While the Vandenberg catalyst was developed originally for the industrial polymerization of epoxides, the activity of the Vandenberg catalyst toward lactones has never been reported to the best of our knowledge. The structure and mechanism of the Vandenberg catalyst are unfortunately unknown due to the uncontrolled nature of its preparation. A structure was proposed by Vandenberg according to the stoichiometry of reactants and the moles of gas evolved from release of the alkyl groups on aluminum during synthesis.<sup>82</sup> This stoichiometrically representative structure is shown in Scheme 2-2a. **Error! Reference source not found.** It should be noted that this structure is one of many possibilities, but a structure with large degrees of rotational freedom is not consistent with the isoselectivity of the Vandenberg-catalyzed epoxide polymerizations. On the basis of foundational work by Atwood<sup>83-85</sup> and Barron,<sup>86-92</sup> we propose that the structure of the Vandenberg catalyst is likely closer to the more rigid bis- $\mu$ -oxo-dialuminum structure shown in Scheme 2-2b. A conclusive structure of the initiating and catalytic motifs for the Vandenberg catalyst have never been substantiated to the best of our knowledge.



Scheme 2-2 (a) Originally Proposed Structure for the Vandenberg Catalyst and (b) a Renewed Stoichiometrically Representative Structure

Before copolymerizations were undertaken, the homopolymerization of DL-lactide (LA) was briefly investigated using the Vandenberg catalyst. Homopolymerizations of LA were carried out until complete consumption of monomer over 48 h for a range of aluminum concentrations. While aluminum concentration typically does not correlate with ultimate molecular weight in Vandenberg-catalyzed epoxide polymerizations, in lactone polymerizations the aluminum loading was effective for controlling molecular weight. For comparison, two size exclusion chromatograms resulting from a LA polymerization and a propylene oxide (PO) polymerization are presented in Figure 2-1 where both poly(propylene oxide) (PPO) and poly(DL-lactide) (PLA) were polymerized at equivalent monomer-to-aluminum ratios ( $[M]_0/[Al]_0 = 140$ ). In general, the homopolymerization of lactones was more controlled than epoxides using the Vandenberg catalyst. For LA, the ratio  $[LA]_0/[Al]_0$  was varied over an order of magnitude from 35 to 350, and the ultimate molecular weight was measured by size exclusion chromatography with multiangle light scattering (SEC-MALS) as shown in Figure 2-2. The ultimate degree of polymerization was approximately two times  $[LA]_0/[Al]_0$  when averaged over all polymerizations. This suggested that approximately two aluminum atoms participated in the production of a single polyester chain. The molecular weight distributions exhibited dispersities of 1.07–1.34 and are shown in the appendix A. These dispersities were lower than those that typically result from Vandenberg-catalyzed epoxide polymerizations which were typically 1.5–3.0. A final characteristic difference between

epoxide and lactone polymerizations using the Vandenberg catalyst is that the epoxide polymerizations are mildly isoselective,<sup>93</sup> whereas lactone polymerizations proceed without any apparent stereochemical preference.<sup>94,95</sup> Having gained a qualitative understanding of the separate homopolymerization of epoxides and lactones using the Vandenberg catalyst, we next carried out the simultaneous statistical copolymerization of lactones DL-lactide and  $\epsilon$ -caprolactone with epoxides epichlorohydrin, butylene oxide, propylene oxide, and ethylene oxide.

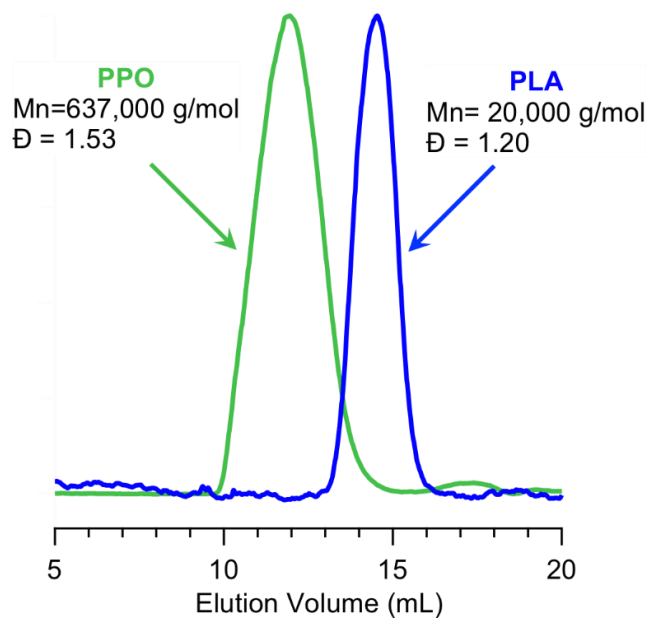


Figure 2-1. Comparison of size exclusion chromatograms (light scattering intensity) of poly(propylene oxide) (PPO) and poly(DL-lactide) (PLA) synthesized using the same monomer-to-aluminum ratio of the Vandenberg catalyst. The polymerization of lactones appears to be more controlled than those of the epoxides.

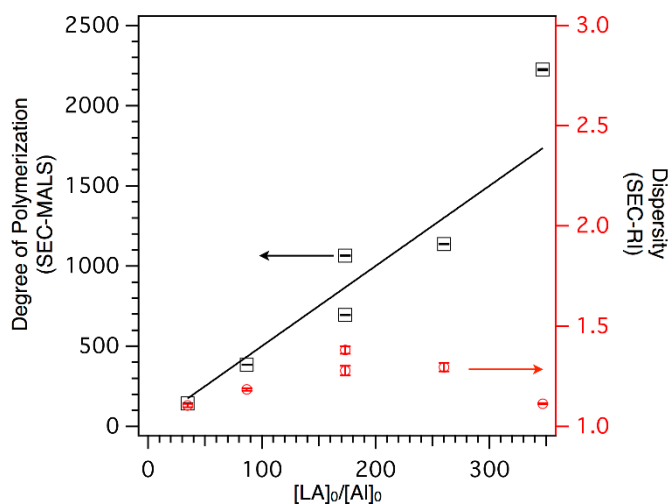


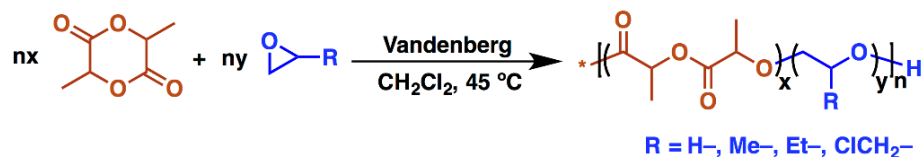
Figure 2-2 Relationship between  $[LA]_0/[Al]_0$  and degree of polymerization indicates that approximately four aluminum atoms are involved in the creation of a single poly(DL-lactide) chain. Degrees of polymerization were determined by size exclusion chromatography with a multiangle light scattering detector in chloroform, and dispersities were calculated from the RI signal. Each data point represents a separate experiment.

### Copolymerization of Epoxides and Lactones

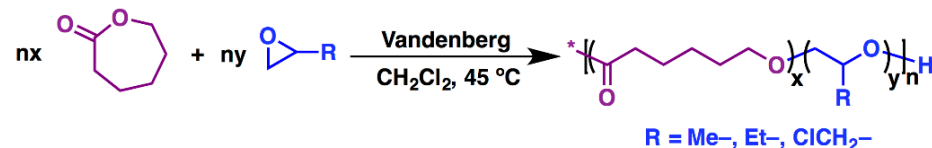
Copolymerizations between lactones and epoxides were conducted by dissolving both monomers in dry dichloromethane under a nitrogen atmosphere. The copolymerization was initiated by the addition of a measured quantity of Vandenberg catalyst solution in diethyl ether through a septum into the monomer solution. The copolymerizations were conducted at 45 °C for 24 h. Typically, magnetic stirring ceased as the reaction viscosity increased. Polymerization was terminated by the addition of a methanol/dichloromethane solution. The copolymers were dried by rotary evaporation and then *in vacuo* overnight. The copolymers were characterized by  $^1\text{H}$  and  $^{13}\text{C}$  NMR spectroscopy and size exclusion chromatography (SEC) with light scattering (LS), differential refractive index (RI), and viscosity detectors to determine molecular weight distribution. Comonomer feed stoichiometry was 2:1, 1:1, and 1:2 by mole for most lactone:epoxide combinations. The following seven copolymer species were synthesized:

poly[(DL-lactide)-*co*-(ethylene oxide)] (P(LA-*co*-EO)), poly[(DL-lactide)-*co*-(epichlorohydrin)] (P(LA-*co*-ECH)), poly[(DL-lactide)-*co*-(butylene oxide)] (P(LA-*co*-BO)), poly[(DL-lactide)-*co*-(propylene oxide)] (P(LA-*co*-PO)), poly[( $\epsilon$ -caprolactone)-*co*-(epichlorohydrin)] (P(CL-*co*-ECH)), poly[( $\epsilon$ -caprolactone)-*co*-(butylene oxide)] (P(CL-*co*-BO)), and poly[( $\epsilon$ -caprolactone)-*co*-(propylene oxide)] (P(CL-*co*-PO)). The general copolymerization scheme is shown in Scheme 2-3, and the results of the copolymerizations are summarized in Table 2-1. Generally, the molecular weights and dispersities of the copolymers were consistent with the characteristics and performance of the Vandenberg catalyst for pure epoxide systems. However, the yields of the recovered copolymers were generally not quantitative, and the molecular weights ranged from the lowest at 29 kg/mol to the highest at 16 Mg/mol. We attribute the nonquantitative yield of the copolymerizations to the sharp increase in solution viscosity during the latter stages of the polymerization. Molecular weight distributions ranged from narrowly distributed, unimodal distributions with dispersities of 1.2 to broadly distributed materials with dispersities as high as 20. The polymer composition ( $F_{\text{lactone}}$ ) followed the general trend in monomer feed ( $f_{\text{lactone}}$ ). However, we attribute discrepancies to the inherent reactivity ratios of each copolymerization and the ultimate conversion.

(a) Copolymerization of DL-lactide and epoxides



(b) Copolymerization of  $\epsilon$ -caprolactone and epoxides



Scheme 2-3 General Statistical Copolymerization of Lactones and Epoxides

Table 2-1. Characteristics of Poly(ester-co-ether)s

entry	copolymer	$f_{\text{lactone}}^{\text{a}}$	$F_{\text{lactone}}^{\text{b}}$	$M_n^{\text{c}}$ (kg/mol)	$M_w^{\text{c}}$ (kg/mol)	$D^{\text{d}}$	$T_g^{\text{e}}$	$T_m^{\text{e}}$
1	P(LA <sub>0.45</sub> -co-EO <sub>0.55</sub> )	0.50	0.45	93	114	1.2	-26	62
2	P(LA <sub>0.08</sub> -co-ECH <sub>0.92</sub> )	0.33	0.08	1630	2900	1.8	-24	n.o.
3	P(LA <sub>0.45</sub> -co-ECH <sub>0.55</sub> )	0.50	0.45	4160	5730	1.5	-30	n.o.
4	P(LA <sub>0.22</sub> -co-ECH <sub>0.78</sub> )	0.66	0.22	16840*	24730	1.5*	-33	n.o.
5	P(LA <sub>0.40</sub> -co-BO <sub>0.60</sub> )	0.33	0.40	166	1860	11.1	30	n.o.
6	P(LA <sub>0.25</sub> -co-BO <sub>0.75</sub> )	0.50	0.25	29	327	11.2	26	n.o.
7	P(LA <sub>0.24</sub> -co-BO <sub>0.76</sub> )	0.66	0.24	99	1540	15.5	34	n.o.
8	P(LA <sub>0.19</sub> -co-PO <sub>0.81</sub> )	0.33	0.19	2760	3180	1.2	18	n.o.
9	P(LA <sub>0.20</sub> -co-PO <sub>0.80</sub> )	0.50	0.20	1100	3680	3.4	19	n.o.
10	P(LA <sub>0.34</sub> -co-PO <sub>0.66</sub> )	0.66	0.34	80	514	6.5	18	n.o.
11	P(CL <sub>0.67</sub> -co-ECH <sub>0.33</sub> )	0.33	0.67	150	2710	18.0	-47	28
12	P(CL <sub>0.48</sub> -co-ECH <sub>0.52</sub> )	0.50	0.48	110	2290	20.7	-50	14
13	P(CL <sub>0.93</sub> -co-ECH <sub>0.07</sub> )	0.66	0.93	41	500	12.2	n.o.	32
14	P(CL <sub>0.32</sub> -co-BO <sub>0.68</sub> )	0.33	0.32	2500	3790	1.5	n.o.	51
15	P(CL <sub>0.29</sub> -co-BO <sub>0.71</sub> )	0.50	0.29	515	1570	3.1	n.o.	55
16	P(CL <sub>0.59</sub> -co-BO <sub>0.41</sub> )	0.66	0.59	57	550	9.6	n.o.	52
17	P(CL <sub>0.20</sub> -co-PO <sub>0.80</sub> )	0.33	0.20	137	794	5.8	n.o.	52
18	P(CL <sub>0.28</sub> -co-PO <sub>0.72</sub> )	0.50	0.28	126	677	5.4	n.o.	51
19	P(CL <sub>0.51</sub> -co-PO <sub>0.49</sub> )	0.66	0.51	45	372	8.3	n.o.	50

a Initial mole fraction of lactone flactone = nlactone/(nlactone + nepoxide). b Final cumulative mole fraction composition of copolymer measured by 1H NMR spectroscopy. c Number- and weight-average molecular weight determined by size exclusion chromatography in chloroform using light scattering and differential refractometer detectors. In instances where ultrahigh molecular weight materials are beyond the exclusion limit of size exclusion columns (~10 MDa), Mn will be inaccurate. These values are indicated by an asterisk. d Dispersity was determined by size exclusion chromatography in chloroform using the differential refractometer signal. In instances where ultrahigh molecular weight materials were beyond the exclusion limit of the size exclusion columns (~10 MDa), D will be inaccurate. These values are indicated by an asterisk. e Thermal properties were measured by differential scanning calorimetry and recorded in °C.

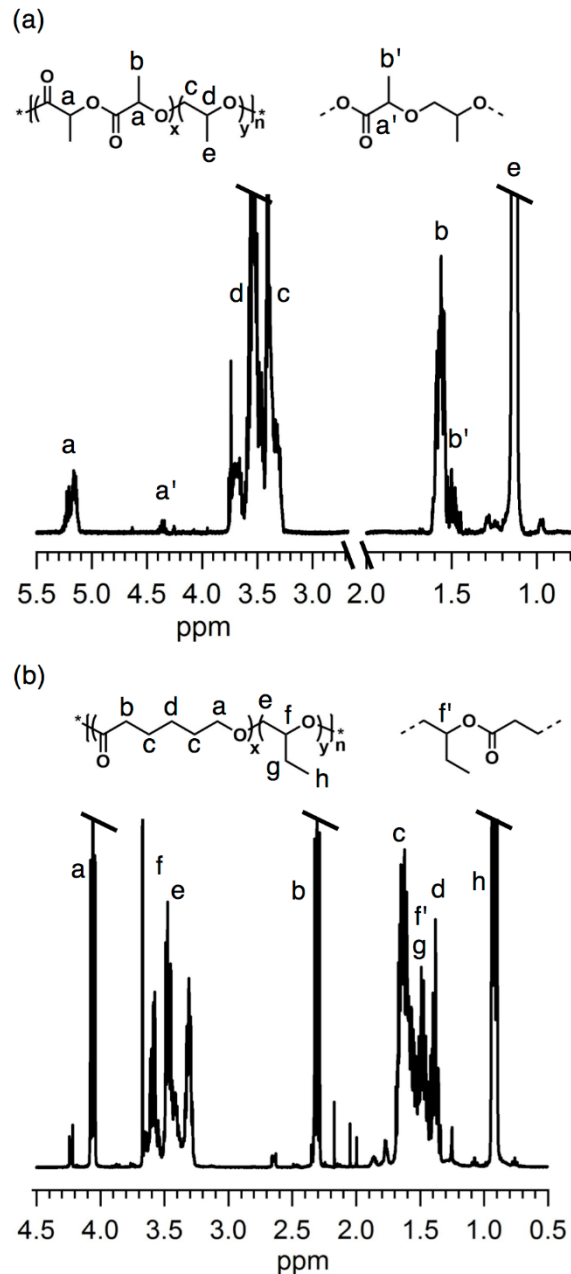


Figure 2-3 Representative <sup>1</sup>H NMR spectra (400 MHz, CDCl<sub>3</sub>) of (a) P(LA-co-PO) and (b) P(CL-co-BO). The spectra can be viewed as a superposition of the two homopolymer spectra with the addition of distinct signals consistent with dyad formation. Signals were assigned based on COSY NMR spectra shown in Appendix A.

NMR spectroscopy is sensitive to copolymer composition and can also identify characteristic dyad or triad heterosequences that are characteristic of copolymerization. A representative <sup>1</sup>H NMR spectrum of poly[(dl-lactide)-co-(propylene oxide)] is shown in Figure

2-3a, and a representative spectrum of poly[( $\epsilon$ -caprolactone)-co-(butylene oxide)] is shown in Figure 2-3b. Peak assignments are supported by  $^1\text{H}$ - $^1\text{H}$  COSY NMR spectra shown in the appendix. For poly[(dl-lactide)-co-(propylene oxide)] (Figure 2-3a) a dyad signal that was diagnostic for the presence of the lactide methine immediately adjacent to a propylene oxide LA-PO repeat unit was observed at ca. 4.4 ppm (a', 1H). This assignment was consistent with the chemical shifts reported for block junctions in low molecular weight diblock copolymers of poly(lactide) with various polyethers<sup>96-99</sup> and a recent report on the post polymerization oxidation of poly(ethylene oxide) introducing randomly dispersed glycolide repeat units.<sup>100</sup> Additional signals consistent with methyl (b', 3H) protons on lactide in the LA-PO dyad were observed at 1.5 ppm (Figure 2-3a). For the  $^1\text{H}$  NMR spectrum of poly[( $\epsilon$ -caprolactone)-co-(butylene oxide)] shown in Figure 2-3b, the overlapping methine signal of a butylene oxide repeat unit in a BO-CL dyad was observed at 1.5 ppm (f', 1H). The  $^1\text{H}$ - $^1\text{H}$  COSY spectrum that supports this assignment is shown in the appendix A. Additional  $^{13}\text{C}$ ,  $^1\text{H}$ , and  $^1\text{H}$ - $^1\text{H}$  COSY NMR spectra of all copolymers are shown in appendix A.

Differential scanning calorimetry was used to assess the impact of copolymerization on the glass-transition temperature ( $T_g$ ) and melting point ( $T_m$ ) where applicable. For a sufficiently random statistical copolymer, the  $T_g$  should be an intermediate between the  $T_g$  of each corresponding pure component. The copolymers containing dl-lactide (Table 2-1, entries 1-10) exhibited  $T_g$  between that of pure poly(dl-lactide) (60 °C) and that of poly(ethylene oxide) (-60 °C), poly(butylene oxide) (-70 °C), and poly(propylene oxide) (-60 °C) as shown in Table 2-1. Poly[(dl-lactide)-co-(epichlorohydrin)] exhibited  $T_g$  ranging from -33 to -24 °C. For copolymers containing  $\epsilon$ -caprolactone (Table 2-1, entries 11-19) glass-transition temperatures were not observed in every sample. Poly[( $\epsilon$ -caprolactone)-co-(epichlorohydrin)] exhibited  $T_g$  of -50 to -47 °C as the fractional molar composition of caprolactone repeat units ( $F_{\text{lactone}}$ ) increased from 0.48

to 0.67 (Table 2-1, entries 11 and 12). Once the  $\epsilon$ -caprolactone  $F_{\text{lactone}}$  increased further to 0.93 by mole, a glass transition was no longer observed. The melting temperature increased with  $\epsilon$ -caprolactone  $F_{\text{lactone}}$  from 14 to 32 °C. These melting temperatures were depressed from the melting point of pure poly( $\epsilon$ -caprolactone) due to the defects provided by epichlorohydrin repeat units. For the remainder of the copolymers containing  $\epsilon$ -caprolactone, the crystallinity of the poly( $\epsilon$ -caprolactone) component appeared to be relatively unaffected by comonomer incorporation. This suggested that the architecture of the copolymer was consistent with a stronger gradient than observed in poly[( $\epsilon$ -caprolactone)-co-(epichlorohydrin)]. To quantify the gradient character of the poly(ester-co-ether) copolymers, reactivity ratios were determined for representative epoxide/lactone pairs.

Kinetic data were collected for copolymerizations of dl-lactide/propylene oxide (LA/PO) as well as  $\epsilon$ -caprolactone/propylene oxide (CL/PO). The consumption of both monomers was measured with time by  $^1\text{H}$  NMR spectroscopy as shown respectively in Figure 2-4 and Figure 2-5.<sup>99</sup> The initial mole fraction of the feed was  $f_{\text{LA}} = 0.57$  ( $f_{\text{PO}} = 0.43$ ). In the stacked  $^1\text{H}$  NMR spectra shown in Figure 2-4, the simultaneous consumption of LA and PO could be observed by the decrease in the integral (3H) of epoxide signals at 2.3–3.0 ppm, and the methine signal at 5.15 ppm corresponding to 2H per LA, as well as the methyl signal at 1.62 ppm corresponding to 6H per LA. PO was consumed preferentially over LA. While simultaneous consumption of comonomers with time is sufficient to determine reactivity ratios, it does not uniquely define true copolymerization. In Figure 2-4, the characteristic dyad signal at 4.2 ppm (a') increased in intensity while PO and LA were both being consumed. After complete consumption of PO, the growth of the dyad signal at 4.2 ppm (a') stopped. The direct observation of the growth of this characteristic dyad signal during copolymerization is only consistent with a copolymerization where both LA and PO are incorporating into a single polymer backbone and would not be consistent with transesterification.

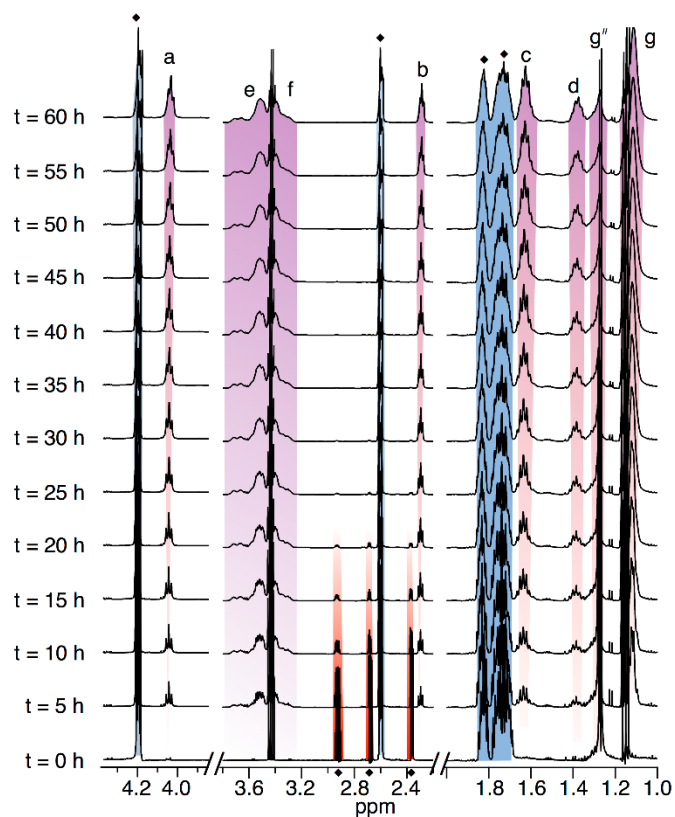


Figure 2-4 <sup>1</sup>H NMR spectroscopy (600 MHz, CD<sub>2</sub>Cl<sub>2</sub>) of the copolymerization of LA and PO over 65 h at room temperature. LA resonances at δ 5.15 (2H) and 1.62 (6H) are shaded in blue, and PO resonances at δ 2.4–3.0 (3H) are shaded in red. Resonances associated with the copolymer are shaded in purple: (a) δ 5.2 2H, (a') δ 4.2 1H, (c', d, c) δ 3.4–3.7 3H, (b, b') δ 1.58 6H.

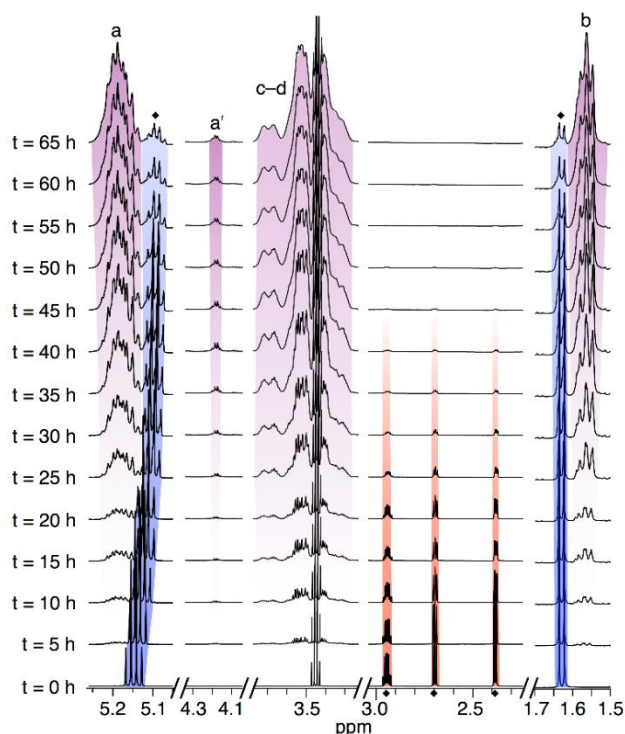


Figure 2-5.  $^1\text{H}$  NMR spectroscopy (600 MHz,  $\text{CD}_2\text{Cl}_2$ ) of the copolymerization of CL and PO over 65 h at room temperature. CL resonances at  $\delta$  4.20 (2H),  $\delta$  2.59 (2H),  $\delta$  1.81 (2H), and  $\delta$  1.71 (4H) are shaded in blue, and PO resonances at  $\delta$  2.39,  $\delta$  2.9–2.6 (3H), and  $\delta$  1.26 (3H) are shaded in red. Resonances associated with the copolymer are shaded in purple: (a)  $\delta$  4.03 (2H), (e, f)  $\delta$  3.3–3.6 (3H), (b)  $\delta$  2.3 (2H), (c)  $\delta$  1.63 (4H), (d)  $\delta$  1.37 (2H), (g)  $\delta$  1.10 (3H).

The copolymerization of  $\epsilon$ -caprolactone (CL) and propylene oxide (PO) was similarly monitored by  $^1\text{H}$  NMR spectroscopy. The spectra are shown in Figure 2-5. The initial mole fraction of the feed was  $f_{\text{CL}} = 0.62$  ( $f_{\text{PO}} = 0.38$ ). The consumption of propylene oxide was monitored by the combined integral of the epoxide signals at 2.5–3.1 ppm corresponding to 3H on PO. PO was consumed preferentially over CL over the course of 32 h at room temperature. The consumption of 4H on CL was monitored by its methylene signals 4.4 and 2.8 ppm corresponding to 4H per monomer. CL was not consumed completely during the course of the copolymerization. However, sufficient data were acquired to calculate reactivity ratios.

The time-dependent composition of LA/PO and CL/PO copolymerizations were interpreted within the context of two integrated models of copolymerization capable of producing reactivity ratios from the spectroscopic data in Figure 2-4 and Figure 2-5. For nonterminal copolymerization kinetics common in coordination–insertion, ionic, and pseudoionic type polymerization mechanisms, the simple model for compositional drift reported by Beckingham et al. (BSL) was employed.<sup>77</sup> For a terminal model of copolymerization kinetics, we employed the classical model of Meyer and Lowry (ML).<sup>101</sup>

The BSL and ML fits to the compositional drift data for LA/PO are shown in Figure 2-6a and b, respectively. The nonterminal model yielded reactivity ratios of  $r_{PO} = 4.50 \pm 0.47$  and  $r_{LA} = 0.37 \pm 0.02$ . The terminal model was utilized to extract reactivity ratios by fitting the same data formatted for the ML equation. The reactivity ratios that resulted were consistent with those obtained by BSL:  $r_{PO} = 2.29 \pm 0.24$  and  $r_{LA} = 0.36 \pm 0.02$ . On the basis of these reactivity ratios, we concluded that P(LA-co-PO) materials were most consistent with a gradient copolymer. We believe the discrepancy in  $r_{PO}$  between the two fitting models is due to the reversible nature of lactone ring-opening polymerization, which neither BSL nor ML accounts for. Including partial reversibility into an integrated model for copolymerization will be the subject of future investigation.

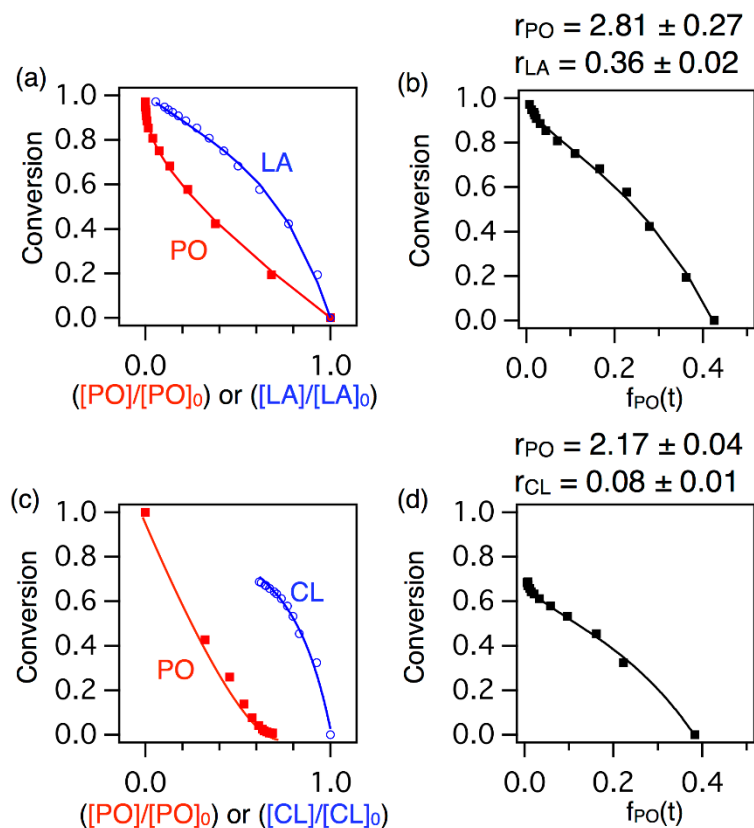


Figure 2-6 Reactivity ratios could be estimated from the raw  $^1\text{H}$  NMR spectroscopy data shown in Figure 2-4 and Figure 2-5 by two methods: (a) The nonterminal model of copolymerization kinetics reported by Beckingham et al. was used to produce an estimate of the reactivity ratios:  $r_{\text{PO}} = 4.50 \pm 0.47$  and  $r_{\text{LA}} = 0.37 \pm 0.02$ . (b) The Meyer–Lowry equation for the traditional terminal model of copolymerization produced similar values:  $r_{\text{PO}} = 2.81 \pm 0.27$  and  $r_{\text{LA}} = 0.36 \pm 0.02$ . The results of fitting by both methodologies were consistent with a gradient copolymer. (c)  $\epsilon$ -Caprolactone and propylene oxide reactivity ratios could not be accurately described by the model of Beckingham et al. Curves are drawn to guide the eye. (d) The Meyer–Lowry equation produced a fit that was consistent with a strong gradient copolymer with generally isolated CL repeat units  $r_{\text{PO}} = 2.17 \pm 0.04$  and  $r_{\text{CL}} = 0.08 \pm 0.01$ .

The determination of reactivity ratios for the copolymerization of  $\epsilon$ -caprolactone and propylene oxide was comparably conducted. Propylene oxide was consumed earlier in the copolymerization with  $\epsilon$ -caprolactone incorporating more slowly and did not polymerize beyond a conversion of *ca.* 40% over the course of the experiment. Lactone polymerizations can exhibit significant equilibrium behavior that results in an equilibrium concentration of monomer. If the

lactone chain end was to have any appreciable tendency toward alternation, then isolated ester repeat units would be present, and a fraction of unconsumed lactone would be expected for a range of monomer feeds. Likewise, a combination of both monomer equilibrium and alternation could account for the remaining fraction of unreacted  $\epsilon$ -caprolactone. A detailed investigation of these aspects is currently underway in a separate study. Because of the unreacted fraction of  $\epsilon$ -caprolactone, the BSL analysis of compositional drift was not possible. The compositional drift data, formatted for BSL, are shown in Figure 2-6c. The extraction of reactivity ratios using the ML equation was possible, but these values are offered with the caveat that while they will describe the changes in bulk monomer composition with time, all the unreacted  $\epsilon$ -caprolactone will be interpreted by the ML model as being due to alternation in that monomer, i.e., a small  $r_{CL}$ . This is reflected in the reactivity ratio values that resulted:  $r_{PO} = 2.17 \pm 0.04$  and  $r_{CL} = 0.08 \pm 0.01$ . Further detailed investigation of the thermodynamics, kinetics, and mechanism of copolymerization is currently underway. In summary, reactivity ratios were determined for two representative copolymerizations between DL-lactide and  $\epsilon$ -caprolactone copolymerized with propylene oxide using compositional data. The appearance of specific spectroscopic signatures of copolymerization through ester–ether dyad formation was observed as well. These observations are consistent with copolymerization of lactones and epoxides.

The visual appearance of a multicomponent material can be diagnostic for its purity, morphology, and also miscibility in the case of homopolymer mixtures. Immiscible homopolymer mixtures will generally appear opaque due to light scattering associated with phase separation, whereas copolymers will appear optically clear if spatially homogeneous or if phase separation is limited to small length scales (<100 nm). Dry copolymers were pressed into films between Teflon sheet at 70 °C. A representative film of poly[(dl-lactide)<sub>0.24</sub>-co-(butylene oxide)<sub>0.76</sub>] ( Table 2-1, entry 7) is shown in Figure 2-7. All films were optically clear consistent with majority

copolymer compositions and not homopolymer mixtures which could phase-separate, coarsen, and appear opaque. An image of a blend of PLA and PBO homopolymers is shown for comparison in Figure A2-28.

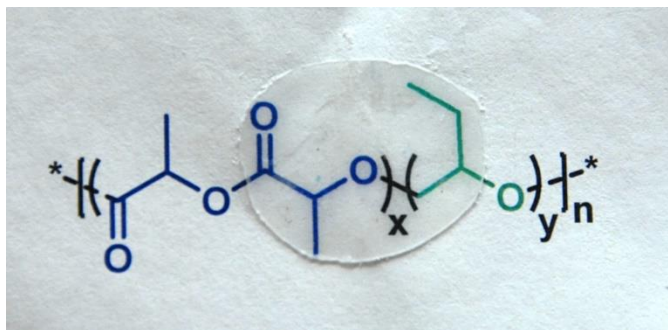


Figure 2-7 A pressed film of poly[(DL-lactide)-co-(butylene oxide)] (Table 2-1, entry 7) was optically clear and homogeneous.

Degradability is an important feature for environmental and biomedical applications of new polymer materials. In order to explore the degradability of our copolymers, poly[(dl-lactide)-co-(ethylene oxide)] (Table 2-1, entry 1) was pressed into several 1.0 cm × 1.0 cm × 0.4 cm cubes at 70 °C. These solid samples were subjected to basic and neutral aqueous conditions over the course of several days in triplicate. The mass of the remaining samples was recorded as a function of time by blotting the excess liquid using a paper towel and measuring the remaining weight of the cube. As can be seen in Figure 2-8, there was a decrease in average mass with time after the material initially swelled to equilibrium within the first 24 h. Measurement of the molecular weight of the solid portions of the sample remained nearly unchanged from the parent material as the experiment progressed. The degradation of the P(LA<sub>0.45</sub>-co-EO<sub>0.55</sub>) cubes was consistent with surface erosion due to ester cleavage and dissolution of remaining PEO oligomers. The solid samples experienced a 75–80% decrease in weight of the starting polymer versus the ending material in both neutral and basic mixtures over the course of 15 days. As expected, the basic conditions (0.5 M NaOH in 40 vol % water/methanol) led to a higher rate of degradation.<sup>102</sup> We

attribute the swelling and high rate of degradation to the increased hydrophilicity imparted to the material by the presence of ethylene oxide moieties in the poly(ester-co-ether) backbone.<sup>103</sup>

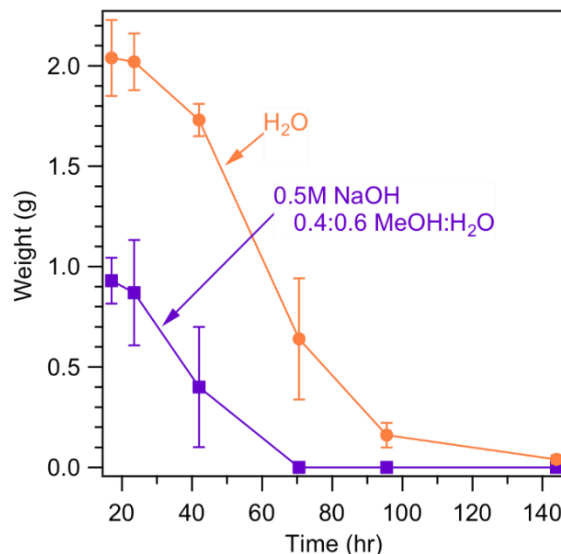


Figure 2-8 Degradation of poly[(DL-lactide)-co-(ethylene oxide)] cubes was conducted under standard aqueous and basic conditions. Experiments were conducted in triplicate, and error bars represent the standard deviation among the three samples.

## CONCLUSIONS

We reported a synthetic technique for the general statistical copolymerization of lactones and epoxides using the Vandenberg catalyst developed originally for the industrial production of high molecular weight polyethers. Copolymers were synthesized from DL-lactide and ethylene oxide, propylene oxide, butylene oxide, and epichlorohydrin, while  $\epsilon$ -caprolactone was copolymerized with propylene oxide, butylene oxide, and epichlorohydrin. Spectroscopic compositional and sequential information combined with thermal and optical properties were consistent with copolymer formation from mixed lactone and epoxide monomer feedstocks. The presence of ester-ether heterodyads was directly observed by <sup>1</sup>H NMR spectroscopy. Reactivity ratios were determined for poly[(DL-lactide)-co-(propylene oxide)] and were consistent with a gradient copolymer. A tentative reactivity ratio estimation for poly[( $\epsilon$ -caprolactone)-co-(propylene

oxide)] was also consistent with a gradient copolymer but with isolated  $\epsilon$ -caprolactone-derived repeat units. These new synthetic concepts expand the ability of modular and versatile copolymerization to encompass a greater diversity of repeat unit structures and to tune thermal, mechanical, and reactive properties of new functional polymeric materials derived from readily available and structurally diverse precursors.

## **EXPERIMENTAL SECTION**

### **Materials**

Chemicals were obtained from Sigma-Aldrich, Fisher Scientific, and TCI-America, Inc., and were used without further purification unless otherwise specified. Toluene and diethyl ether were drawn from a dry solvent system (J.C. Meyer) and used immediately afterward. Deuterated chloroform ( $\text{CDCl}_3$ ) and deuterated methylene chloride ( $\text{CD}_2\text{Cl}_2$ ) were purchased from Cambridge Isotope Laboratories, Inc. DL-Lactide was recrystallized from ethyl acetate, and all epoxides except ethylene oxide were dried over calcium hydride and degassed via three freeze–pump–thaw cycles. These monomers were kept in an inert nitrogen environment until use. Ethylene oxide was purchased from Airgas (99.9%+) and condensed into a tared and dried high-pressure round-bottom flask fitted with Chemglass stopcocks.

### **Measurements and Characterization**

$^1\text{H}$  and  $^{13}\text{C}$  NMR spectroscopy was carried out on an Agilent MR 400 MHz spectrometer, a Varian DirectDrive 400 MHz, a Varian Inova 500 MHz, and a Varian Mercury 400 MHz. Spectra were collected in deuterated chloroform except where specified. Differential scanning calorimetry (DSC) was performed using a TA Instruments Q2000 MDSC equipped with an autosampler. The temperature ranged from  $-70$  to  $+150$  °C and was controlled by heating at  $10$  °C/min and cooling at  $5$  °C/min. Size exclusion chromatography (SEC) was carried out on an Agilent system with a

1260 Infinity isocratic pump, degasser, and thermostated column chamber held at 30 °C containing Agilent PLgel 10 µm MIXED-B and 5 µm MIXED-C columns with a combined operating range of 200–10 000 000 g/mol relative to polystyrene standards. Chloroform with 50 ppm amylene was used as the mobile phase at 0.5 mL/min for the copolymer measurement and tetrahydrofuran at 0.5 mL/min for polylactide. Measurement of polymer concentration, molecular weight, and viscosity was provided by a suite of detectors from Wyatt Technologies. Static light scattering was measured using a DAWN HELEOS II Peltier system, differential refractive index was measured with an Optilab TrEX, and differential viscosity was measured using a Viscostar II. Change in refractive index with concentration ( $dn/dc$ ) was estimated by assuming 100% mass recovery from the column.

#### ***Synthesis of the Aluminum Chelate (Vandenberg) Catalyst***

To an 80 mL solution of 0.5 M triethylaluminum in diethyl ether at  $-78$  °C was added dropwise 0.5 equiv of dry acetyl acetone. The reaction mixture was stirred and vented under an inert nitrogen purge until all gas evolution ceased. 0.5 equiv of deionized water was added *slowly* to the rapidly stirring solution under inert nitrogen at 0 °C. The solution was allowed to warm and stir overnight before use.

#### ***Synthesis of Poly[(dl-lactide)]***

DL-Lactide (2 g) was added to a dry reaction vial under nitrogen with a Teflon-coated stir bar. 6 mL of dichloromethane was added to the reaction mixture, after which the vial was sealed to maintain an inert nitrogen atmosphere. The catalyst was added from a stock solution to target monomer-to-aluminum ratios of 35, 87, 173, 260, and 350. The solvent in these polymerizations was used as received. The reaction was heated at 45 °C and magnetically stirred for 48 h. Conversion of DL-lactide was quantitative. Molecular weight was determined by SEC using the

differential refractive index and multiangle light scattering detectors with a  $dn/dc = 0.042$  mL/g for PLA in the tetrahydrofuran mobile phase.

#### ***Synthesis of Poly[(dl-lactide)-co-(ethylene oxide)] (P(LA-co-EO))***

DL-Lactide (13.25 g) was added to a glass reactor, after which 43 mL of dry dichloromethane was added. Ethylene oxide (4.18 g) was added in a 1:1 molar feed ratio relative to DL-lactide. The Vandenberg catalyst was added from a stock solution to target a monomer-to-aluminum ratio of 208. The reaction was then stirred and heated to 45 °C for 24 h. As the reaction proceeded the viscosity increased dramatically. The reaction was quenched with a mixture of methylene chloride and methanol. The polymer was dried *in vacuo*. The sample was weighed at this time to determine yield and analyzed with  $^1\text{H}$  and  $^{13}\text{C}$  NMR spectroscopy and SEC.  $^1\text{H}$  NMR (400 MHz, 2:1  $\text{CD}_2\text{Cl}_2:\text{CDCl}_3$ ):  $\delta$  5.2, 4.4 ( $-\text{C}(=\text{O})\text{CH}(\text{CH}_3)-\text{O}-$ ),  $\delta$  1.5 ( $-\text{C}(=\text{O})\text{CH}(\text{CH}_3)-\text{O}-$ ),  $\delta$  3.5–3.8 ( $-\text{OCH}_2\text{CH}_2\text{O}-$ ).  $^{13}\text{C}$  NMR (100 MHz,  $\text{CD}_2\text{Cl}_2:\text{CDCl}_3$ ):  $\delta$  169.2, 71.1, 69.8, 69.6, 17.1.

#### ***Synthesis of Poly[(dl-lactide)-co-(epichlorohydrin)] (P(LA-co-ECH))***

DL-Lactide (1 g) was added to a reaction vial, after which the corresponding molar amount of epichlorohydrin was added. To this monomer mixture, 6 mL of dry dichloromethane was added, after which the vial was sealed under an inert nitrogen atmosphere. The catalyst was added from a stock solution to target monomer-to-aluminum ratios of 169, 182, and 157 for LA:ECH molar feed ratios of 1:1, 1:2, and 2:1 of LA:ECH. The reaction was stirred and heated at 45 °C for 24 h. As the reaction proceeded, the viscosity increased dramatically. The polymerization was terminated with a mixture of dichloromethane and methanol. The polymer was then dried on a rotary evaporator at 150 mbar and 45 °C to remove solvent before being dried *in vacuo* to a pressure of 20 mTorr. The sample at this time was weighed to determine yield and used for characterization by  $^1\text{H}$  and  $^{13}\text{C}$  NMR spectroscopy and SEC.  $^1\text{H}$  NMR (400 MHz, 1:2  $\text{CD}_2\text{Cl}_2:\text{CDCl}_3$ ):  $\delta$  5.2–5.1, 4.3

(-C(=O)CH(CH<sub>3</sub>)-O-),  $\delta$  1.6–1.4 (-C(=O)CH(CH<sub>3</sub>)-O-),  $\delta$  3.8–3.6 (-OCH<sub>2</sub>CH(CH<sub>2</sub>Cl)O-). <sup>13</sup>C NMR (100 MHz, CD<sub>2</sub>Cl<sub>2</sub>:CDCl<sub>3</sub>):  $\delta$  80.0, 70.5, 69.9, 44.6, 21.3, 17.6.

#### ***Synthesis of Poly[(dl-lactide)-co-(butylene oxide)] (P(LA-co-BO))***

DL-Lactide (1 g) was added to a reaction vial, after which the corresponding molar amount of butylene oxide was added to create molar feed ratios of 1:1, 1:2, and 2:1 of LA:BO. 6 mL of dry dichloromethane was added, after which the vial was sealed and kept in an inert nitrogen atmosphere. The catalyst was added from a stock solution to target monomer-to-aluminum ratios of 185, 208, and 164 for the LA:BO molar feed ratios of 1:1, 1:2, and 2:1. Reaction conditions, product work-up, and analysis were carried out equivalently to P(LA-co-ECH). <sup>1</sup>H NMR (400 MHz, CDCl<sub>3</sub>):  $\delta$  5.3–5.1, 4.4 (-C(=O)CH(CH<sub>3</sub>)O-),  $\delta$  1.6–1.4 (-C(=O)CH(CH<sub>3</sub>)O-),  $\delta$  3.7–3.3 (-OCH<sub>2</sub>CH(CH<sub>2</sub>CH<sub>3</sub>)O-),  $\delta$  1.6 (-OCH<sub>2</sub>CH(CH<sub>2</sub>CH<sub>3</sub>)O-),  $\delta$  0.9 (-OCH<sub>2</sub>CH(CH<sub>2</sub>CH<sub>3</sub>) O-). <sup>13</sup>C NMR (100 MHz, CDCl<sub>3</sub>):  $\delta$  81.0, 72.5, 69.1, 24.9, 20.3, 16.8, 10.0.

#### ***Synthesis of Poly[(dl-lactide)-co-(propylene oxide)] (P(LA-co-PO))***

DL-Lactide (1 g) was added to a reaction vial, after which the corresponding molar amount of propylene oxide was added to create a molar feed ratios of 1:1, 1:2, and 2:1. To this monomer mixture, 6 mL of dry dichloromethane was added, after which the vial was sealed and kept in an inert nitrogen atmosphere. The catalyst was added from a stock solution to target a monomer-to-aluminum ratio of 198, 230, and 173 for the LA:PO molar feed ratios of 1:1, 1:2, and 2:1. Reaction conditions, product work-up, and analysis were carried out equivalently to P(LA-co-ECH). <sup>1</sup>H NMR (400 MHz, CDCl<sub>3</sub>):  $\delta$  5.2–5.1, 4.4 (-C(=O)CH(CH<sub>3</sub>)O-),  $\delta$  1.6–1.5(-C(=O)CH(CH<sub>3</sub>)O-),  $\delta$  3.8–3.3 (-OCH<sub>2</sub>CH(CH<sub>3</sub>)O-),  $\delta$  1.1 (-OCH<sub>2</sub>CH(CH<sub>3</sub>)O-). <sup>13</sup>C NMR (100 MHz, CDCl<sub>3</sub>):  $\delta$  169.5, 75.7, 73.6, 69.3, 52.4, 20.3, 18.25, 17.45, 16.8.

### ***Synthesis of Poly[( $\epsilon$ -caprolactone)-co-(epichlorohydrin)] (P(CL-co-ECH))***

$\epsilon$ -Caprolactone (1 g) was added to a reaction vial, after which the corresponding molar amount of epichlorohydrin was added to create a molar feed ratio of 1:1, 1:2, and 2:1 of CL:ECH. To this monomer mixture, 6 mL of dry dichloromethane was added, after which the vial was sealed and kept in an inert nitrogen atmosphere. The catalyst was added from a stock solution to target a monomer-to-aluminum ratio of 194, 200, and 187 for EL:ECH molar feed ratios of 1:1, 1:2, and 2:1. Reaction conditions, product work-up, and analysis were carried out equivalently to P(LA-co-ECH).  $^1\text{H}$  NMR (400 MHz, 1:2  $\text{CD}_2\text{Cl}_2:\text{CDCl}_3$ ):  $\delta$  4.0 ( $-\text{C}(=\text{O})\text{CH}_2\text{CH}_2\text{CH}_2\text{CH}_2\text{CH}_2\text{O}-$ ),  $\delta$  2.3 ( $-\text{C}(=\text{O})\text{CH}_2\text{CH}_2\text{CH}_2\text{CH}_2\text{CH}_2\text{O}-$ ),  $\delta$  1.7–1.6 ( $-\text{C}(=\text{O})\text{CH}_2\text{CH}_2\text{CH}_2\text{CH}_2\text{CH}_2\text{O}-$ ),  $\delta$  1.4–1.3 ( $-\text{C}(=\text{O})\text{CH}_2\text{CH}_2\text{CH}_2\text{CH}_2\text{CH}_2\text{O}-$ ),  $\delta$  3.8–3.6 ( $-\text{OCH}_2\text{CH}(\text{CH}_2\text{Cl})\text{O}-$ ),  $\delta$  1.53 ( $-\text{OCH}_2\text{CH}(\text{CH}_2\text{Cl})\text{O}-$ ).  $^{13}\text{C}$  NMR (100 MHz,  $\text{CD}_2\text{Cl}_2:\text{CDCl}_3$ ):  $\delta$  174.1, 79.8, 70.3, 64.8, 44.5, 34.8, 29.1, 26.2, 26.5.

### ***Synthesis of Poly[( $\epsilon$ -caprolactone)-co-(butylene oxide)] (P(CL-co-BO))***

$\epsilon$ -Caprolactone (1 g) was added to a reaction vial, after which the corresponding molar amount of butylene oxide was added to create a molar feed ratio of 1:1, 1:2, and 2:1 of CL:BO. To this monomer mixture, 6 mL of dry dichloromethane was added, after which the vial was sealed and kept in an inert nitrogen atmosphere. The catalyst was added from a stock solution to target a monomer-to-aluminum ratio of 185, 208, and 164 for the EL:BO molar feed ratios of 1:1, 1:2, and 2:1. Reaction conditions, product work-up, and analysis were carried out equivalently to P(LA-co-ECH).  $^1\text{H}$  NMR (400 MHz,  $\text{CDCl}_3$ ):  $\delta$  4.2 ( $-\text{C}(=\text{O})\text{CH}_2\text{CH}_2\text{CH}_2\text{CH}_2\text{CH}_2\text{O}-$ ),  $\delta$  2.3 ( $-\text{C}(=\text{O})\text{CH}_2\text{CH}_2\text{CH}_2\text{CH}_2\text{CH}_2\text{O}-$ ),  $\delta$  1.7–1.5 ( $-\text{C}(=\text{O})\text{CH}_2\text{CH}_2\text{CH}_2\text{CH}_2\text{CH}_2\text{O}-$ ),  $\delta$  1.4–1.3 ( $-\text{C}(=\text{O})\text{CH}_2\text{CH}_2\text{CH}_2\text{CH}_2\text{CH}_2\text{O}-$ ),  $\delta$  3.7–3.3 ( $-\text{OCH}_2\text{CH}(\text{CH}_2\text{CH}_3)\text{O}-$ ),  $\delta$  1.5

(-OCH<sub>2</sub>CH<sub>1</sub>(CH<sub>2</sub>CH<sub>3</sub>)O-),  $\delta$  0.9 (-OCH<sub>2</sub>CH(CH<sub>2</sub>CH<sub>3</sub>)O-). <sup>13</sup>C NMR (100 MHz, CDCl<sub>3</sub>):  $\delta$  173.6, 81.0, 72.5, 64.3, 34.3, 28.5, 25.6, 25.2, 24.8, 9.9.

### ***Synthesis of Poly[( $\epsilon$ -caprolactone)-co-(propylene oxide)] (P(CL-co-PO))***

$\epsilon$ -Caprolactone (1 g) was added to a reaction vial, after which the corresponding molar amount of propylene oxide was added to create a molar feed ratio of 1:1, 1:2, and 2:1 of CL:PO. To this monomer mixture, 6 mL of dry dichloromethane was added, after which the vial was sealed and kept in an inert nitrogen atmosphere. The catalyst was added from a stock solution to target a monomer-to-aluminum ratio of 214, 232, and 200 for the EL:PO molar feed ratios of 1:1, 1:2, and 2:1. Reaction conditions, product work-up, and analysis were carried out equivalently to P(LA-co-ECH). <sup>1</sup>H NMR (400 MHz, CDCl<sub>3</sub>):  $\delta$  4.1 (-C(=O)CH<sub>2</sub>CH<sub>2</sub>CH<sub>2</sub>CH<sub>2</sub>CH<sub>2</sub>O-),  $\delta$  2.3 (-C(=O)CH<sub>2</sub>CH<sub>2</sub>CH<sub>2</sub>CH<sub>2</sub>CH<sub>2</sub>O-),  $\delta$  1.7 (-C(=O)CH<sub>2</sub>CH<sub>2</sub>CH<sub>2</sub>CH<sub>2</sub>CH<sub>2</sub>O-),  $\delta$  1.4 (-C(=O)CH<sub>2</sub>CH<sub>2</sub>CH<sub>2</sub>CH<sub>2</sub>CH<sub>2</sub>O-),  $\delta$  3.6–3.3 (-OCH<sub>2</sub>CH(CH<sub>3</sub>)O-),  $\delta$  1.6 (-OCH<sub>2</sub>CH<sub>1</sub>(CH<sub>2</sub>CH<sub>3</sub>)O-),  $\delta$  1.1 (-OCH<sub>2</sub>CH(CH<sub>3</sub>)O-). <sup>13</sup>C NMR (100 MHz, CDCl<sub>3</sub>):  $\delta$  173.7, 75.6, 73.5, 64.3, 34.3, 28.5, 25.6, 24.7, 17.6.

### ***Kinetic Experiments***

DL-Lactide (0.1 g) was added to an NMR sample tube after which 0.6 mL of deuterated dichloromethane was added. The corresponding molar amount of propylene oxide (0.04 g) was added to create a molar feed ratio of nearly 1:1 LA:PO. To this monomer mixture, 0.03 mL of the Vandenberg catalyst solution was added. The reaction was then quickly placed in a Varian Inova 500 MHz NMR spectrometer. Data were collected for 65 h. The NMR spectrometer was held at room temperature and collected scans at periodic time intervals. The same procedure was used with  $\epsilon$ -caprolactone (0.1 g) and propylene oxide (0.05 g).

### ***Degradation Experiments***

P(LA-*co*-EO) was compression molded to yield several samples of  $1 \times 1 \times 0.4$  cm<sup>3</sup> of approximately 300 mg in weight. Each sample was introduced into either a flask filled with 100 mL of 0.5 M NaOH solution in 40:60 methanol:water by volume or pure water. The flasks were held at room temperature. Three specimens were withdrawn from each solution every few hours over 2 weeks, dried with a paper towel, weighed, and then returned into the solution. At the end of the 15 days, the solution was dried on a rotary evaporator and dried *in vacuo* to record the change in final mass of polymer.

### **ACKNOWLEDGMENT**

This work was supported by start-up funds provided by the McKetta Department of Chemical Engineering, the Cockrell School of Engineering, and the Science and Technology Acquisition and Retention Program at the University of Texas at Austin. M.C. is grateful for a Cockrell School fellowship. N.A.L. acknowledges support through the Welch Foundation (Grant F-1904). The authors also thank Prof. Nicholas A. Peppas for access to the Institute for Biomaterials, Drug Delivery, and Regenerative Medicine.

## Chapter 3: Simple bis( $\mu$ -alkoxo-dialkylaluminum) initiators for ring-opening polymerization of lactone and mixed monomer feeds<sup>2</sup>

### INTRODUCTION

Degradable polymeric materials address the emerging crisis of incomplete recycling and the associated environmental and biological accumulation of plastics.<sup>29,104–109</sup> Greater compositional diversity in new degradable polymers is required to achieve the right properties that either match or exceed the properties of petroleum-derived incumbents. Significant progress in this area has been made with a large diversity of new materials derived from heterocyclic monomers with wide variation in desirable physical properties.<sup>75,110–118</sup> It is also important to develop versatile Earth-abundant and inexpensive initiators and catalysts for reasons of cost and environmental impact. Synthetic platforms which provide the greatest range of monomer substrate could allow for the use of existing capital equipment to produce a variety of polymeric materials economically. Additionally, residual metals or other compounds resulting from synthesis must themselves be environmentally benign and consist of components already found widely in the environment.

Aluminum, as the most abundant metal in the Earth's crust, is a good option for catalyst design.<sup>119</sup> Aluminum is generally nontoxic, ubiquitous in our environment, and is commonly used in many consumer products.<sup>120,121</sup> These characteristics make aluminum the primary candidate for Earth-abundant and sustainable polymerization catalyst development. Aluminum based catalysts have been applied to many ring opening polymerizations such as the classical aluminum chelate catalyst for epoxide polymerization,<sup>82,122</sup> aluminum salen catalyst for lactone polymerization,<sup>123–</sup>

---

<sup>2</sup> This work was performed by the following authors: Malgorzata Chwatko, Carol Huang, Christina Rodriguez, Robert Ferrier, Jr., Nathaniel Lynd. Malgorzata Chwatko and Nathaniel Lynd designed the study. Malgorzata Chwatko and Carol Huang performed all polymerizations. Christina Rodriguez and Robert Ferrier Jr. synthesized the catalyst used in the study. All authors assisted in the data analysis and writing of this work.

<sup>128</sup> or aluminum porphyrin for lactones, epoxides, acrylates and methacrylates.<sup>129–135</sup> This overall versatility in monomer substrates suggests that a simple aluminum-based catalyst may exhibit sufficient versatility in monomer-type to enable compositional control of structure-property relationships from mixed monomer feeds.<sup>136</sup>

Copolymerization enables compositional control of structure-property relationships. Ring-opening polymerization is amenable to the heterocopolymerization of monomers that belong to distinct classes, *e.g.*, lactones and epoxides. The investigation of Earth-abundant catalysts and initiators with balanced reactivity for a variety of heterocycle monomers will meet the challenge of tuning polymer properties within the scope of available monomers.

Aluminum-based chemistry as it applies to polymer synthesis originated with Ziegler and classical olefin polymerization. Vandenberg was a contemporary and introduced the idea of aluminum-coordination catalysis for epoxides. Both the Ziegler-Natta and Vandenberg catalysts use hydrolyzed organoaluminum complexes of unknown architecture. Barron and Atwood carried out groundbreaking structural characterization of similar hydrolyzed organoaluminum bis( $\mu$ -alkoxo-dialkylaluminum) (BOD).<sup>87,137–139</sup> Similar structures have been explored by Lewiński *et al.* for lactone polymerizations.<sup>140</sup> These studies have inspired us to study the application of these structures in heterocyclic copolymerization.

We synthesized five homologous bis( $\mu$ -alkoxo-dialkylaluminum) (BOD) structures and explored their reactivity for a diverse array of heterocyclic monomers. The BOD species were found to initiate and control the degree of polymerization with low dispersity for diverse monomer feeds such as lactones, lactone/carbonate, and lactone/anhydride comonomers systems.

## EXPERIMENTAL SECTION

### Materials

Chemicals were obtained from Sigma-Aldrich, Fisher Scientific and TCI-America Inc. and were used without further purification unless otherwise specified. Toluene was drawn from a dry solvent system (J. C. Meyer) and used immediately afterwards. Deuterated chloroform ( $\text{CDCl}_3$ ) was purchased from Cambridge Isotope Laboratories, Inc. DL-Lactide was recrystallized from ethyl acetate. The monomer was kept in an inert nitrogen environment until use.

### Measurements and characterization

$^1\text{H}$  and  $^{13}\text{C}$  NMR spectroscopy was carried out on an Agilent MR 400 MHz spectrometer, Varian DirectDrive 400 MHz, and Varian Mercury 400 MHz. Spectra were collected in deuterated chloroform. Size exclusion chromatography (SEC) was carried out on one of two systems: (1) An Agilent system with a 1260 Infinity isocratic pump, degasser, and thermostated column chamber held at 30 °C containing Agilent PLgel 10  $\mu\text{m}$  MIXED-B and 5  $\mu\text{m}$  MIXED-C columns with a combined operating range of 200–10 000 000  $\text{g mol}^{-1}$  relative to polystyrene standards, or (2) an Agilent system with a 1260 Infinity II isocratic pump, degasser, and thermostated column chamber held at 30 °C containing Agilent PLgel 10  $\mu\text{m}$  MIXED-B with a combined operating range of 500–10 000 000  $\text{g mol}^{-1}$  relative to polystyrene standards. Chloroform with 50 ppm amylene was used as the mobile phase on both systems. System (1) was equipped with an Agilent 1260 Infinity refractometer, dual angle dynamic and static light scattering. System (2) was equipped with a suite of detectors supplied by Wyatt Technologies, which provided measurement of polymer concentration, molecular weight, and viscosity. Static light scattering was measured using a DAWN HELEOS II Peltier system with differential refractive index measured with an Optilab TrEX, and differential viscosity measured with a Viscostar II.

### ***Synthesis of Bis( $\mu$ -alkoxo-dialkylaluminum)s (BODs)***

A representative synthesis of a BOD1 begins with adding a stir bar to a reaction vial followed by trimethylaluminum (12.7 mmol, 12.7 mL). The solution was cooled to  $-78\text{ }^{\circ}\text{C}$  and 2-methoxyethanol was added dropwise into the reaction vial. The solution was allowed to warm to RT and stirred overnight. The solution was cooled to  $-40\text{ }^{\circ}\text{C}$  to induce crystallization of the desired product. The resultant crystals were washed three times with anhydrous hexanes and dried *in vacuo*.

### ***General procedure for synthesis of polymers***

All polymerizations were performed neat in a septum-capped reaction vial unless otherwise noted. The vials were charged with a stir bar, monomer, and BOD initiator in an inert nitrogen environment. The solutions were then heated to the final reaction temperature ( $30\text{--}80\text{ }^{\circ}\text{C}$ , dependent on monomer) and polymerizations were carried out for 2 h–288 h (up to 12 days). Reactions were quenched with methanol and dissolved before precipitation. The supernatant solution was discarded, and the polymer was dried *in vacuo*.

### ***[DL-lactide]<sub>0</sub>/[Al]<sub>0</sub> sweep***

DL-Lactide (2 g) was added to a dry reaction vial under nitrogen with a Teflon-coated stir-bar. 6.0 mL of toluene was added to the reaction mixture after which the vial was sealed to maintain an inert nitrogen atmosphere. The catalyst was either added from a stock solution or from dry crystals to target monomer-to-aluminum ratios of 70, 94, 170, 210, 50, 550, 700, 1030, 1300, and 1390. The reaction was heated at  $90\text{ }^{\circ}\text{C}$  and magnetically stirred for 48 hours. Conversion of DL-lactide was above 96%. Molecular weight was determined by SEC using the differential refractive

index, and multi-angle light scattering detectors with a  $(dn/dc) = 0.024 \text{ mL/g}$  for PLA in chloroform mobile phase.

***[ $\epsilon$ -caprolactone]<sub>0</sub>/[Al]<sub>0</sub> sweep***

$\epsilon$ -Caprolactone (2 g) was added to a dry reaction vial under nitrogen with a Teflon-coated stir-bar. The catalyst was either added from a stock solution or from dry crystals to target monomer-to-aluminum ratios of 70, 94, 170, 210, 50, 550, 700, 1030, 1300, and 1390. The reaction was heated at 90 °C and magnetically stirred for two hours. Conversion of monomer was above 96%. Molecular weight was determined by SEC using the differential refractive index, and multi-angle light scattering detectors with a  $(dn/dc) = 0.062 \text{ mL/g}$  for PCL in chloroform mobile phase.

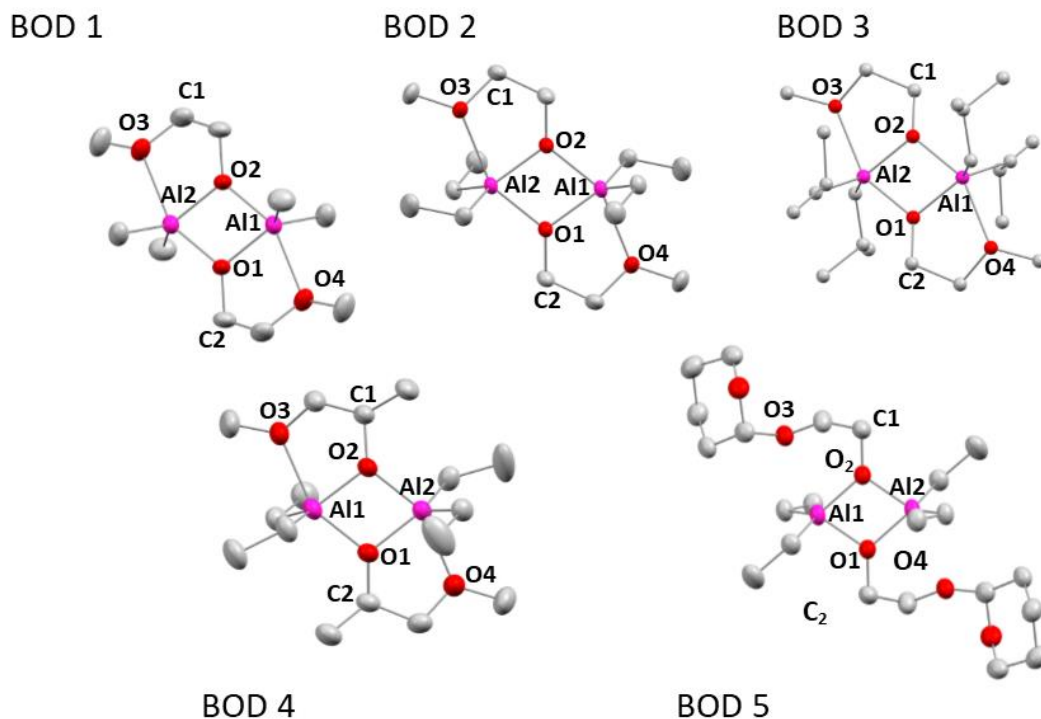


Figure 3-1 Structures obtained by X-ray crystallography contain variation in alkyl groups on aluminum, and in the initiator moiety. Thermal ellipsoids are drawn at 50% probability.

## RESULTS AND DISCUSSION

### Initiator characterization

We synthesized BOD initiators by adding an alcohol such as 2-(Tetrahydro-2H-pyran-2-yloxy)ethanol or 2-methoxyethanol to a rapidly stirring solution of 1.0 M trimethyl-, triethyl-, or triisobutylaluminum at  $-78\text{ }^{\circ}\text{C}$  in hexane. The reaction was allowed to warm to room temperature overnight, and the product was isolated directly from the reaction medium by crystallization at  $-40\text{ }^{\circ}\text{C}$ . Figure 3-1 shows structures of the resultant BOD initiators. Relevant bond lengths and angles were extracted from the crystallographic data and are shown in Table 3-1. Complete crystallographic data for the BOD initiators can be found in the appendix.  $^1\text{H}$  NMR spectra of the initiators were consistent with crystallographic data and can also be found in the appendix.

Table 3-1 Selected bond lengths and angles for BOD initiators.

	BOD-1	BOD-2	BOD-3	BOD-4	BOD-5
<b>Bond Length (<math>\text{\AA}</math>)</b>					
Al <sub>1</sub> -O <sub>1</sub>	1.904	1.910	1.917	1.910	1.880
O <sub>1</sub> -Al <sub>2</sub>	1.836	1.843	1.847	1.843	1.828
Al <sub>2</sub> -O <sub>2</sub>	2.231	2.251	2.221	2.251	2.702
O <sub>1</sub> -C <sub>1</sub>	1.418	1.416	1.420	1.416	1.422
<b>Bond Angle (<math>^{\circ}</math>)</b>					
Al <sub>1</sub> -O <sub>1</sub> -Al <sub>2</sub>	103.83	104.40	103.80	103.11	101.89
O <sub>1</sub> -Al <sub>1</sub> -O <sub>1</sub> '	76.17	75.60	76.20	76.47	78.11
O <sub>1</sub> -Al <sub>2</sub> -O <sub>1</sub> '	76.17	75.60	76.20	<b>76.93</b>	78.11
C <sub>1</sub> -O <sub>1</sub> -Al <sub>1</sub>	131.56	130.22	130.53	129.37	127.25
C <sub>1</sub> -O <sub>1</sub> -Al <sub>2</sub>	124.10	124.33	121.67	125.09	130.83
O <sub>1</sub> -Al <sub>2</sub> -O <sub>2</sub>	76.24	75.80	76.06	75.57	69.99

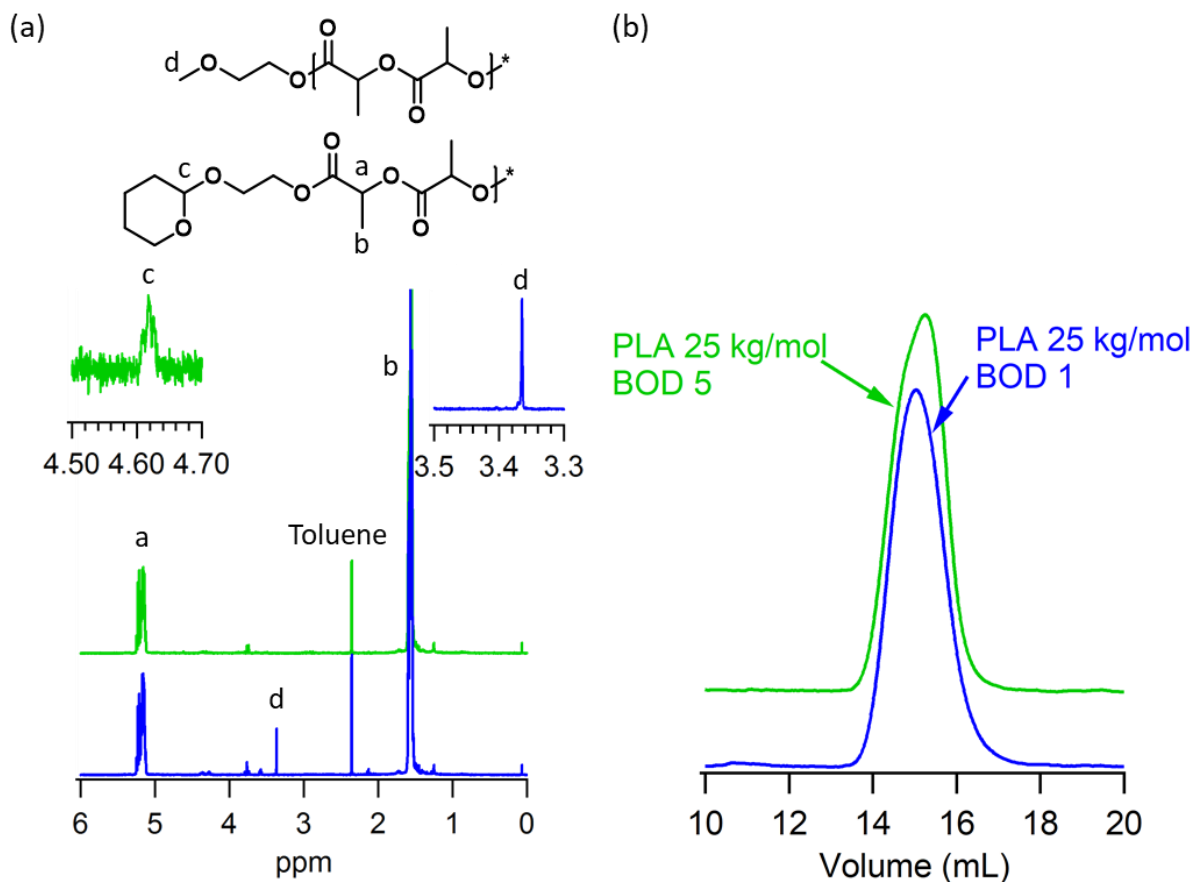


Figure 3-2.  $^1\text{H}$  NMR spectra and SEC traces of two poly(lactide) polymers created with BOD 5 in green and BOD 1 in blue showing the end groups produced from these initiators.

The BODs proved generally effective for lactone polymerizations. Figure 3-2 shows the resultant  $^1\text{H}$  NMR spectroscopy and SEC characterization of poly(DL-lactide)s (PLA) resultant from initiation by two different BODs: BOD 1 and BOD 5. After purification,  $^1\text{H}$  NMR spectroscopy revealed the end groups of the PLAs, which were derived from each initiator. Similarly, molecular weights obtained from end group analysis matched those obtained from GPC. To investigate the control of molecular weight, the monomer-to-initiator ratio was varied, and the results are shown in Figure 3-3. Polymerizations proceeded for two days for DL-lactide and two hours for  $\epsilon$ -caprolactone. In the case of lactide and  $\epsilon$ -caprolactone polymerization, we note that as the ratio of monomer to aluminum increased, the degree of polymerization linearly increased.

Based on the slope, it appeared that each BOD initiated two chains. We propose that this is because the BODs are symmetric and can yield a coordination insertion mechanism at each aluminum alkoxide. Ultimately, the BOD initiators were capable of high molecular weights, *e.g.*, PLA was synthesized to 130 kg/mol.

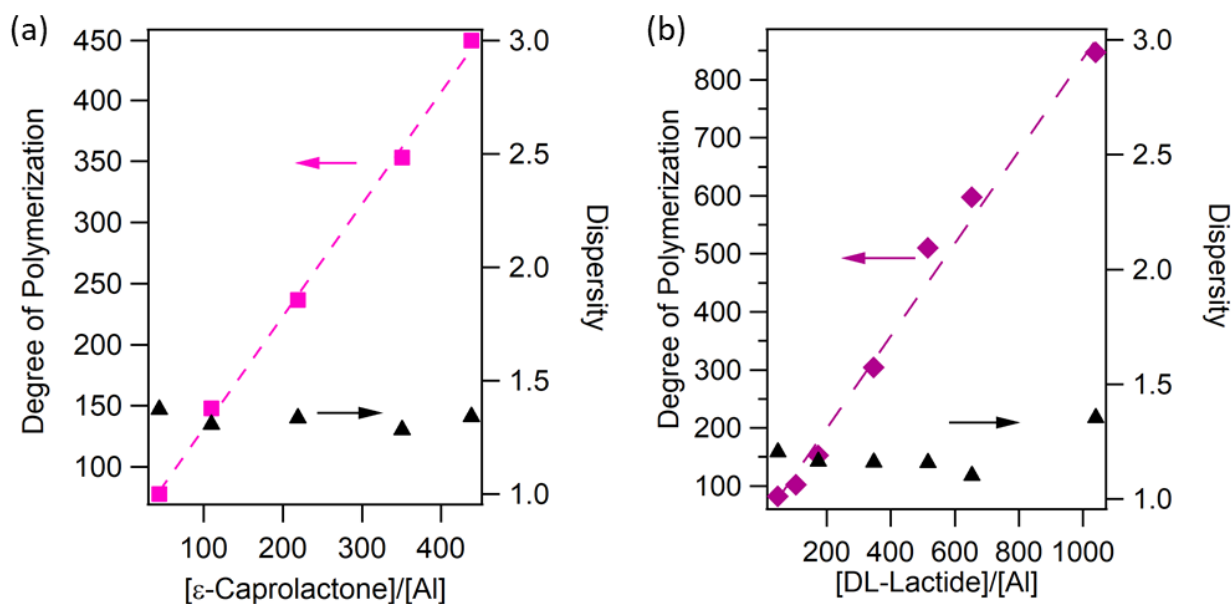


Figure 3-3 Control of molecular weight was demonstrated in homopolymerization of lactones a)  $\epsilon$ -caprolactone b) DL-lactide.

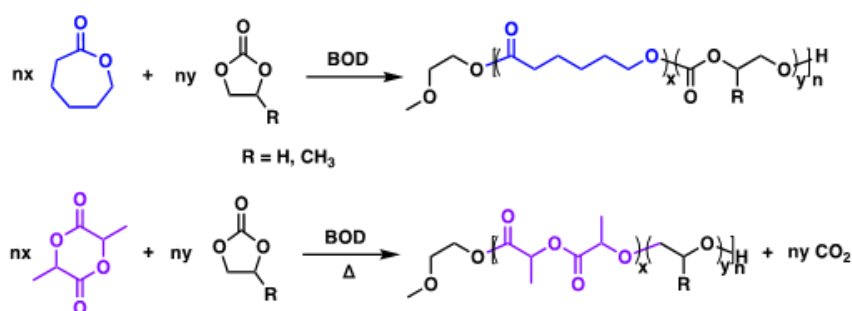
### Copolymerization

Copolymerization allows for a development of materials with targeted properties drawing upon a larger scope of constituent monomers. Typically, these are conducted with structurally homologous monomers which copolymerize via a consistent mechanism. For ring opening polymerization, while a consistent mechanism may underlie propagation, differences in active-site affinity and ring-strain may affect copolymer incorporation. In this work, we apply the BOD system to

lactone/carbonate and anhydride/epoxide copolymerization in order to explore the balance of the kinetic and thermodynamic considerations for copolymerization with this system.

***Copolymerization of carbonates and lactones.***

Polycarbonates are a desirable class of polymeric materials due to their good mechanical properties and degradability.<sup>141</sup> Carbonate polymerization has a low ceiling temperature, around room temperature, such that polymerization at a higher temperature occurs with the carbonate losing a carbon dioxide moiety and results in a polyether.<sup>112</sup> To keep the easily degradable carbonate functionality, copolymerization between carbonates and lactones has only recently been explored.<sup>112,141–143</sup>



Scheme 3-1 Copolymerization of lactones and carbonates.

Copolymerizations of carbonates, ethylene carbonate and propylene carbonate, with lactones, DL-lactide and  $\epsilon$ -caprolactone, were analyzed via NMR and GPC. Figure 3-4B shows a typical NMR of these copolymers. Peaks around 4.1-4.2ppm has been identified as the dyad carbonate-lactone peak. The total conversion of the reactions did not exceed over 60% as seen in Table 3-1. This nonqualitative conversion is due to a minimal incorporation of carbonate which could be a result of the catalyst's incompatibility with epoxides which are produced when the carbonate moiety loses a carbon dioxide. The poor incorporation of carbonate was also seen in other studies and was attributed to a large difference in reactivity.<sup>141,144</sup> The fraction of lactone in the copolymers usually maintained around 90% of lactone, however even a minimal amount of carbonate addition still influenced the glass transition temperature significantly.

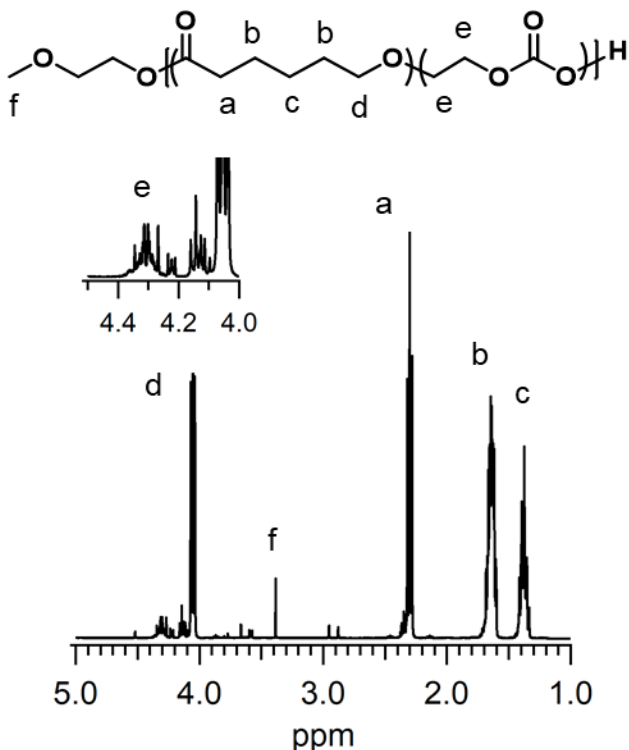


Figure 3-4 Copolymerization of carbonates and lactones gives a lower than theoretical incorporation of carbonates as seen by the presence of peak e in the case of formation of poly[(D,L-lactide)-(ethylene carbonate)].

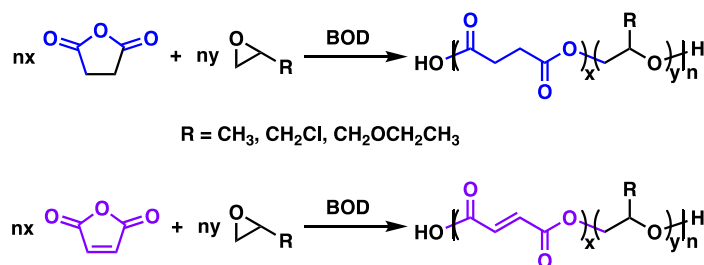
Table 3-2 Properties of lactone carbonate copolymers

Copolymer	Solvent	$\frac{[M]_0}{[AI]}$	Time (h)	Conversion Lactone: Carbonate	$F_{\text{lactone}}^a$	$M_n$ (g/mol) <sup>b</sup>	$M_n$ (g/mol) <sup>c</sup>	$\bar{D}^d$	$T_g^e$ (°C)
P(CL <sub>0.5</sub> EC <sub>0.5</sub> )	Methylene Chloride	84	16	0.53: 0.06	0.82	8,500	8,300	1.25	-71
P(CL <sub>0.5</sub> PC <sub>0.5</sub> )	Neat	46	18h	1: 0.08	0.94	9,300	6,100	1.59	-
P(CL <sub>0.5</sub> PC <sub>0.5</sub> )	Neat	97	18h	1: 0.07	0.92	11,700	11,000	1.25	-
P(LA <sub>0.5</sub> EC <sub>0.5</sub> ) <sup>f</sup>	Neat	48	120h	0.98: 0.08	0.95	8,900	5,600	1.52	29
P(LA <sub>0.5</sub> PC <sub>0.5</sub> ) <sup>g</sup>	Toluene	166	96h	0.48: 0.07	0.91	8,400	7,800	1.27	9

<sup>a</sup> Final cumulative mole fraction composition of copolymer measured by <sup>1</sup>H NMR spectroscopy <sup>b</sup> Determined by end group analysis by <sup>1</sup>H NMR spectroscopy. <sup>c</sup> Determined by size exclusion chromatography with multi-angle light scattering. <sup>d</sup> Determined by size exclusion chromatography. <sup>e</sup> Determined by differential scanning calorimetry and recorded in °C. All reactions were done at 25 °C except <sup>f</sup> done at 30°C and <sup>g</sup> done at 90°C

### Copolymerization of anhydrides and epoxides.

Aliphatic polyesters offer good degradability and biocompatibility.<sup>145,146</sup> There are two common routes to polyesters synthesis, step-growth or chain-growth polymerization. Step-growth method requires the removal of a small-molecule byproducts that necessitates high temperatures and typically produces low molecular weight materials. In response, catalytic chain-growth polymerization approaches have been developed based on chromium, zinc, aluminum and cobalt with good polymerization rates.<sup>65,66,75,116–118,147,148</sup> However, these catalysts typically involve complex, multistep synthesis in contrast to the simplicity of the BOD synthesis.



Scheme 3-2 Copolymerization of anhydrides and epoxides.

The effectiveness of BODs to copolymerize maleic anhydride or succinic anhydride with epichlorohydrin, propylene oxide or ethyl glycidyl ether was investigated via NMR spectroscopy and GPC. Figure 3-5 describes the results of the copolymerization between succinic anhydride and epichlorohydrin. The end group of the BODs was visible in the copolymer of succinic anhydride and epichlorohydrin but was otherwise obscured with the epoxide portion of the other copolymers. The anhydride copolymerizations were performed at different temperatures ranging from room temperature to 90 °C. The molecular weights achieved match those typically reported by others for these copolymers, as seen in Table 3-3. The dispersities ( $\bar{D}$ ) were higher than the homopolymerizations with lactides, discussed previously, which were around 1.7 and increase with increasing temperature as would be expected. As the degree of polymerization of maleic anhydride increases, the polymer solubility was significantly reduced which might have impacted the polymerization. Polymers formed were still of good molecular weight and relatively low dispersity.

Table 3-3 Properties of anhydride epoxide copolymers

Copolymer	Solvent	$\frac{[M]}{[AI]}$	Temp	Time	Total Conversion	$M_n$ (g/mol) <sup>a</sup>	$M_n$ (g/mol) <sup>b</sup>	$\bar{D}$ <sup>c</sup>	$T_g$ <sup>d</sup>
P(MA <sub>0.5</sub> ECH <sub>0.5</sub> )	Neat	131	70	23h	0.76	12,700	16,300	1.9	-11
P(MA <sub>0.5</sub> PO <sub>0.5</sub> )	Neat	92	45	72h	0.63	-	12,700	1.2	-18
P(MA <sub>0.5</sub> EGE <sub>0.5</sub> )	DMF	125	70	72h	0.62	-	32,200	1.70	-37
P(SA <sub>0.5</sub> ECH <sub>0.5</sub> )	Neat	130	90	23h	0.74	-	11,600	1.74	-12
P(SA <sub>0.5</sub> EGE <sub>0.5</sub> )	Neat	122	90	24h	1	-	13,500	1.83	-31

<sup>a</sup> Determined by end group analysis by <sup>1</sup>H NMR spectroscopy. <sup>b</sup> Determined by size exclusion chromatography with multi-angle light scattering. <sup>c</sup> Determined by size exclusion chromatography. <sup>d</sup> Determined by differential scanning calorimetry and recorded in °C.

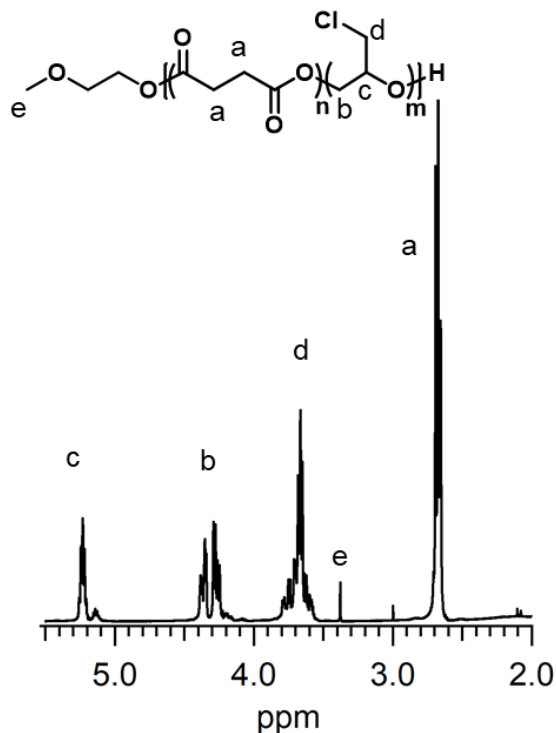


Figure 3-5 Copolymerization of anhydrides and epoxides provides new polymeric structures.

***Comparison to mono- $\mu$ -oxo- dialuminium initiator (MOB).***

In order to gain a better understanding about the BODs polymerizations, we have compared the BODs to a similar aluminum-based catalyst, mono( $\mu$ -alkoxo)bis(alkylaluminum) (MOB).<sup>122</sup> The MOB catalyst variants have been shown to have good activity for epoxide polymerization.<sup>122,149</sup> In previous work<sup>150</sup>, we have noted that the BOD initiators exhibit a significantly lower epoxide polymerization rate compared to the MOB system.<sup>150,151</sup> In this study we compare MOB 1 [(Me)<sub>2</sub>NCH<sub>2</sub>CH<sub>2</sub>( $\mu$ -O)Al(iBu)<sub>2</sub>·Al(iBu)<sub>3</sub>] and BOD 3. While the BOD and MOB initiator are compositionally similar, differences can be noted in the polymerization of lactones and copolymerization of carbonates and lactones. The MOB produced high molecular weight polylactide similar to the BODs and similarly produce two polymer chains per initiator (Figure B3-15). However, the copolymerization of carbonates and lactones yielded only

homopolymers of instead of copolymers produced by the BODs (Figure B-13). Lastly, copolymerization of anhydride and epoxides yielded alternating copolymers comparable to those resulting from BOD-initiated copolymerization (Figure B-11 and B-14).

To compare kinetics, time dependent NMR spectroscopy measurements of *in-situ* polymerizations were performed. The rates of homopolymerization of lactide and a copolymerization of ethyl glycidyl ether and maleic anhydride is reported in Figure 3-6. The pseudo-first-order apparent rate constant for lactide homopolymerization were about 0.46 and 0.35 h<sup>-1</sup> for both the BODs and MOB 1, which could be attributed to the formation of a BOD intermediate.<sup>151</sup> When considering the copolymerization, it was found that the copolymerization rate initiated with the MOB 1 initiator was approximately three times faster than the BOD-initiated copolymerization.

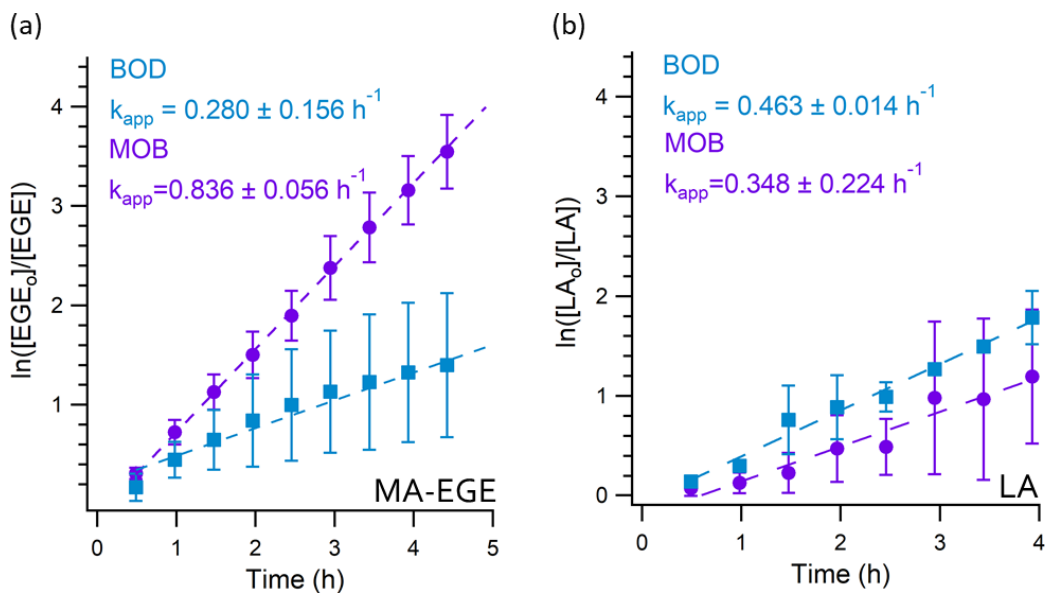


Figure 3-6 Comparison of polymerization rates of MOB 1 vs BODs with heterocyclic monomers (a) copolymerization of EGE and MA at 60°C at [M]/[Al]=25 (b) polymerization of PLA at 90°C at [M]/[Al]=50.

## **CONCLUSION**

Development of new sustainable synthetic strategies to create degradable polymers is an important goal. In this chapter, we investigated a set of initiators, BODs, which are capable of polymerizing a variety of different heterocyclic monomers such as lactones and anhydrides. Due to their simplicity and versatility in monomer substrate, we believe they may serve as a starting point for selecting catalysts for heterocopolymerizations among differing classes of monomers.

## **ACKNOWLEDGMENTS**

This work was supported by start-up funds provided by the McKetta Department of Chemical Engineering and the Cockrell School of Engineering. M.C. is grateful for a Cockrell School fellowship and Eastman Chemical Summer Fellowship. N.A.L. acknowledges support through the Welch Foundation (Grant F-1904).

## Chapter 4: Synthesis of barrier materials from biologically derived monomers<sup>3</sup>

### INTRODUCTION

The current global consumption of plastics is surpassing 200 million tonnes overall.<sup>152</sup> Oil derived polymers such as polyethylene (PE) and polypropylene (PP) are widely used in widely varying applications. One specific application is in the packaging industry because of their tunable performance and low cost. However, these polymers possess very slow degradability in marine and terrestrial environments. Moreover, due to the contamination with organic matter, recycling of thin films of PE and PP is impractical and not economically viable.<sup>152-154</sup>

Food packaging can extend the shelf life of fresh fruit and vegetables. When harvested, produce continues to consume oxygen and release carbon dioxide. Fruits also produce ethylene, which helps in the ripening process.<sup>155</sup> Cooling and lowering the O<sub>2</sub> concentration in the package reduces the respiration rate and therefore extends shelf life. Adding temperature responsiveness to the plastic barrier materials can additionally better match the changes in produce respiration rate. Semicrystalline materials can achieve this thermal responsiveness but it is important to achieve these properties sustainably.

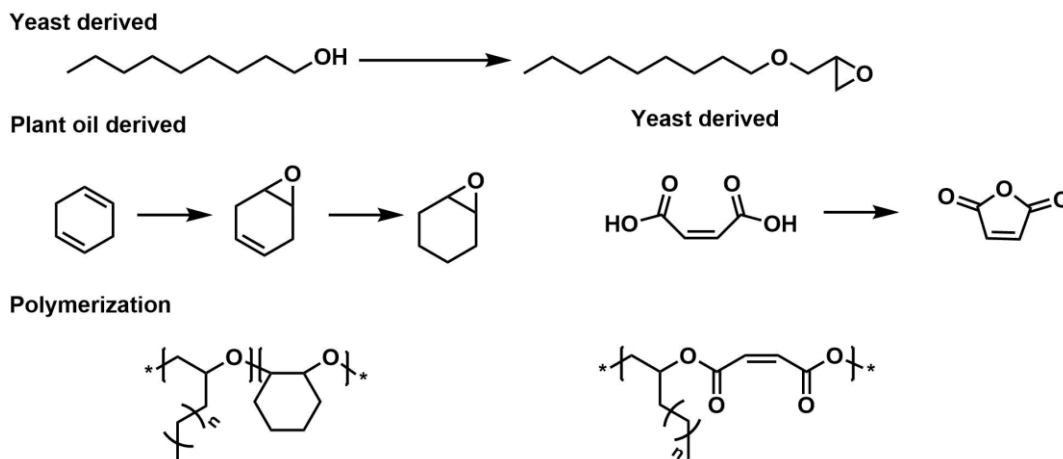
Sustainable replacements for oil-based polymers are essential for a sustainable future. Many different renewable resources can be used to create monomers. For lactide, corn and beets can be used as feedstock.<sup>25,156</sup> In addition to using plants, microorganisms can also be a pathway for sustainable monomer synthesis. Microorganisms are unique in that they can be used to create both polymers and monomers, in particular fatty alcohols.<sup>157-162</sup> Fatty acids and fatty alcohols are a particularly attractive platform due to their versatility in synthesis, and biocompatibility. By

---

<sup>3</sup> This work was performed by the following authors: Malgorzata Chwatko, Christina Rodriguez, Melanie Merrick, Nathaniel Lynd and Benny Freeman. Malgorzata Chwatko, Melanie Merrick and Benny Freeman designed the study. Malgorzata Chwatko performed all polymerizations. Christina Rodriguez and Melanie Merrick performed gas transport measurements. All authors assisted in the analysis of the data. The authors acknowledge Lauren Cordova and Hal Alper for discussions on fatty alcohol synthesis.

modifying the fatty alcohols into epoxides, the resulting polyethers would contain flexibility and side chain crystallinity which could be beneficial for barrier materials.

In this work, we synthesized semicrystalline polyethers using the mono( $\mu$ -alkoxo)bis(alkylaluminum) (MOB) chemistry developed in the Lynd lab. Copolymers of long chain epoxides were synthesized and used to create thin films. The thin films were tested to identify their thermal and gas transport properties.



Scheme 4-1 Scheme of sustainable synthesis of crosslinked liquid crystalline films

## Materials

Chemicals were obtained from Sigma-Aldrich, Fisher Scientific and TCI-America Inc. They were used without further purification unless otherwise specified. Deuterated chloroform ( $\text{CDCl}_3$ ) was purchased from Cambridge Isotope Laboratories, Inc. The monomers were kept in an inert nitrogen environment until use.

## Measurements and characterization

### *Polymer Characterization*

$^1\text{H}$  NMR spectroscopy was carried out on an Agilent MR 400 MHz spectrometer, Varian DirectDrive 400 MHz, and Varian Mercury 400 MHz. Spectra were collected in deuterated

chloroform. Size exclusion chromatography (SEC) was carried out on one of two systems: (1) an Agilent system with a 1260 Infinity isocratic pump, degasser, and thermostatted column chamber held at 30 °C containing Agilent 5  $\mu\text{m}$  MIXED-C columns with a combined operating range of 200–2 000 000  $\text{g mol}^{-1}$  relative to polystyrene standards, or (2) an Agilent system with a 1260 Infinity II isocratic pump, degasser, and thermostatted column chamber held at 30 °C containing Agilent PLgel 10  $\mu\text{m}$  MIXED-B with a combined operating range of 500–10 000 000  $\text{g mol}^{-1}$  relative to polystyrene standards. Chloroform with 50 ppm amylene was used as the mobile phase on system (2) while tetrahydrofuran was used as a mobile phase on system (1). System (1) was equipped with an Agilent 1260 Infinity refractometer, bi dual angle dynamic and static light scattering. System (2) was equipped with a suite of detectors from Wyatt Technologies, which provided measurement of polymer concentration, molecular weight, and viscosity. Static light scattering was measured using a DAWN HELEOS II Peltier system with differential refractive index measured with an Optilab TrEX, and differential viscosity measured using a Viscostar II.

### ***General Procedure for Synthesis of linear Polyethers***

Prior to polymer synthesis, MOB1 [(Me)<sub>2</sub>NCH<sub>2</sub>CH<sub>2</sub>( $\mu$ -O)Al(iBu)<sub>2</sub>·Al(iBu)<sub>3</sub>] and MOB2 [(Bn)<sub>2</sub>NCH<sub>2</sub>CH<sub>2</sub>( $\mu$ -O)Al(Et)<sub>2</sub>·Al(Et)<sub>3</sub>] catalyst system were synthesized following an established procedure.<sup>149,151</sup> All polymerizations were performed neat in septum-capped reaction vials.<sup>149,151</sup> The vials were charged with a stir bar, monomer, and MOB initiator in an inert nitrogen environment. The solutions were then heated to the final reaction temperature of 60 °C. Polymerizations were carried out for two days. Reactions were quenched with methanol and dissolved in dichloromethane (DCM) before an extraction to remove the catalyst. The extraction was carried out with three dilute acid washes, followed by one DI water wash, followed by one dilute basic wash and two more DI water washes. The polymer was dried in vacuo.

### ***General Procedure for Synthesis of Crosslinked Block Copolymer Membranes***

Pre-polymer solutions were all initially prepared in 20 mL vials with the MOB initiator and long alkyl chain terminal epoxide monomer. The reaction mixture was heated to 60 °C and

allowed to polymerize overnight until completion under a nitrogen atmosphere inside a glovebox. To the resultant viscous solution containing active chain-ends, cyclohexene oxide and butane diglycidyl ether was added. Once the polymerization mixture was once again viscous due to conversion of the additional monomers, it was degassed via vacuum pump and poured between two quartz plates, which were separated by aluminum spacers to control film thickness. One of the quartz plates was covered with a Teflon film in order to facilitate sample removal after polymerization. The plates were placed inside the antechamber of a glovebox, which was equipped with a heating stage, and left to react overnight under a nitrogen atmosphere.

#### ***General Procedure for Synthesis of Crosslinked Alternating Copolymer Membranes***

Pre-polymer solutions were all initially prepared in a 20 mL vial with MOB initiator, alkyl chain epoxide and maleic anhydride. The reaction mixture was heated to 60 °C (above the maleic anhydride melting point) and reacted until viscosity increased visibly. The viscous solution was degassed by a vacuum pump and was poured between two quartz plates. The quartz plates were separated by aluminum spacers to control film thickness. One of the quartz plates was also covered with a Teflon film in order to facilitate sample removal after polymerization. The plates were placed inside the antechamber of a glovebox, which was equipped with a heating stage, and left to react overnight under a nitrogen atmosphere.

#### ***Density Measurement***

A Micromeritics AccuPyc II 1340 Series Pycnometer was used for density measurements. The density measurements were made via helium gas displacement in a 1 cm<sup>3</sup> sample chamber. Samples were sealed in the sample chamber of known volume. Helium gas was admitted into the sealed chamber and then expanded into the reference chamber of a fixed internal volume. The

differential pressures observed in the sample chamber from filling and discharging subsequently yields a sample volume using the following equation

$$V_s = V_c - \frac{V_r}{\frac{P_1}{P_2} - 1}$$

where  $V_s$  is the sample volume,  $V_c$  is the volume of the empty sample chamber,  $V_r$  is the volume of the reference chamber,  $P_1$  is the pressure in the sample chamber, and  $P_2$  is the pressure in the reference chamber.

### ***Thermal Characterization***

Samples were prepared by depositing 1–10 mg of each polymer into hermetically sealed aluminum pans. Differential scanning calorimetry (DSC) experiments were performed on a TA Instruments Discovery DSC 250 instrument with the following temperature scan: heat to 120 °C at 10 °C/min, cool to –75 °C at 5 °C/min, heat to 110 °C at 5 °C/min, cool to –75 °C at 10 °C/min, heat to 110 °C at 5 °C/min. The glass transition temperature,  $T_g$ , and melting temperature,  $T_m$ , values of the polymers was obtained from the third heating scan.

### ***Pure Gas Permeation Measurements***

The pure gas permeabilities of H<sub>2</sub>, CH<sub>4</sub>, N<sub>2</sub>, O<sub>2</sub>, CO<sub>2</sub> and C<sub>2</sub>H<sub>4</sub> were obtained at 35°C using a custom-built system based on a constant volume/variable-pressure method. . Film thicknesses were measured using digital calipers (Mitutoyo, ±1 μm). The film samples were masked for permeation tested by adhering them to brass support discs using epoxy (Devcon epoxy gel). After the sample assemblies were installed in the permeation system, the membranes were dried *in vacuo* overnight to remove all sorbed gases. The upstream pressure was maintained at predetermined set values of 4, 6, 8, 11, and 16 or 3, 7, 10, 13, and 17 atmospheres and monitored using a Honeywell STJE transducer. The increase in the downstream pressure across the membrane was measured as a function of time for each upstream pressure setpoint using an MKS Baratron with a

0-10 Torr range. The gas permeabilities ( $P$ ) were determined from the steady-state rate of pressure increase in the downstream. The ideal selectivity was calculated as the permeability of the more permeable gas divided by that of the less permeable gas.

## RESULTS

### Synthesis of linear liquid crystalline polyethers (PLE)

Linear polyethers were synthesized using long chain epoxides by utilizing the MOB initiators. The long alkyl chain monomers have been previously known to have steric hindrance which can limit the achievable molecular weight.<sup>18,22</sup> The  $^1\text{H}$  NMR spectrum of one of the polyethers can be seen in Figure 4-1. The polymerization up to 15,000 g/mol took place in less than 24 hours at 60 °C. The elevated temperature was chosen in order to ensure that both the monomer and polymer remain

Polymers	[M]/[Al]	$M_n$ (g/mol) <sup>a</sup>	$D^a$	$T_g$ (°C) <sup>b</sup>	$T_m$ (°C) <sup>c</sup>	$\Delta H_m$ (J/g) <sup>c</sup>
Poly(dodecane ether) P(PDE)	70	15,000	1.6	-78.4	26.8	56.8
Poly(hexadecyl ether- <i>co</i> -dodecane ether) P(HDE- <i>co</i> -DE)	70	8,200	1.9	-	19.9	73.9

in an amorphous liquid state. The polymer properties are shown in

Table 4-1. Using the MOB catalytic system, both homopolymers and copolymers of the long alkyl chain monomers were possible. The long alkyl chain polyethers exhibit side chain crystallinity with a melting point at 20–25°C and are waxy due to this low melting point and low glass transition temperature. Melting points in this range are optimal to work as a barrier material for food packaging that will be refrigerated as the crystalline polymer will block gas permeation. One way to improve the mechanical properties of such materials is through crosslinking.

Table 4-1 Properties of the long alkyl chain polyethers (PLEs)

Polymers	[M]/[Al]	M <sub>n</sub> (g/mol) <sup>a</sup>	D <sup>a</sup>	T <sub>g</sub> (°C) <sup>b</sup>	T <sub>m</sub> (°C) <sup>c</sup>	ΔH <sub>m</sub> (J/g) <sup>c</sup>
Poly(dodecane ether) P(PDE)	70	15,000	1.6	-78.4	26.8	56.8
Poly(hexadecyl ether- <i>co</i> -dodecane ether) P(HDE- <i>co</i> -DE)	70	8,200	1.9	-	19.9	73.9

Polymerization was done for 20 h at 60°C and reached 100% conversion. <sup>a</sup> Determined by size exclusion chromatography with multi-angle light scattering. <sup>b</sup> Determined by differential scanning calorimetry; glass transition not observed <sup>c</sup> Determined by differential scanning calorimetry. T<sub>m</sub> is reported as the peak temperature

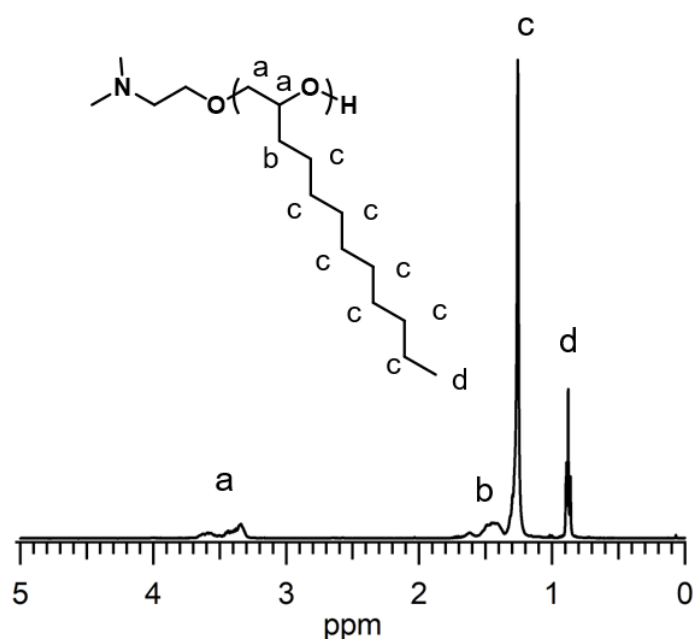


Figure 4-1 Representative <sup>1</sup>H NMR spectra (400 MHz, CDCl<sub>3</sub>) of poly(dodecane ether).

### Film synthesis

Copolymerization of a hard and soft segment can lead to an additive combination of favorable properties from the two materials. The proposed semi-crystalline polymers can act as a barrier material due to crystallinity and hydrophobicity. Scheme 4-1 shows two options to enhance mechanical properties involving different monomers. Block copolymerization with cyclohexene oxide can improve mechanical properties to the materials as poly(cyclohexene oxide) is

glassy.<sup>163,164</sup> Copolymerization with maleic anhydride could likewise increase the rigidity of the material via the polymerization proceeding in an alternating fashion.

Polyether materials are degradable through acidic cleavage of the ether linkage over long time scales.<sup>165,166</sup> In order to induce greater degradability, copolymerization can also be utilized. A more rapidly degradable ester linkage can be added by the addition of maleic anhydride to the polymerization.

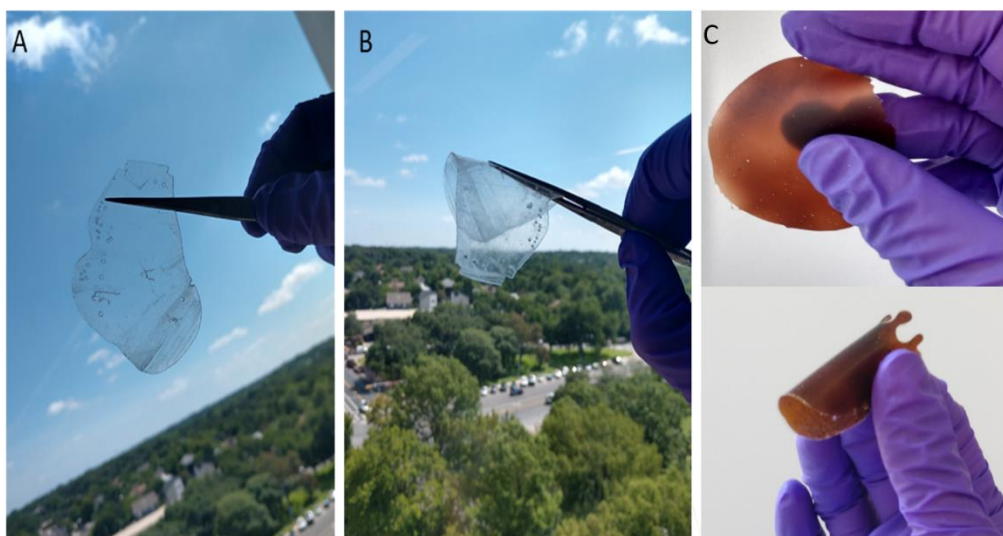


Figure 4-2 Picture of thin films A) P(LE-CHO) film to show transparency, B) folded P(LE-CHO) film shows flexibility C) P(LE-MA) to show color and flexibility of thin films.

To create a thin film using block copolymers, we modified a method developed from our previous work.<sup>167</sup> The first block was polymerized completely, after which the components for the second crosslinked block were added. Similarly, a single pot approach can be undertaken with the statistical copolymerization. Pictures of the films are shown in Figure 4-2. The defects along the edges of the samples are derived from casting the samples. The P(LE-CHO) films were optically clear, with good mechanical integrity while P(MA-LE) copolymer films were opaque and dark orange.<sup>116</sup>

Thermal properties of the material dictate its responsiveness. Table 4-2 shows both density and thermal characteristics. The glass transition of some films was not easily observed, potentially due to it being obscured by the side group melting peak. For this small series of materials, the melting enthalpy decreased with crosslinking and copolymerization. The melting enthalpy also decreased with monomer dilution such that the alternating copolymerization that resulted in a nearly amorphous material. In the P(MA-DE) copolymer however, there was an observable glass transition temperature below room temperature.

Table 4-2 Properties of the synthesized thin films

Sample	Monomers	[M]/[I]	[M <sub>1</sub> ]:[M <sub>2</sub> ]:[M <sub>3</sub> ]	Density (g/cm <sup>3</sup> ) <sup>a</sup>	T <sub>g</sub> (°C) <sup>b</sup>	T <sub>m</sub> (°C) <sup>c</sup>	ΔH <sub>m</sub> (J/g) <sup>c</sup>
1	DE-CHO	70	1:1	1.01	-	16.0	48.1
2	HDE-DE-CHO	70	1:1:2	0.97	-	18.3	60.3
3	MA-DE	70	1:1	1.10	-13.5	-	-

Polymerization was done for 48 h at 60 °C with 10 mol% butane diglycidyl ether crosslinker. <sup>a</sup> Determined by a pycnometer. <sup>b</sup> Determined by differential scanning calorimetry; glass transition not observed in all cases <sup>c</sup> Determined by differential scanning calorimetry. T<sub>m</sub> is reported as the peak temperature

### Transport Characterization

Understanding gas permeability behavior of the thin films is essential for their application in food packaging. Table 4-3 shows the resultant permeabilities of the films at 35 °C. The two films have very similar selectivity of gases while the permeability of P(MA-DDE) for some gases is double than that of P(DDE-CHO) films. Comparing to the standard polylactide barrier, both films have better selectivity for CO<sub>2</sub>/O<sub>2</sub>, however the permeabilities are approximately one to two orders of magnitude higher than that of the control.

Ethylene permeability is not commonly reported in the food barrier literature, even though it has been identified as crucial in the ripening process. High permeability of ethylene in barrier materials would allow the produced ethylene to exit the bag and not speed up the ripening process. The reported ethylene permeabilities are relatively high for both materials, being approximately half of the CO<sub>2</sub> permeabilities. Comparing the ethylene permeability results to those of low density polyethylene study both the oxygen and ethylene permeability is approximately an order of magnitude higher.<sup>168</sup> While the commercial standards outperform the membranes synthesized in this work, our platform allows for tunability of crystallinity in the samples via alkyl chain length with a broad melting transition between room temperature and refrigeration temperatures which will be studied in future work with preliminary data shown in Figure C5.

Table 4-3 Gas transport properties of thin films

Sample	Composition	Film Thickness (μm)	Permeability (Barrer) <sup>a</sup>					Ideal Selectivity (α <sub>x/y</sub> ) <sup>b</sup>	
			CH <sub>4</sub>	N <sub>2</sub>	O <sub>2</sub>	CO <sub>2</sub>	C <sub>2</sub> H <sub>4</sub>	CO <sub>2</sub> /N <sub>2</sub>	CO <sub>2</sub> /O <sub>2</sub>
1	P(DDE <sub>0.5-b-</sub> CHO <sub>0.5</sub> )	337± 16	10.2 ±	3.3 ±	9.6 ±	44.6 ±	25.3 ±	13.5 ±	4.7 ± 0.4
			0.7	0.2	0.6	3.0	1.7	1.2	
3	P(DDE <sub>0.5-co-</sub> MA <sub>0.5</sub> )	353± 25	15.6 ±	5.3 ±	15.5 ±	88.3 ±	47.1 ±	16.7 ±	5.7 ± 0.7
			1.4	0.5	1.4	8.1	4.3	2.2	
control	PLA	27± 2	-	0.054 ±	0.34 ±	1.27 ±	-	-	3.7 ± 0.2
				0.004	0.02	0.004			

<sup>a</sup> Measured using the constant-volume/variable pressure method at 3–4 atm and 35 °C. <sup>b</sup> Calculated from  $\alpha_{x/y} = P_x/P_y$ . Polylactide (PLA) data is shown as a sustainable and degradable polymer reference with 25% crystallinity. The data is taken from reference <sup>169</sup> at 35 °C.

## **CONCLUSION**

The production of sustainable and degradable food packaging films is a necessary step to achieve a future with less plastic waste. Utilizing fatty alcohol derived monomers as the base of the design could achieve these goals due to their hydrophobicity and side chain crystallinity. In this work it was found that the MOB chemistry can polymerize long alkyl chain terminal epoxides. To create thin films, two approaches were used, block copolymerization and copolymerization with a comonomer and a crosslinker. The films were free standing and had comparable or better barrier properties than a polylactide film.

## **ACKNOWLEDGMENT**

Research supported as part of the Center for Materials for Water and Energy Systems (M-WET), an Energy Frontier Research Center funded by the U.S. Department of Energy (DOE), Office of Science, Basic Energy Sciences (BES), under Award #DE-SC0019272 (material support) and Welch Foundation Grant F-1904 (material support). M.C. is grateful for a Cockrell School fellowship. We would like to thank Lauren Cordova and Hal Alper for initial discussion about the application of fatty alcohols and fatty acids.

## Chapter 5: Impact of polyether polarity on ionic conductivity<sup>4</sup>

### INTRODUCTION

Due to concerns over climate change, the world needs to reduce its reliance on greenhouse gas emitting energy sources such as coal, and natural gas. New energy sources such as wind and solar energy have been identified however, a new gap in technology has been also created. When it comes to both of those energy sources, we can't control peak energy production to match that of consumption. This means that we need to develop better energy storage devices such as lithium ion batteries.<sup>170,171</sup>

Current lithium ion batteries consist of an inert metal current collector in electrical contact with two electrodes separated by an ionically conductive and electronically insulating material known as the electrolyte. This electrolyte typically consists of a lithium salt dissolved in a blend of liquid, polar, organic solvents. Unfortunately, liquid electrolytes suffer from low electrochemical stability, high vapor pressures at elevated operating temperatures and incompatibility with a lithium metal anode which would offer high power densities.<sup>38,170-174</sup>

Wright's discovery of the dissolution and conduction of NaI in poly(ethylene oxide) (PEO) triggered an immense research effort to identify polymers best suited for use as polymer electrolytes.<sup>175</sup> Based on this work, it is generally accepted that low glass transition temperature ( $T_g$ )<sup>171</sup> and low molecular weight<sup>176</sup> are vital for high ionic conductivity. However, the development of structure-property relationships with respect to ionic conductivity is still ongoing.<sup>177-182</sup>

One relationship not explored very thoroughly is the influence of polarity on ionic conductivity. Work by Kumar and Sekhon identified that the addition of a plasticizer with higher polarity than PEO increased the conductivity by more than three orders of magnitude.<sup>183</sup> Whereas the addition of plasticizer with lower polarity than PEO does not enhance the conductivity. Choi

---

<sup>4</sup> This work was performed by the following authors: Malgorzata Chwatko, Alysha Helenic, and Nathaniel Lynd. Malgorzata Chwatko and Nathaniel Lynd designed the study. Malgorzata Chwatko, Alysha Helenic designed and performed polymerizations. Malgorzata Chwatko, All authors assisted in the data analysis and writing of this work.

et al. have used a polysiloxane polymer series to identify a trade of between segmental dynamics and polarity which both effect ionic conductivity.<sup>184</sup> Similarly, Barteau *et al.* examined ion transport in a series of poly(glycidyl ether)-based LiTFSI electrolytes of varying polarity.<sup>183</sup> In their systems' ionic conductivities surprisingly did not correlate directly with the polymer glass transition. Instead, they found that ionic conductivity increased as a function of the polymer dielectric constant (relative permittivity) in the range of four to six.

The findings of Barteau and coworkers suggest a new regime where the ionic conductivity of the polyether electrolyte is sensitive to the host polymer polarity. In this chapter, we discuss the synthesis of four polyethers with varying dielectric constants shown in Figure 5-1. The polymers' ionic conductivity was determined with varying temperature and salt content. The impact of both segmental dynamics, and polarity of the host polymers on conductivity was evaluated.

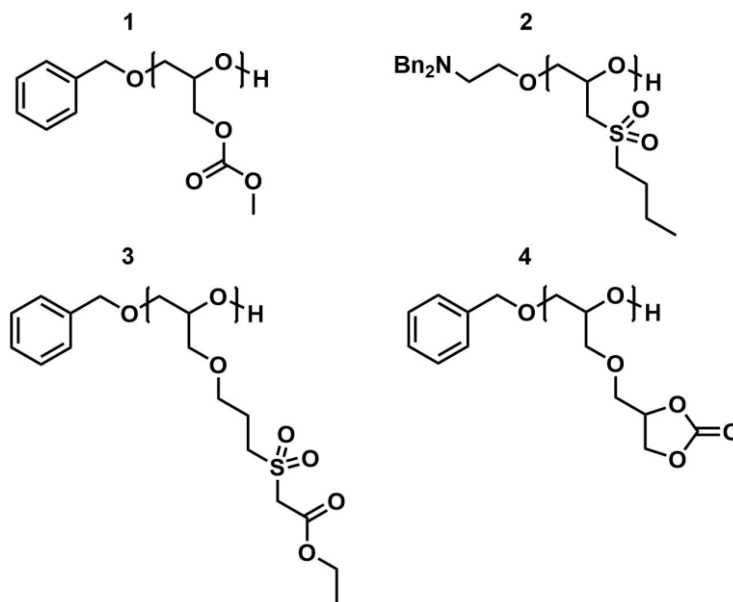


Figure 5-1 Structures of synthesized polyethers.

## **MATERIALS AND METHODS**

### **Polymer synthesis and characterization**

The polyethers used in this study were synthesized using techniques described in Appendix. Table 5-1 provides the number-averaged molecular weight,  $M_n$ , and polydispersity,  $\mathcal{D}$ , dielectric constant,  $\epsilon$ , and glass transition temperature,  $T_g$ , for each polymer.

### **Electrolyte preparation**

Electrolytes were prepared by mixing each polymer with lithium bis(trifluoromethanesulfonyl) imide (LiTFSI) salt. Due to the hygroscopic nature of LiTFSI, all sample preparation was carried out in an argon glovebox (MBraun) where  $H_2O$  and  $O_2$  levels were maintained below 0.1 ppm and 5 ppm respectively. All of the polymers were dried, *in vacuo* to a pressure of 10 milliTorr before being used. Dry polymer and LiTFSI salt were dissolved into anhydrous tetrahydrofuran (THF) or *N,N*-dimethylformamide (DMF) and the solutions were mixed at 60 °C for a minimum of 5 h. Once the solutes were fully dissolved, the polymers were taken out of the glovebox and dried *in vacuo* to a pressure of 10 mTorr before use.

Most of the dry electrolytes were very viscous liquids at room temperature. The salt concentrations chosen in the study were 5, 9, 13, 23, 31 and 50 w% LiTFSI. These values were chosen to span a wide range of salt concentrations.

### **Differential scanning calorimetry**

Samples were prepared by depositing 3–10 mg of each electrolyte into hermetically sealed aluminum pans. The samples were dried *in vacuo* at 70°C until they reached 10 milliTorr. Differential scanning calorimetry (DSC) experiments were performed on a TA Instruments Discovery DSC 250 instrument with the following temperature scan: heat to 120 °C at 10 °C/min,

cool to  $-75\text{ }^{\circ}\text{C}$  at  $5\text{ }^{\circ}\text{C}/\text{min}$ , heat to  $110\text{ }^{\circ}\text{C}$  at  $5\text{ }^{\circ}\text{C}/\text{min}$ , cool to  $-75\text{ }^{\circ}\text{C}$  at  $10\text{ }^{\circ}\text{C}/\text{min}$ , heat to  $110\text{ }^{\circ}\text{C}$  at  $5\text{ }^{\circ}\text{C}/\text{min}$ . The glass transition temperature values of the electrolytes were obtained from the third heating scan.

### Electrochemical measurements

A controlled environment sample holder from Bio-Logic Science Instruments was used with a constant flow of an inert gas. This allows for electrochemical measurements to take place outside of the glovebox while an air and water-free environment is maintained for the electrolyte. The sample holder was placed in the intermediate temperature system (Bio-Logic) to tune the sample holder temperature in the range of  $30\text{ }^{\circ}\text{C}$  to  $90\text{ }^{\circ}\text{C}$ . Complex impedance measurements were acquired using a Bio-Logic MTZ35 impedance analyzer for a frequency range of  $0.1\text{ Hz}$  to  $1\text{ MHz}$  at an amplitude of  $10\text{ mV}$ .

## RESULTS AND DISCUSSION

Table 5-1 Polymer electrolyte properties

Polymer	Molecular weight <sup>a</sup>	$D$ <sup>a</sup>	$\epsilon$ <sup>b</sup>	$T_g$ <sup>c</sup>	$T_g$ <sup>c</sup> (31 w% LiTFSI)
<b>1</b>	13,000	1.9	$10 \pm 9$	$-14 \pm 1$	$-13 \pm$
<b>2</b>	19,800	1.3	$34 \pm 6$	$29 \pm 1$	$20 \pm 7$
<b>3</b>	12,200	1.6	$35 \pm 1$	$-22 \pm 2$	$-14 \pm 2$
<b>4</b>	12,600	1.1	$54 \pm 3$	$-15 \pm 14$	$8 \pm 4$

<sup>a</sup> Determined by size exclusion chromatography with multiangle light scattering. <sup>b</sup> Determined by impedance spectroscopy at  $90\text{ }^{\circ}\text{C}$ . <sup>c</sup> Determined by differential scanning calorimetry

The polymer properties are listed in Table 5-1. The dielectric constants of the polymers varied between 10 to 54 which spanned a wide range of properties for this study. The glass transition temperatures varied from  $-20\text{ }^{\circ}\text{C}$  to  $30\text{ }^{\circ}\text{C}$ . Upon the addition of 31 w% LiTFSI, the glass transition of the measured polymers typically increased, except in the case of polymer **4**. This trend

has been previously reported in a few publications; however, no direct relationship between polymer properties and plasticization by salt has been established.<sup>185–187</sup>

Conductivity,  $\sigma$ , was measured at a wide range of salt concentrations and temperatures (25–90 °C) for each polymer. Results are shown in Figure 5-2 where conductivities of polyethers **1–4** were obtained as a function of temperature (panel A) and at 90 °C as a function of salt concentration (wt. fraction) (panel B). Significantly, the ionic conductivity correlates negatively with the glass transition temperature, which is correlated to segmental dynamics as seen in Figure 5-2A. However, the relationship between LiTFSI concentration and ionic conductivity is not as clear. The higher dielectric constant and lower glass transition temperature polymers (**3** and **4**) exhibit higher ionic conductivity. To attempt to decouple segmental dynamics from dielectric constant, an attempt was made to account for variations in segmental dynamics across polymers.

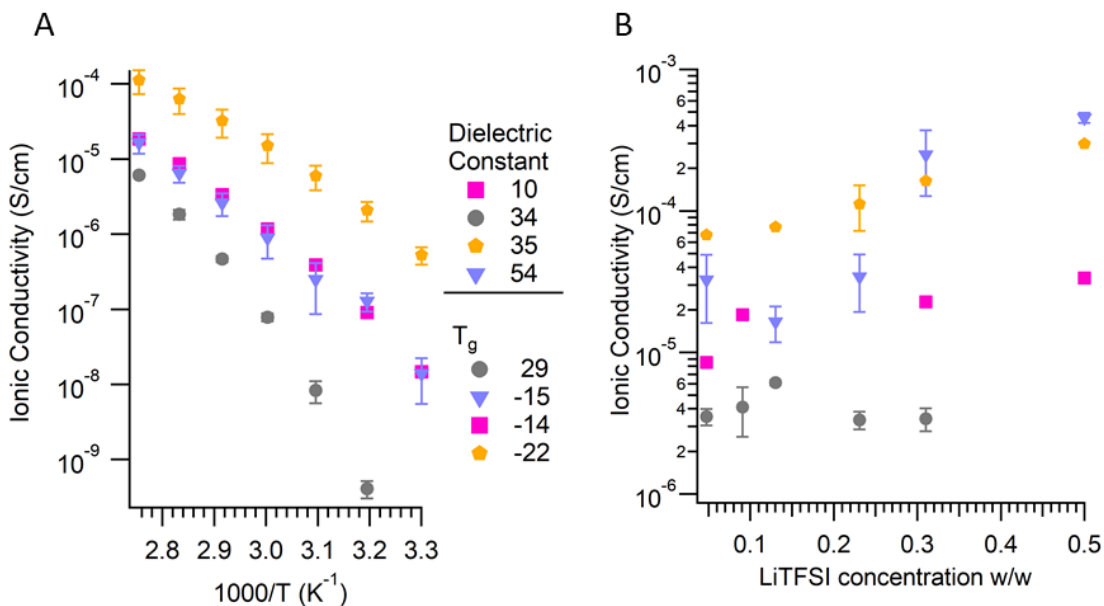


Figure 5-2 Ionic conductivity of the polymers vs A) temperature at 13 wt% LiTFSI and B) salt concentration at 90°C. Segmental dynamics and polarity play an important role in the final ionic conductivity.

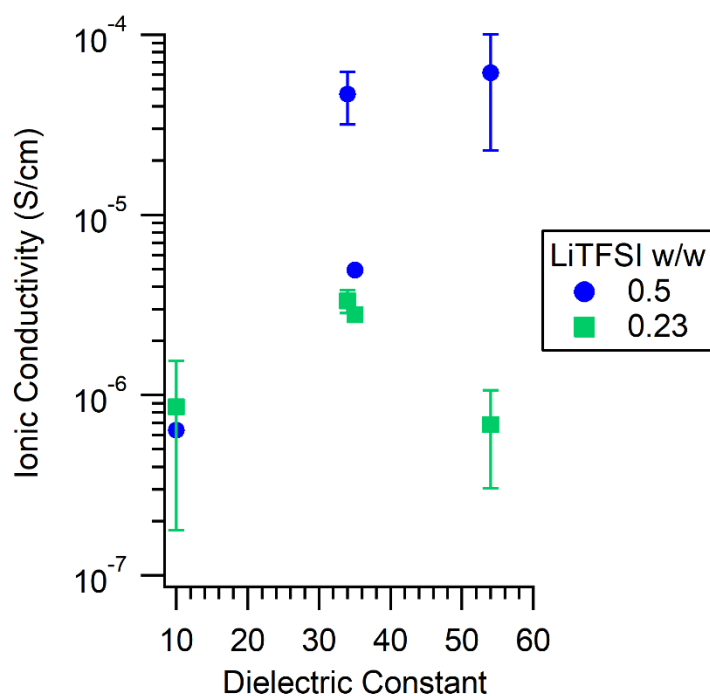


Figure 5-3 Ionic conductivity measured 60 °C below  $T_g$  of each polymer versus dielectric constant. Data without error bars is based off single data points to be remeasured in future.

A common approach to lessen the contributions of segmental dynamics to ionic conductivity is to adjust the measurement temperature for each polymer, such that each is assayed at the same relative temperature compared to its  $T_g$  *e.g.*, at 60 °C above the glass transition.<sup>188,189</sup> This  $T_g$  normalized data can be found in Figure 5-3. At the lower salt concentration, the ionic conductivity seems to obtain maximum at an intermediate dielectric constant. A possible explanation for this behavior is that as the polarity in the system increases, salt is dissociated more readily, however, when polarity increases too high, the large number of dipoles in the system restricts ion motion. Carbonyl functionalities especially has been known to be able solvate Li more effectively than ether oxygens.<sup>169</sup> However, at a higher salt concentration, there is a more general increase in ionic conductivity with dielectric constant. The greatest increase in ionic conductivity

with salt concentration can be seen in polymer **4** which has the highest dielectric constant. It is possible that at the higher salt concentration the carbonyl groups can allow for a secondary Li ion hopping transport mechanism in addition to diffusion.<sup>169</sup> Further studies utilizing high dielectric constant polymers are needed to better understand the physics behind ion transport in these systems.

## **CONCLUSION**

Polymer electrolytes offer a pathway to increase the safety and power density of lithium batteries. Typically, much of the literature focus has been on new polymer structures or a reduction in glass transition temperature to improve performance. In this work, we focused on the impact of polymer polarity on ionic conductivity by designing polyethers with variation in dielectric constant. Ionic conductivity appeared to correlate with glass transition temperature but was influenced by the dielectric constant as LiTFSI salt concentration was increased. By normalizing for differences in glass transition temperature, ionic conductivity was found to generally increase with dielectric constant especially at high salt loadings, suggesting that polymer polarity also plays a key role in ionic transport.

## **ACKNOWLEDGMENT**

This work was supported by start-up funds provided by the Welch Foundation (Grant F-1904) and National Science Foundation. M.C. is grateful for a Cockrell School fellowship.

## Chapter 6: **Hydrophobic or Hydrophilic: Polymerization of Dopamine on Surfaces**<sup>5</sup>

### **INTRODUCTION**

The impact of polymers on our society ranges from improvements in electronics and medicine to the deleterious effects of plastic waste on our environment. In this day and age, everyone will use countless polymers in their everyday life. However, as many studies have noted, students are not formally introduced to the macromolecular concepts underlying plastics and rubbers until after secondary school and often after undergraduate studies in the United States.<sup>190</sup> Difficulties in introducing polymers in the secondary school curriculum include the lack of a formal science requirement and a lack of resources to perform educational activities regarding macromolecules.

This experiment has been developed to help introduce polymers thru a simple surface-active polymerization that can be conducted under ambient conditions. The experiment can fit under chemistry and biology education about hydrophobic/hydrophilic properties and study of pH, monomer vs. polymer, repeat unit structure, and surface modification using polymer coatings. The laboratory can be completed in as little as one one-hour class period, with multiple possibilities for extensions on the core activity. Furthermore, the overall cost of each experiment is minimal due to the small amount of materials required to functionalize a hydrophobic surface with a hydrophilic polydopamine coating.

### **Background**

Marine mussels have an ability to anchor themselves to many surfaces in seawater. These animals do this through the use of adhesive proteins, containing catechol functionality (Figure 6-1). Scientists are now constructing synthetic polymers that contain catechol functionality to

---

<sup>5</sup> This work was performed by the following authors: Malgorzata Chwatko, Kyle Albernaz and Nathaniel Lynd. Malgorzata Chwatko designed the study. Malgorzata Chwatko and Kyle Albernaz performed the activity. All authors assisted in the analysis of the data.

achieve similar properties.<sup>191-193</sup> This application of knowledge from nature is termed biomimicry. Polydopamine (PDA) is a polymer inspired by nature. A proposed structure of polydopamine is shown in Figure 6-1A.<sup>194</sup>

PDA has received much attention due to its ability to polymerize and form a conformal coating on almost any surface to render the surface hydrophilic.<sup>195,196</sup> While the mechanism of dopamine polymerization is still disputed, its applications are not.<sup>197,198</sup> These applications include biomedical materials and modification of membranes for water purification.<sup>195,197,199,200</sup> These applications are derived from the ability of PDA to change surface chemistry to yield an increase in surface hydrophilicity. The hydrophilicity of PDA allows for macroscopic observations of the behavior of water on the surfaces, which can be observed simply by visible inspection. The many applications of catechol-based polymers offer multiple avenues to engage students through experimentation and independent inquiry in the classroom. Due to our goal of fitting within existing curriculum, we aim not to introduce too many new definitions but rather to introduce polymers into the curriculum within the context of currently covered topics.

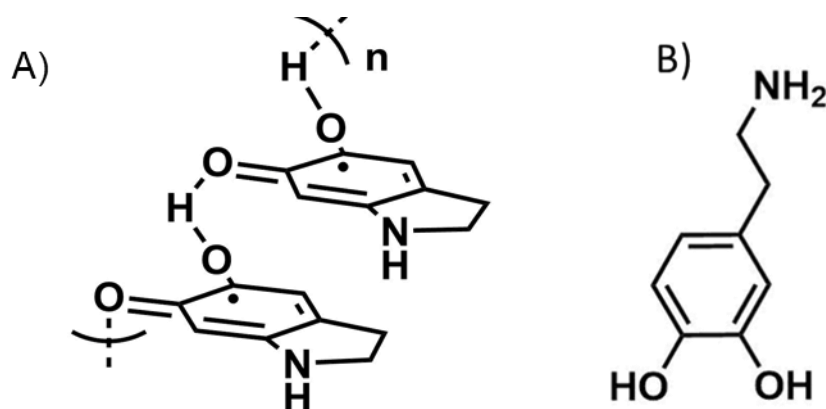


Figure 6-1 A) The proposed chemical structure of a poly(dopamine) B) chemical structure of dopamine.

## **HAZARDS**

Ammonium persulfate is an oxidizer and can cause skin irritation. Dopamine and ammonium persulfate are harmful to aquatic life. Dispose of the liquid waste properly after this activity.

## **EXPERIMENT**

Applying dopamine monomer and polymerizing it on surfaces allows students ample opportunity for critical and creative thinking. The experiment starts with each pair of students finding three labeled solutions, A, B, C and being asked to identify the pH each using a litmus paper. The students are then asked to add 10 mL of each solution into centrifuge tubes or beakers. Next, the students receive a piece of prewetted Teflon they are going to cut into three small pieces. The pieces are then weighed and placed into beakers filled with solution A, B or C. The students are subsequently asked how much dopamine they need to add to create a 2 mg/ml concentration. After the calculation is completed, dopamine is measured and added to the respective beakers. At this point, the polymerization proceeds for 24 hour or 15 minutes if ammonium persulfate is added. After the time passes, the Teflon pieces are taken out from the solution and patted dry. The student should note the appearance of the Teflon pieces. When dry, each piece can be weighed and used in a droplet test. The weight of the Teflon pieces should increase with increase in solution pH. Be mindful, that weight increase should only be a few milligrams and would be best captured by an analytical balance if available. The droplet test is a visual test in which a droplet of water is placed on a sheet and the appearance of the droplet is observed. If the droplet retains shape, the surface is hydrophobic, however if the droplet spreads then the surface is hydrophilic. After the droplet test, the students again will note that the surface hydrophilicity increased with solution pH.

## **RESULTS**

The lab was performed with four different classes, three pre-AP chemistry classes and one biology class. The class periods were an hour and fifteen minutes during which the students received a short lecture about biomimicry and polymers in addition to performing the experiment.

The experiment required *ca.* 40 minutes. During the experiment, the students were provided additional guidance to perform the experiment successfully. The student opinions and knowledge were assessed in comparison to a separate titration experiment that is normally used to illustrate the pH scale. The assessment was done as a pre- and post-assessment survey, where the post assessment survey was given two weeks after the experiment. The survey consisted of open-ended questions and those on the Likert scale.

## DISCUSSION

The experiment was designed to teach students about polymers during standard lectures on pH. This allows for facile introduction of macromolecular chemistry within the normal required secondary school chemistry curriculum. Overall, the experiment introduces polymer-based terminology, while using the discussion of pH as a contextual platform.

Student observation was recorded during the experiments. As the polymerization proceeded, students found that the color of the reaction solution changed from clear to orange. At the end of the allotted time, students identified that the piece of Teflon has changed color from a white to brown. The students were able to make conclusions using colors change observation and data collected via the droplet shape test.

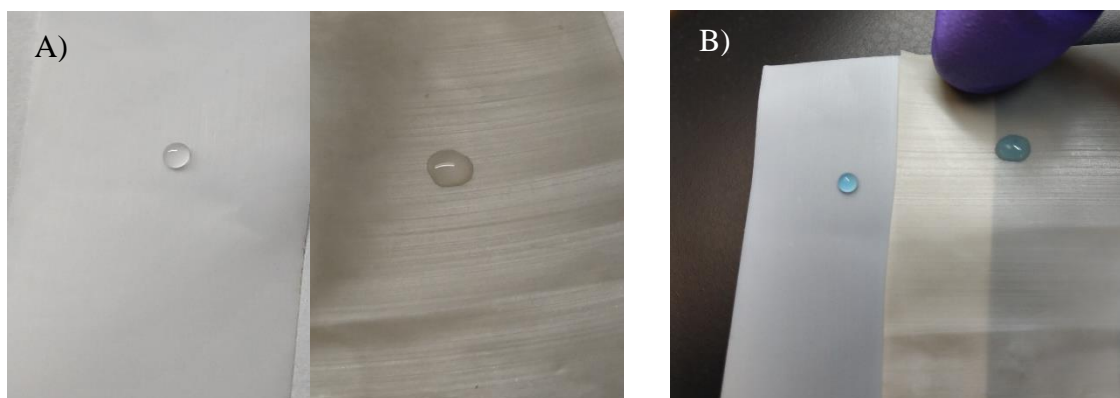


Figure 6-2 Picture of the droplet test on the modified and unmodified Teflon sheet. A) pure water B) methylene blue dyed droplet. The droplet retains shape on the unmodified Teflon, and smears on the PDA modified sample.

The students' pre-assessment and post-assessment were analyzed to learn about potential effects of replacing the existing pH titration lab with the proposed polydopamine experiment. There were no significant changes in the knowledge of the groups regarding pH or polymer science. This may be due to the fact that both the control and experiment group obtained a lecture about polymer information ahead of the proposed polymerization experiment. In general, there was a slight increase in the average for all the activity-based questions for the experimental group vs the control group which performed the normal titration experiment. There was also less deviation which indicates that the experiment reached all students more effectively than the control.

Table 6-1 Survey results post laboratory experiments. The survey used a 4-point Likert scale where Strongly Disagree = 1, Disagree = 2, Agree = 3, Strongly Agree = 4

	Control Group N=24	Experimental Group N=61
The activity was about the right length	3.13 ± 0.78	3.24 ± 0.29
This activity increased my interest in going to college	3.29 ± 0.82	3.43 ± 0.31
This activity increased my interest in a degree or career related to science and engineering	2.90 ± 0.72	3.29 ± 0.30
This activity should be offered again	2.19 ± 0.55	2.67 ± 0.24

## EXTENSIONS

For an activity to be applicable across many age groups and subjects it helps to be amendable to extensions in subject matter and activities. This experiment can be extended beyond testing material properties after polymerization by having the students track reaction kinetics. The kinetics of this polymerization are related to the color of the solution, thus in schools equipped with a UV-spectrophotometer it is possible to obtain quantitative results.<sup>201,202</sup> Another alternative could be to take images on smartphones and use image processing tools to determine an average RGB value which can also be used to track conversion. The data obtained will be similar to the data shown in Figure 6-3. This method is not as accurate but can be used to track reaction kinetics semi-quantitatively without specialized equipment but shows expected trends where polymerization occurs at more basic solution pH.

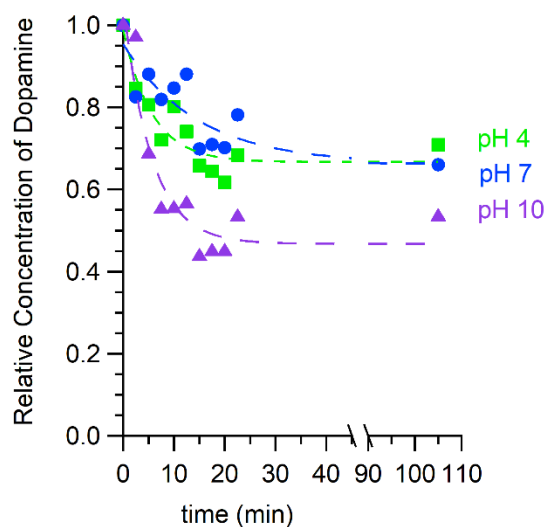


Figure 6-3 Sample of kinetic data of polydopamine formation at different pHs obtained from RGB smartphone method.

## CONCLUSIONS

Polymers are used every day by individuals of all ages, however there are not many simple experiments which can teach students what polymers are. The proposed laboratory experiment is

designed to introduce the concept of polymers to high school chemistry and biology classes. The experiment is simple to run, inexpensive, and can take as little as one class period. Overall, the students had positive impressions of the laboratory.

#### **ACKNOWLEDGMENTS**

We would like to thank Andrea Bucko, Loreni Kerecman and Katye Howell for their helpful discussions relating to the work. MC would like to thank the Scientist-in-Residence Program for help with pedagogical development. This work has been supported via NASCENT Research Experiences for Teachers Program and funding from the University of Texas. NASCENT Engineering Research Center is Cooperative Agreement No. EEC-1160494.

## Chapter 7: Conclusions and Recommendations

Chapter 1 discussed a broad introduction to different concepts described in this dissertation. The major theme of this work is sustainability from monomer feed stock to end of use applications. Polymer synthesis methodology is described to showcase important considerations such as thermodynamics and kinetics of reaction. Polymer electrolytes development is discussed as example of application driven area striving to enhance the power density and safety of the lithium ion batteries.

Chapter 2 discussed the synthesis of lactone epoxide copolymers using the Vandenberg catalyst. This copolymerization is particularly interesting as it can lead to an easily degradable poly(ethylene oxide). The Vandenberg catalyst is an industrially relevant catalyst for epoxide polymerizations. The catalyst was found to polymerize lactide in a controlled fashion. The copolymerization followed the uncontrolled kinetics of the polyether polymerization. The copolymerization was supported via  $^1\text{H}$  NMR and GPC characterization. In the future work in this area, other copolymer pairs should be tested. This can allow for tunable degradation of polyethers, while maintaining their high molecular weight with good mechanical properties.

Chapter 3 discussed the synthesis and application of the BOD catalysts. These catalysts were inspired by the aforementioned Vandenberg catalyst. Typically, catalysts are only tested with one set of monomers. In this work, many classes of cyclic monomers were used. The BODs first were used to polymerize homopolymers of various lactones. Next various copolymers were synthesized and characterized via  $^1\text{H}$  NMR and GPC. The polymers had various thermal properties and molecular weight ranges.

Chapter 4 discussed the application of sustainable fruit and vegetable plastic film wrapping. The plastic barriers allow for the extension of produce shelf life. In this chapter, new polymeric thin films were proposed based on naturally occurring fatty alcohols. Two strategies were used to create thin films; alternating copolymerization and block copolymerization. The two strategies produced polymers with different thermal properties. The gas barrier properties of these films were

also evaluated, and they performed either better or on par with a standard polylactide film. Future work in this area should focus on changing the alkyl chain length of the polyethers and degree of crosslinking.

In Chapter 5, polymer electrolytes of various polarities were synthesized. The polymers have tunable polarity and segmental dynamics. It was found that the polymer ionic conductivity roughly correlated with glass transition temperature. When the segmental dynamics were normalized, there was a secondary trend of ionic conductivity with polymer polarity especially at higher salt loadings. The future work in this area should focus on achieving a good balance between high polarity and high segmental dynamics. One way to do that is increase the polymer polarity and add a plasticizer to increase the system dynamics.

Chapter 6 discusses new educational activities which can be used to teach high school students about polymers. Students typically do not learn about polymers in a standard teaching curriculum. In order to provide an opportunity to learn about polymers, the activity can easily replace or extend the standard pH experiments in the strict teaching requirements. In this activity polydopamine was polymerized on a thin film. The coating allowed for a switch in surface polarity which students studied. No difference was observed in the understanding of pH concepts in the test versus the control group. However, the students who performed the polydopamine experiment cited more interest in science on average.

## **Appendix A**

Supporting Information for Chapter 2: Statistical copolymerization of epoxides  
and lactones to high molecular weight

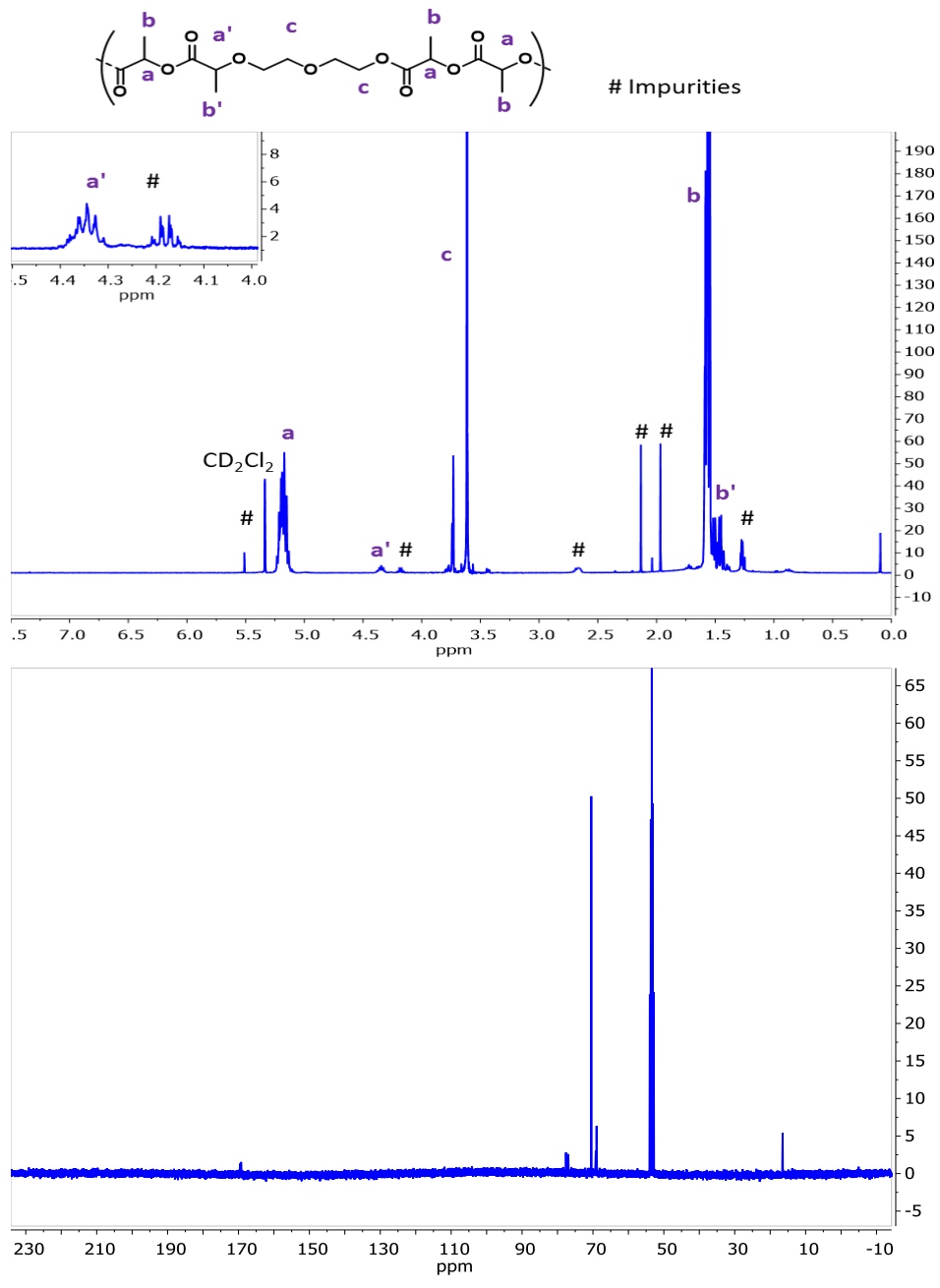


Figure A1 <sup>1</sup>H and <sup>13</sup>C NMR spectra for poly[(DL-lactide)<sub>0.45</sub>-co-(ethylene oxide)<sub>0.55</sub>] in 2:1 CD<sub>2</sub>Cl<sub>2</sub>:CDCl<sub>3</sub>

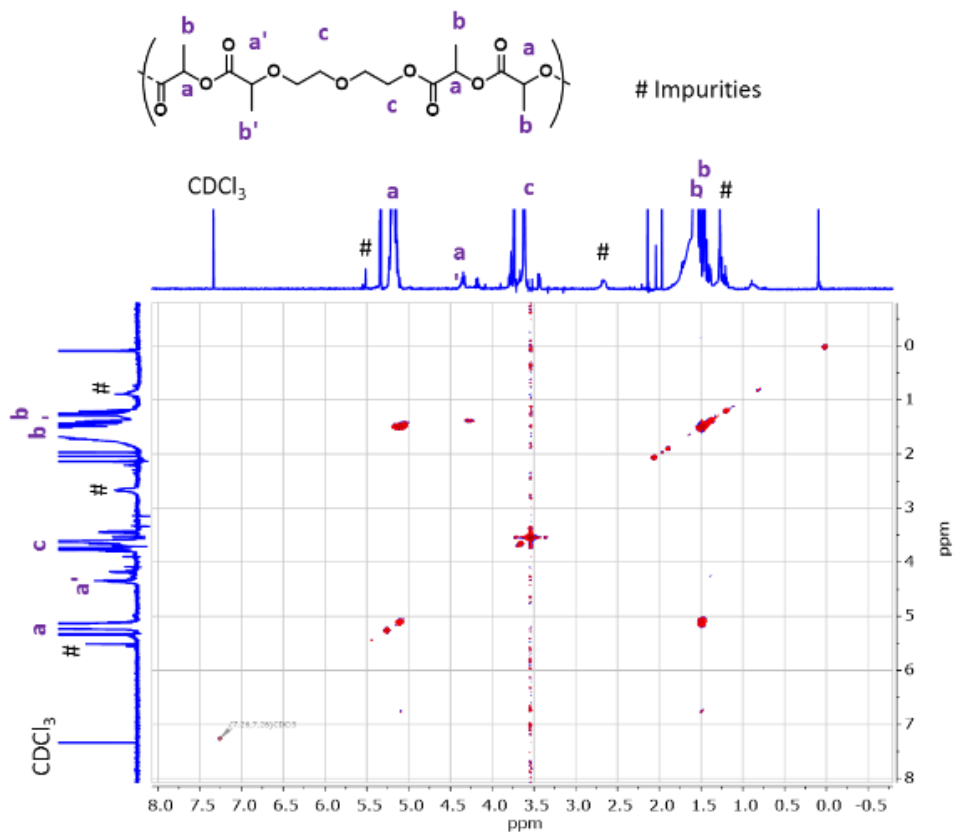


Figure A2 COSY(HH) NMR spectra for poly[(DL-lactide)<sub>0.45</sub>-co-(ethylene oxide)<sub>0.55</sub>] in 2:1 CD<sub>2</sub>Cl<sub>2</sub>:CDCl<sub>3</sub>

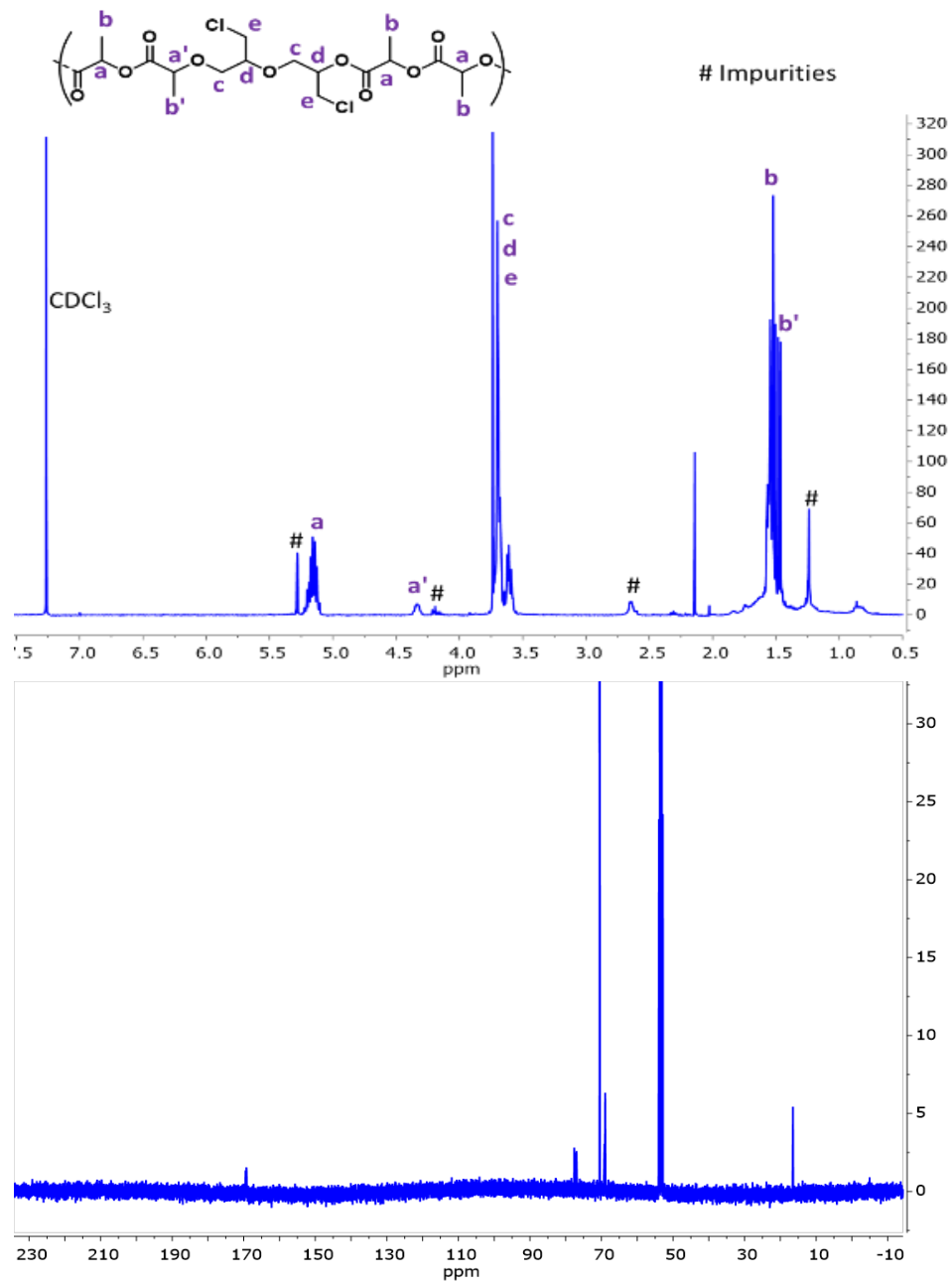


Figure A3 <sup>1</sup>H and <sup>13</sup>C NMR spectra for poly[(DL-lactide)<sub>0.45</sub>-co-(epichlorohydrin)<sub>0.55</sub>] in 1:2 CD<sub>2</sub>Cl<sub>2</sub>:CDCl<sub>3</sub>

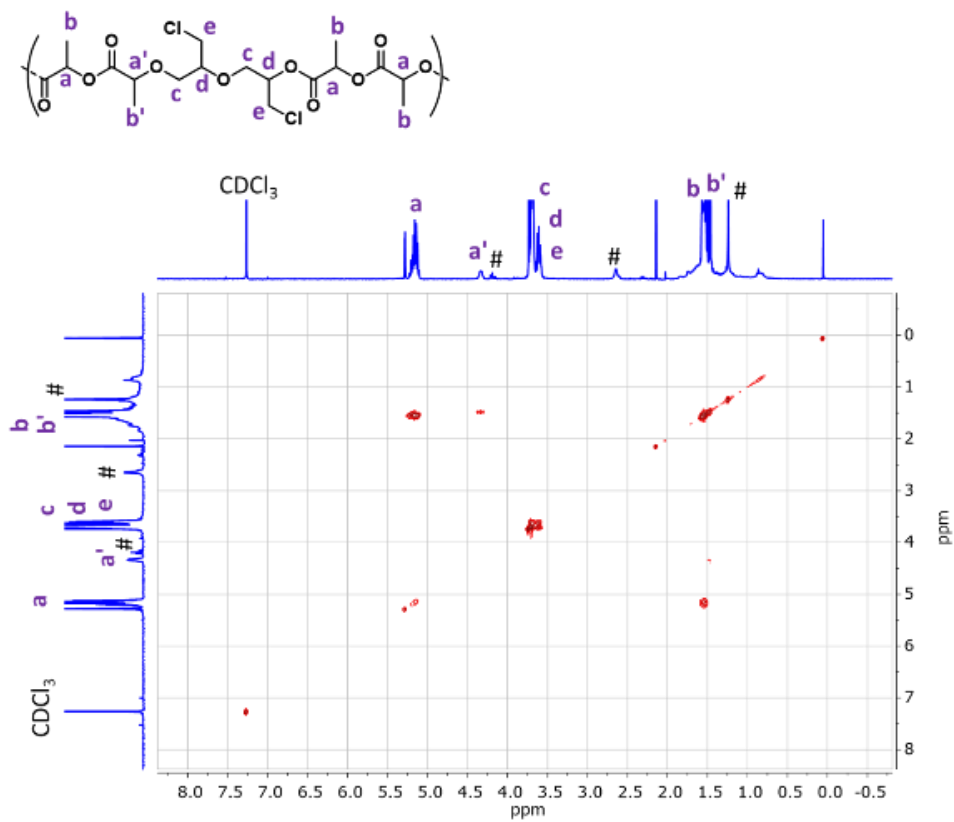


Figure A4 COSY(HH) NMR spectra for poly[(DL-lactide)<sub>0.45</sub>-co-(epichlorohydrin)<sub>0.55</sub>] in 1:2 CD<sub>2</sub>Cl<sub>2</sub>:CDCl<sub>3</sub>

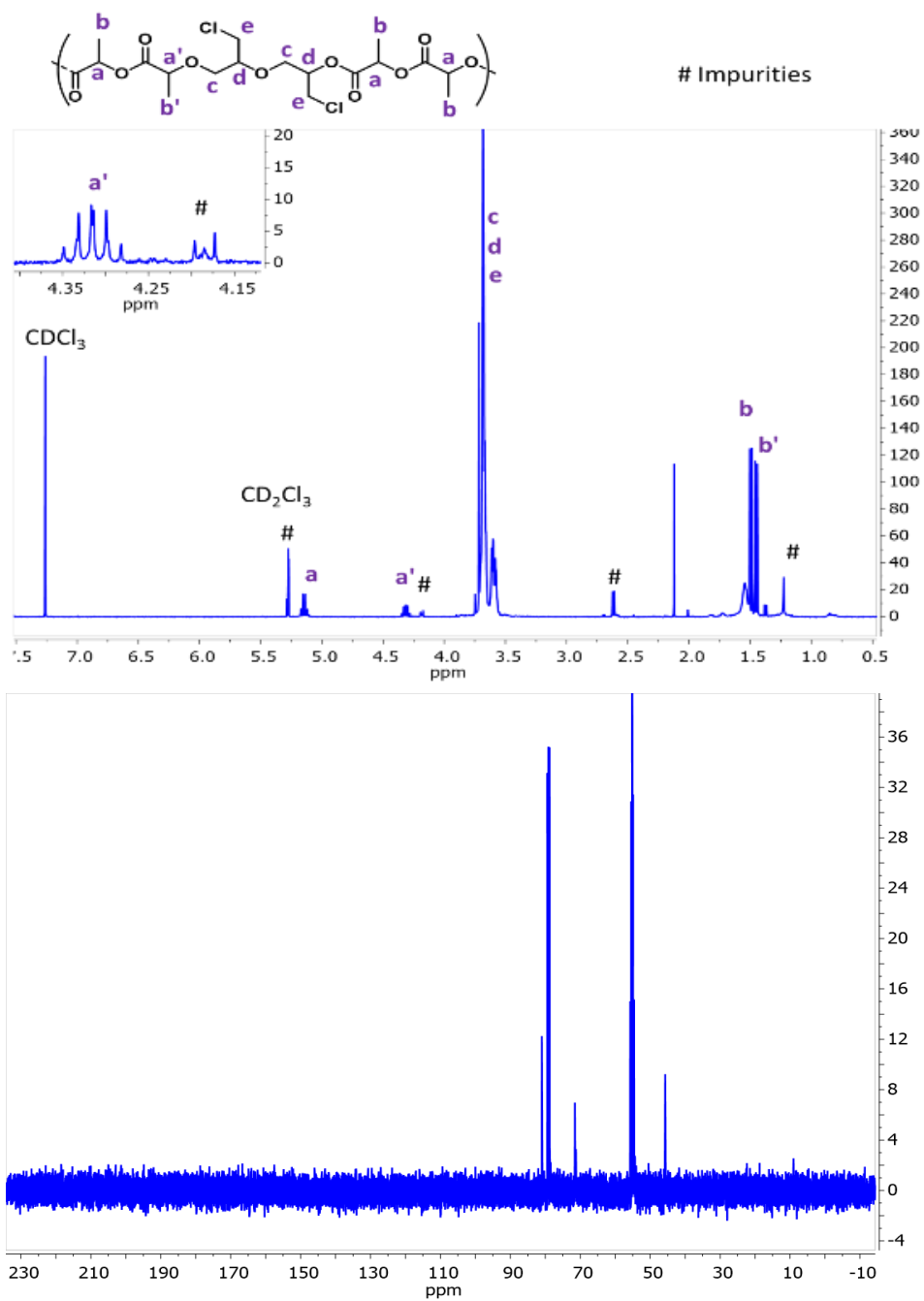


Figure A5 <sup>1</sup>H and <sup>13</sup>C NMR spectra for poly[(DL-lactide)<sub>0.08</sub>-co-(epichlorohydrin)<sub>0.92</sub>] in 1:2 CD<sub>2</sub>Cl<sub>2</sub>:CDCl<sub>3</sub>

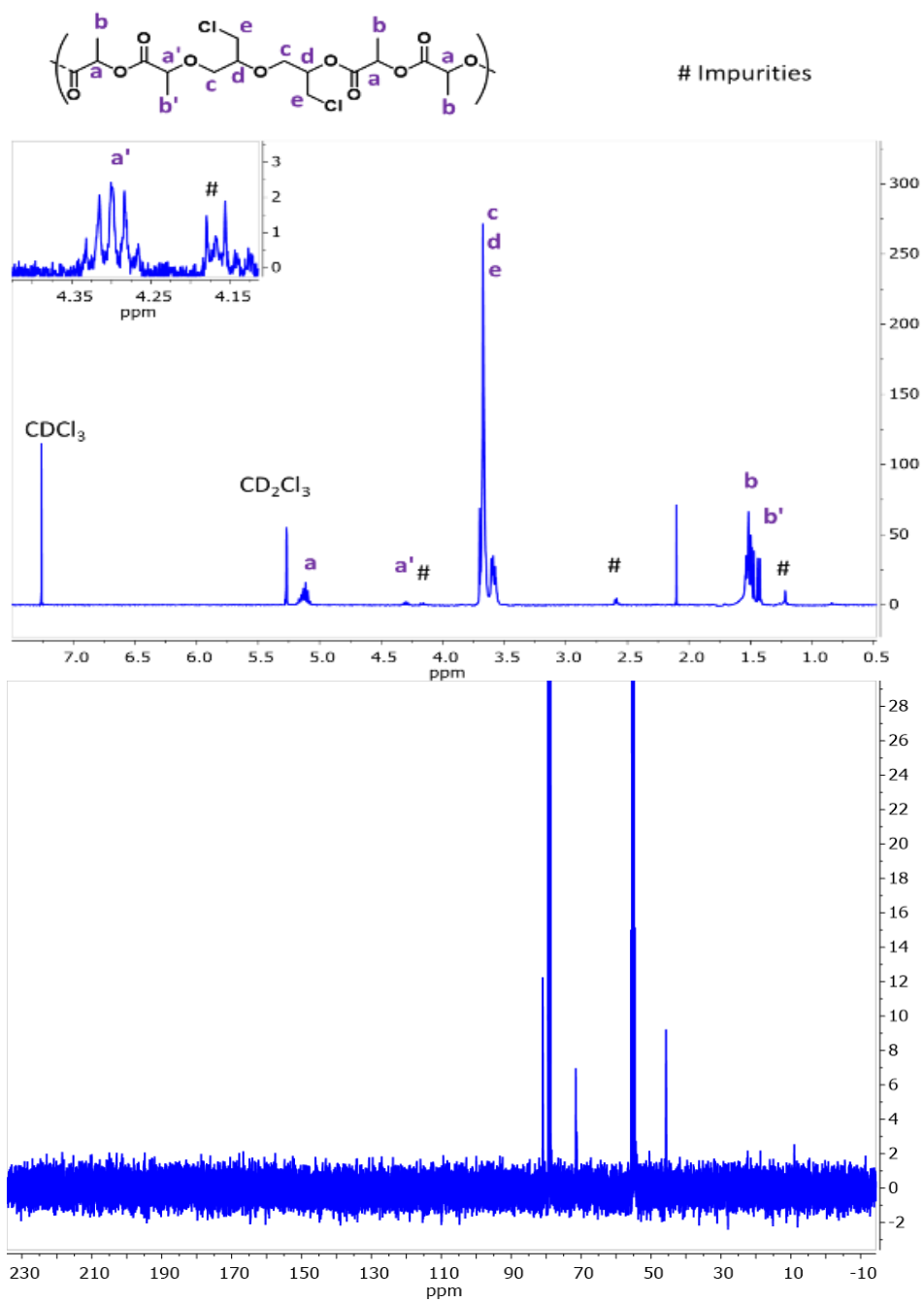


Figure A6 <sup>1</sup>H and <sup>13</sup>C NMR spectra for poly[(DL-lactide)<sub>0.22</sub>-co-(epichlorohydrin)<sub>0.78</sub>] in 1:2 CD<sub>2</sub>Cl<sub>2</sub>:CDCl<sub>3</sub>

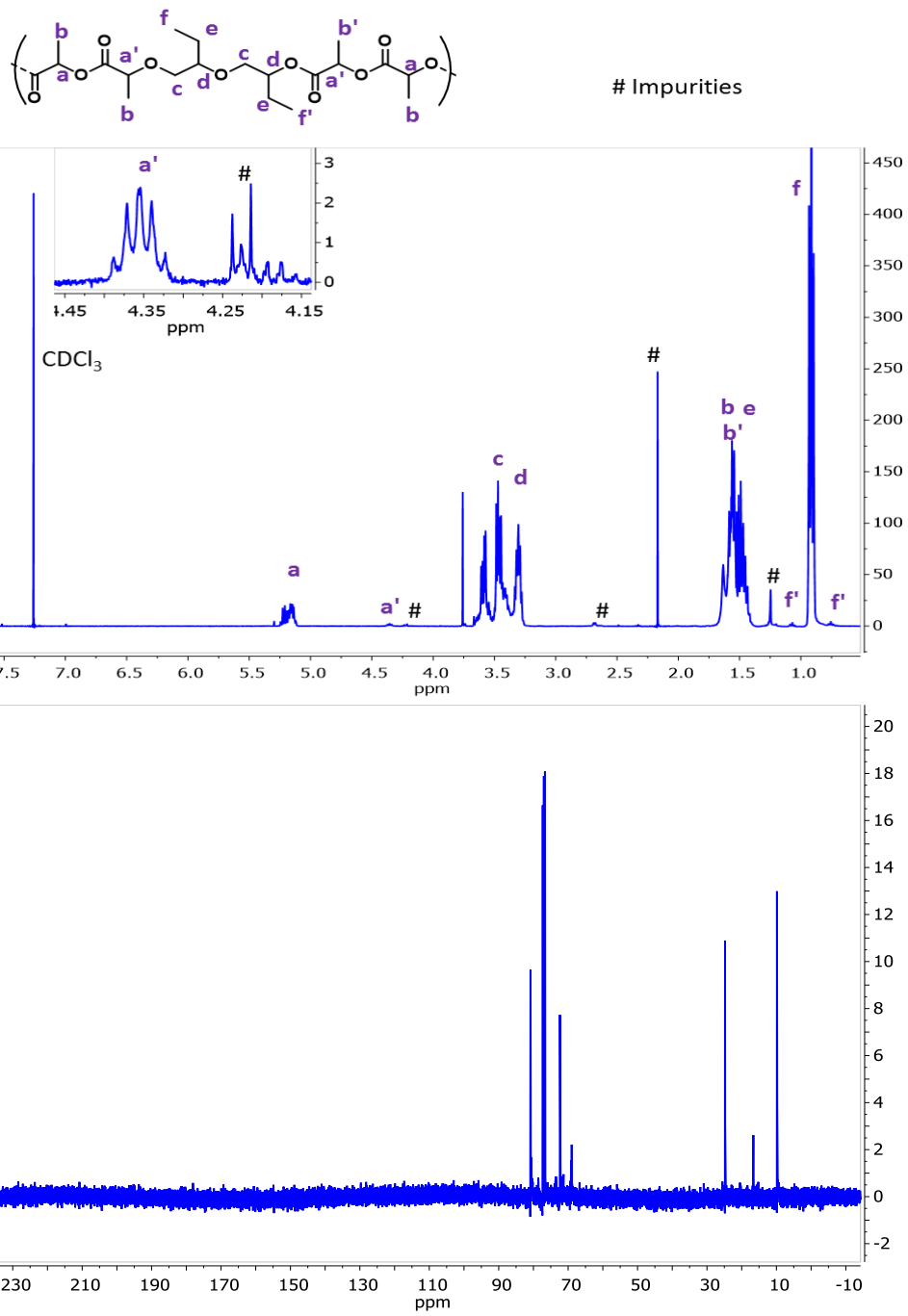


Figure A7 <sup>1</sup>H and <sup>13</sup>C NMR spectra for poly[(DL-lactide)<sub>0.25</sub>-co-(butylene oxide)<sub>0.75</sub>] in CDCl<sub>3</sub>

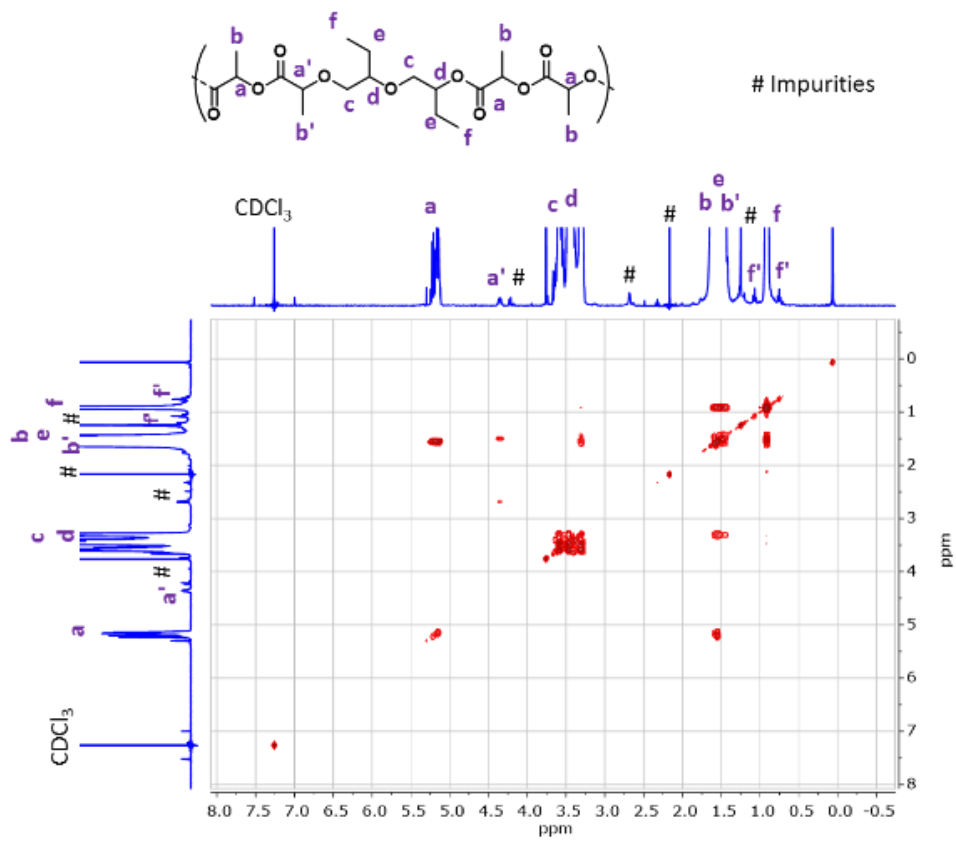


Figure A8 COSY(HH) NMR spectra for poly[(DL-lactide)<sub>0.25</sub>-co-(butylene oxide)<sub>0.75</sub>] in CDCl<sub>3</sub>

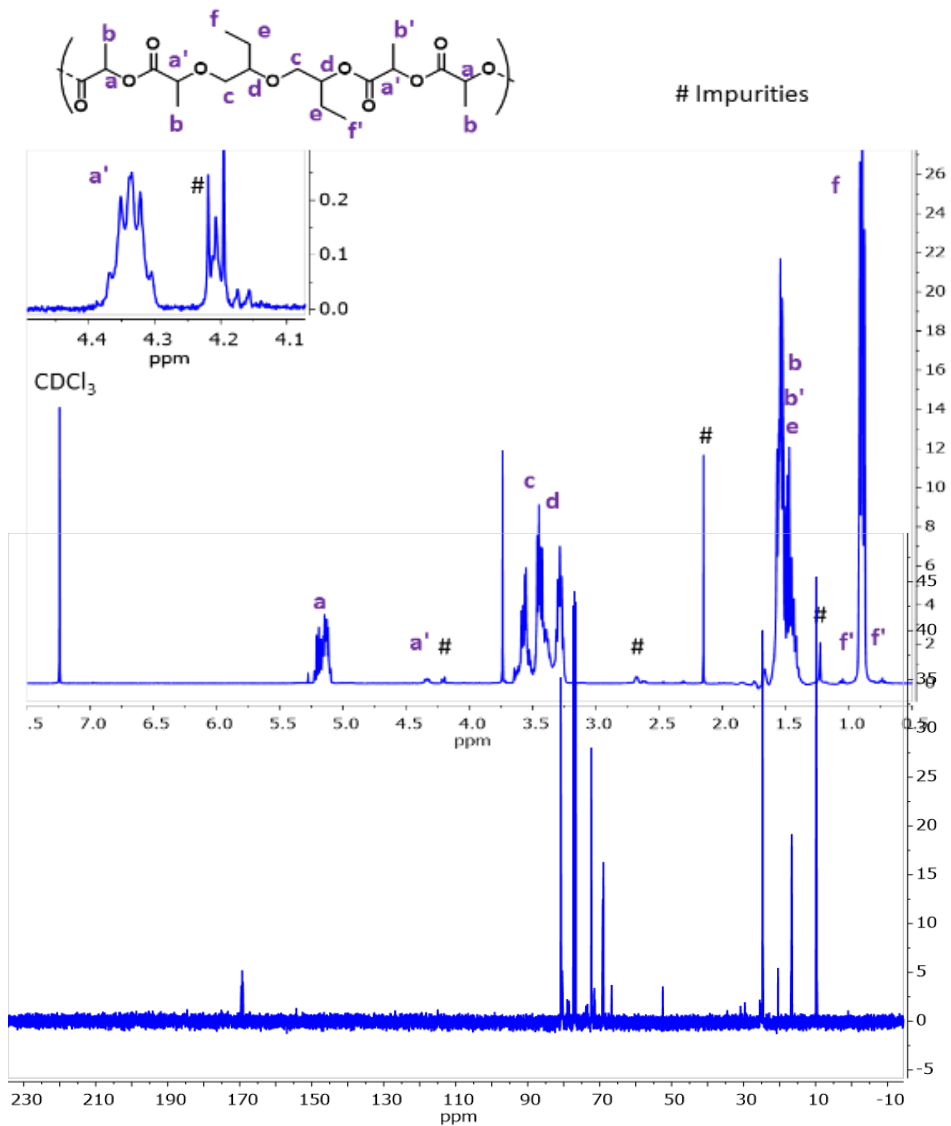


Figure A9 <sup>1</sup>H and <sup>13</sup>C NMR spectra for poly[(DL-lactide)<sub>0.40</sub>-co-(butylene oxide)<sub>0.60</sub>] in CDCl<sub>3</sub>

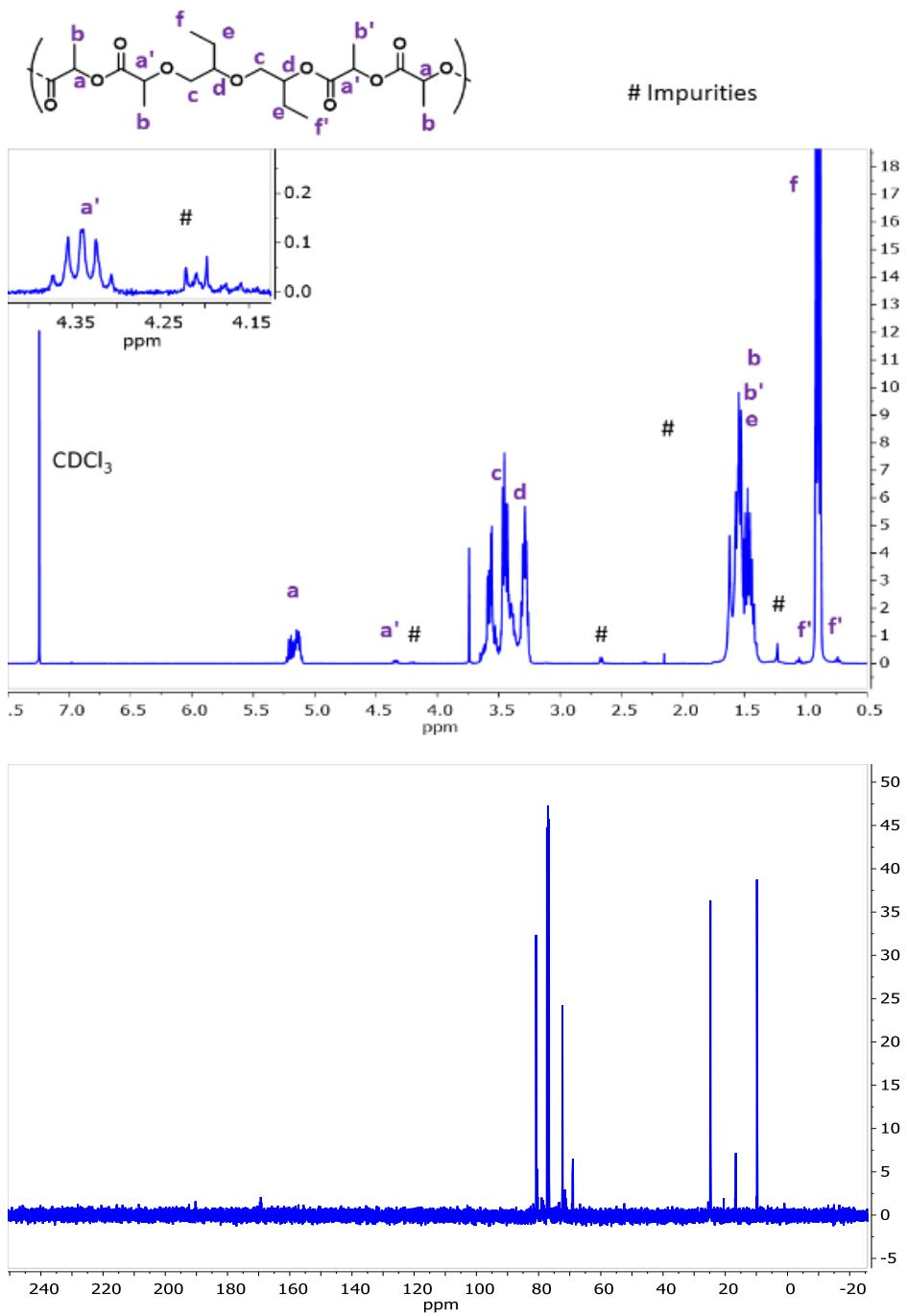


Figure A10 <sup>1</sup>H and <sup>13</sup>C NMR spectra for poly[(DL-lactide)<sub>0.24</sub>-co-(butylene oxide)<sub>0.76</sub>] in CDCl<sub>3</sub>



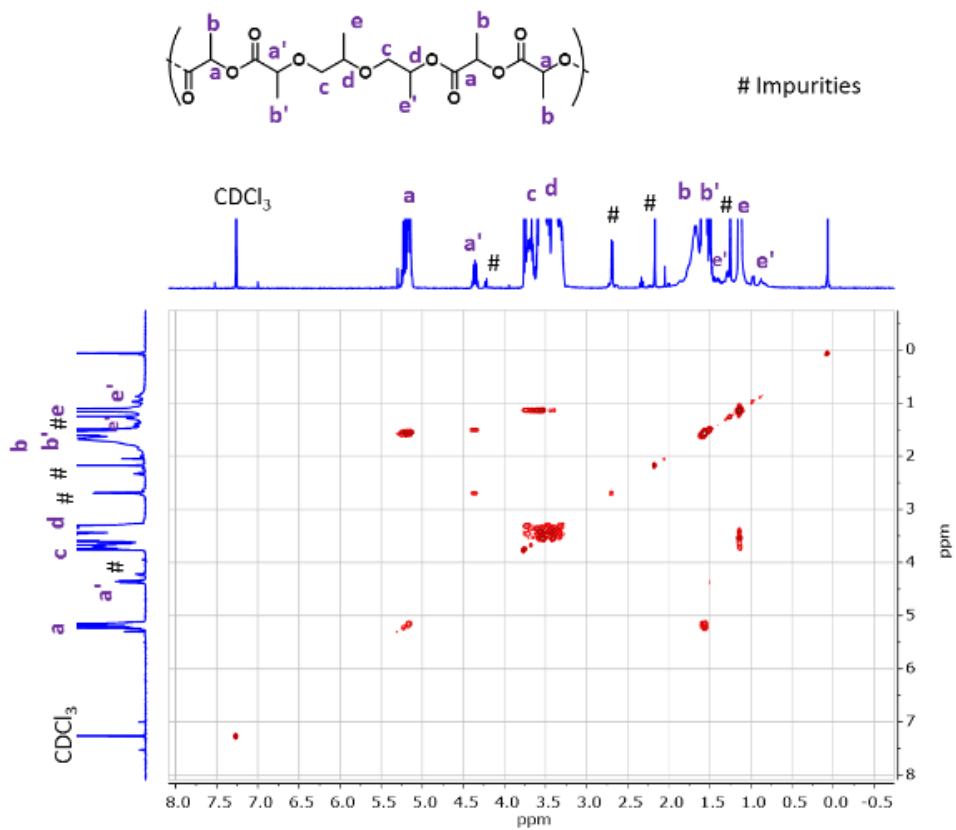


Figure A12 COSY(HH) NMR spectra for poly[(DL-lactide)<sub>0.20</sub>-co-(propylene oxide)<sub>0.80</sub>] in CDCl<sub>3</sub>

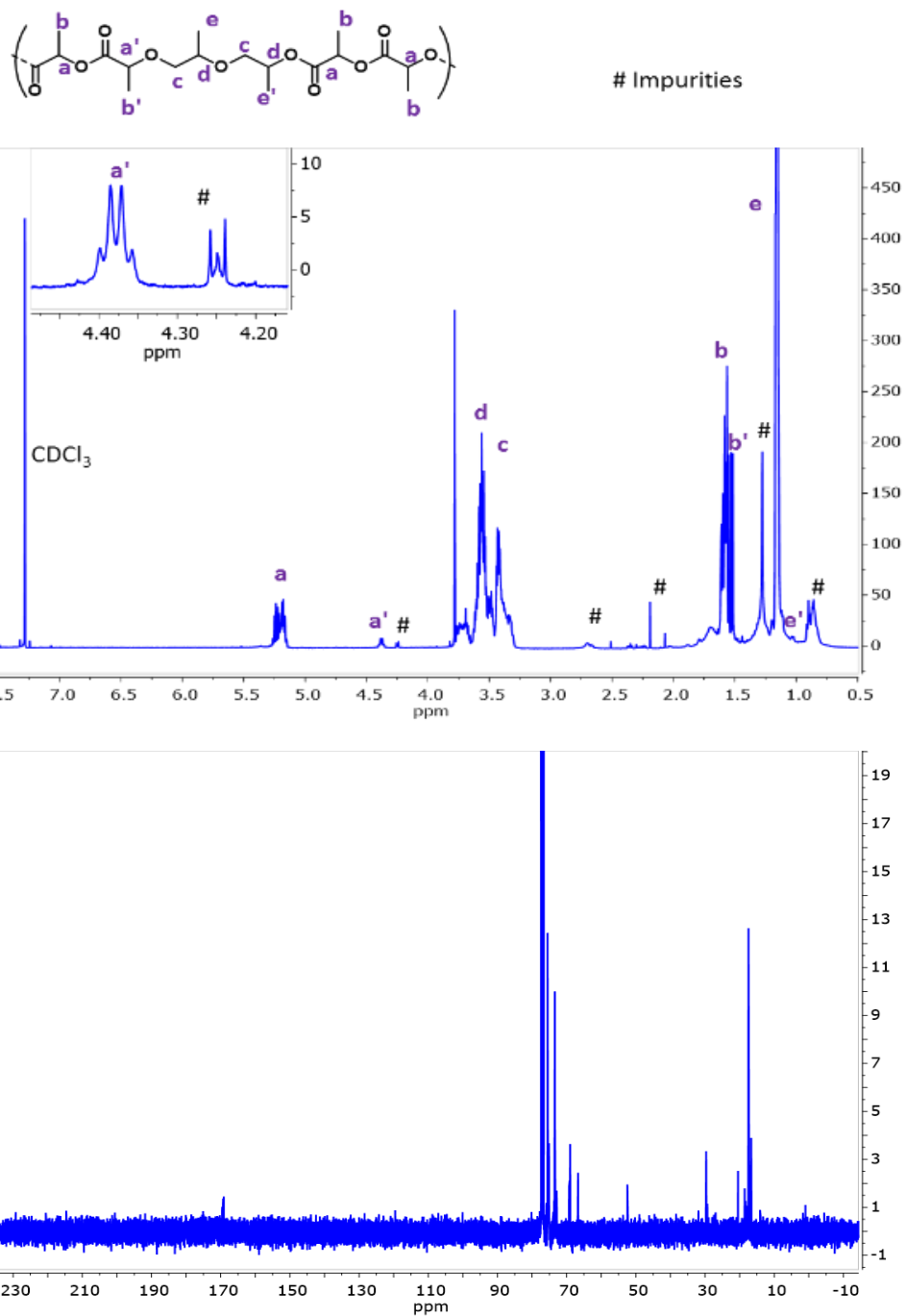
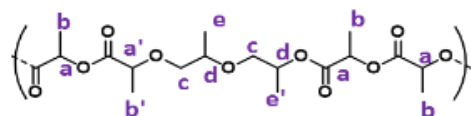


Figure A13 <sup>1</sup>H and <sup>13</sup>C NMR spectra for poly[(DL-lactide)<sub>0.40</sub>-co-(propylene oxide)<sub>0.60</sub>] in CDCl<sub>3</sub>



# Impurities

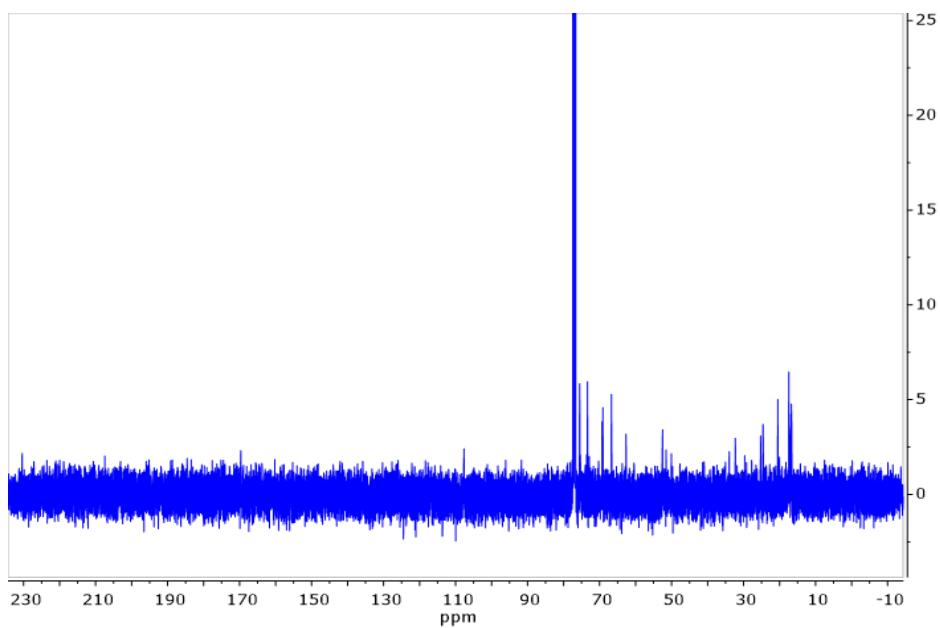
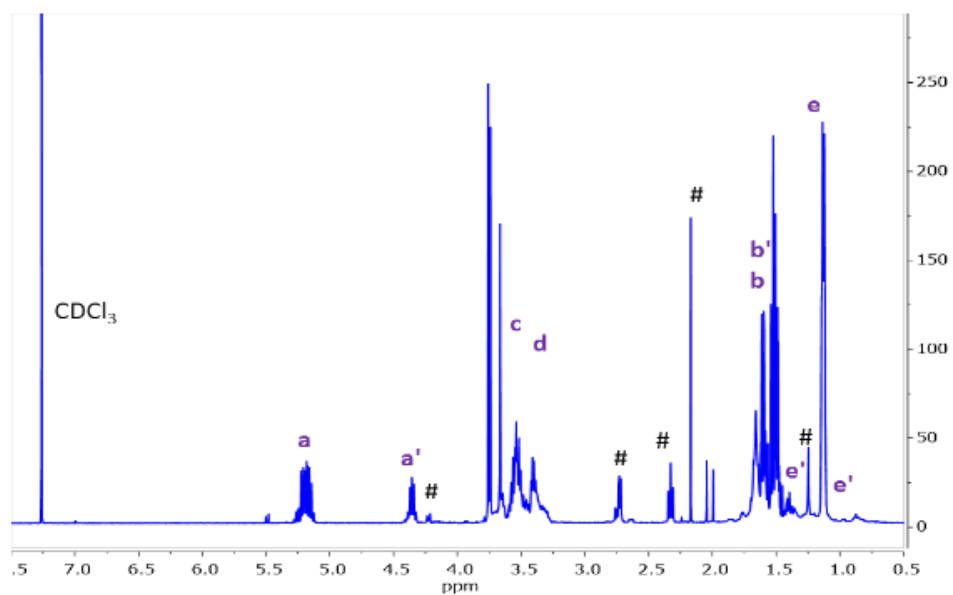


Figure A14 <sup>1</sup>H and <sup>13</sup>C NMR spectra for poly[(DL-lactide)<sub>0.24</sub>-co-(propylene oxide)<sub>0.76</sub>] in CDCl<sub>3</sub>

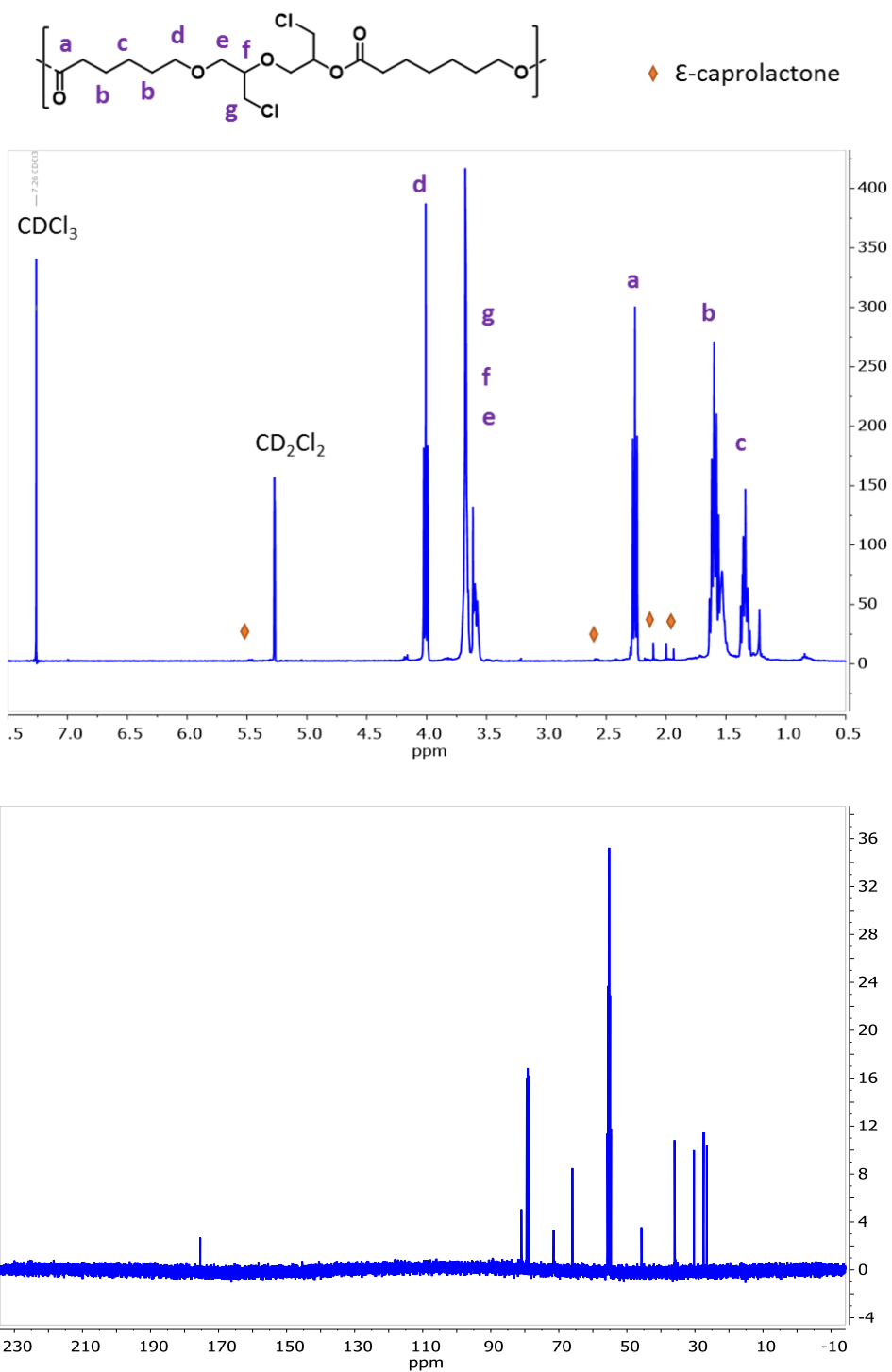


Figure A15  $^1\text{H}$  and  $^{13}\text{C}$  NMR spectra for poly[( $\epsilon$ -caprolactone) $_{0.48}$ -co-(epichlorohydrin) $_{0.52}$ ] in  $\text{CDCl}_3$

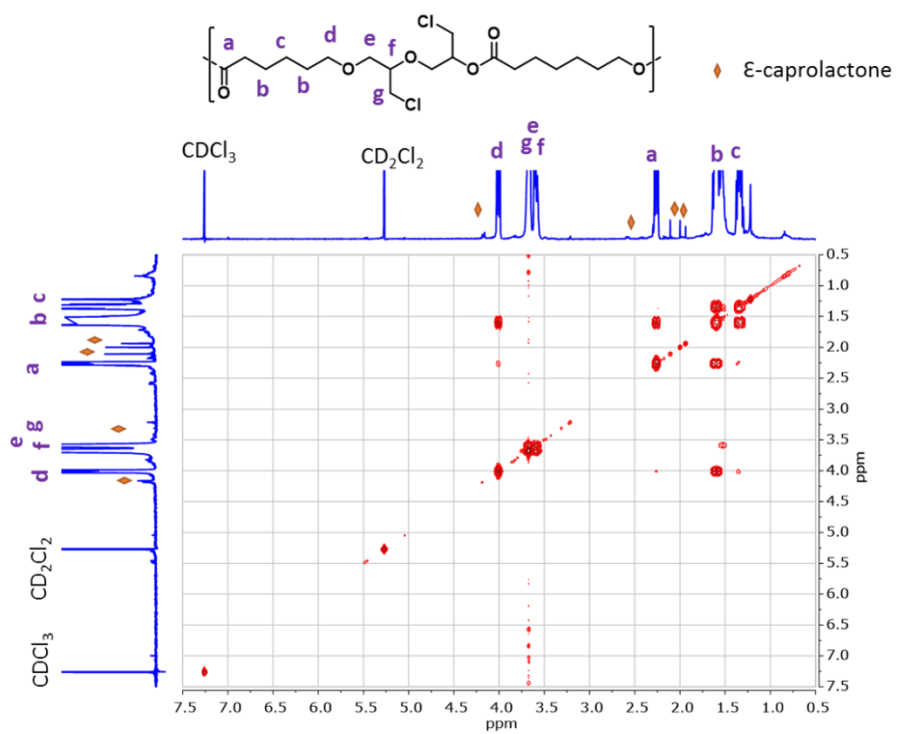


Figure A16 COSY(HH) NMR spectra for poly[( $\epsilon$ -caprolactone)<sub>0.48</sub>-co-(epichlorohydrin)<sub>0.52</sub>] in CDCl<sub>3</sub>

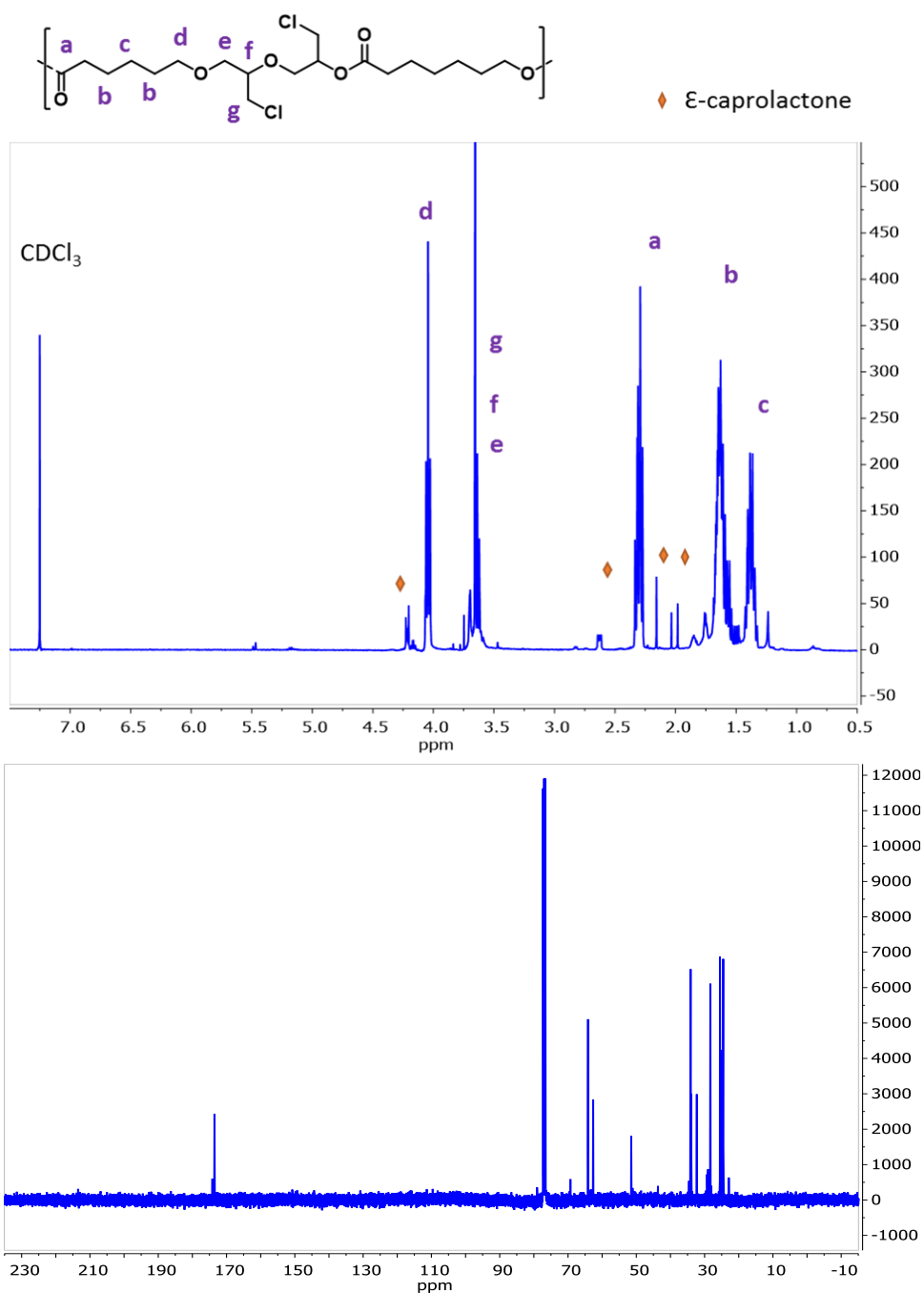


Figure A17  $^1\text{H}$  and  $^{13}\text{C}$  NMR spectra for poly[( $\epsilon$ -caprolactone) $_{0.67}$ -co-(epichlorohydrin) $_{0.33}$ ] in  $\text{CDCl}_3$

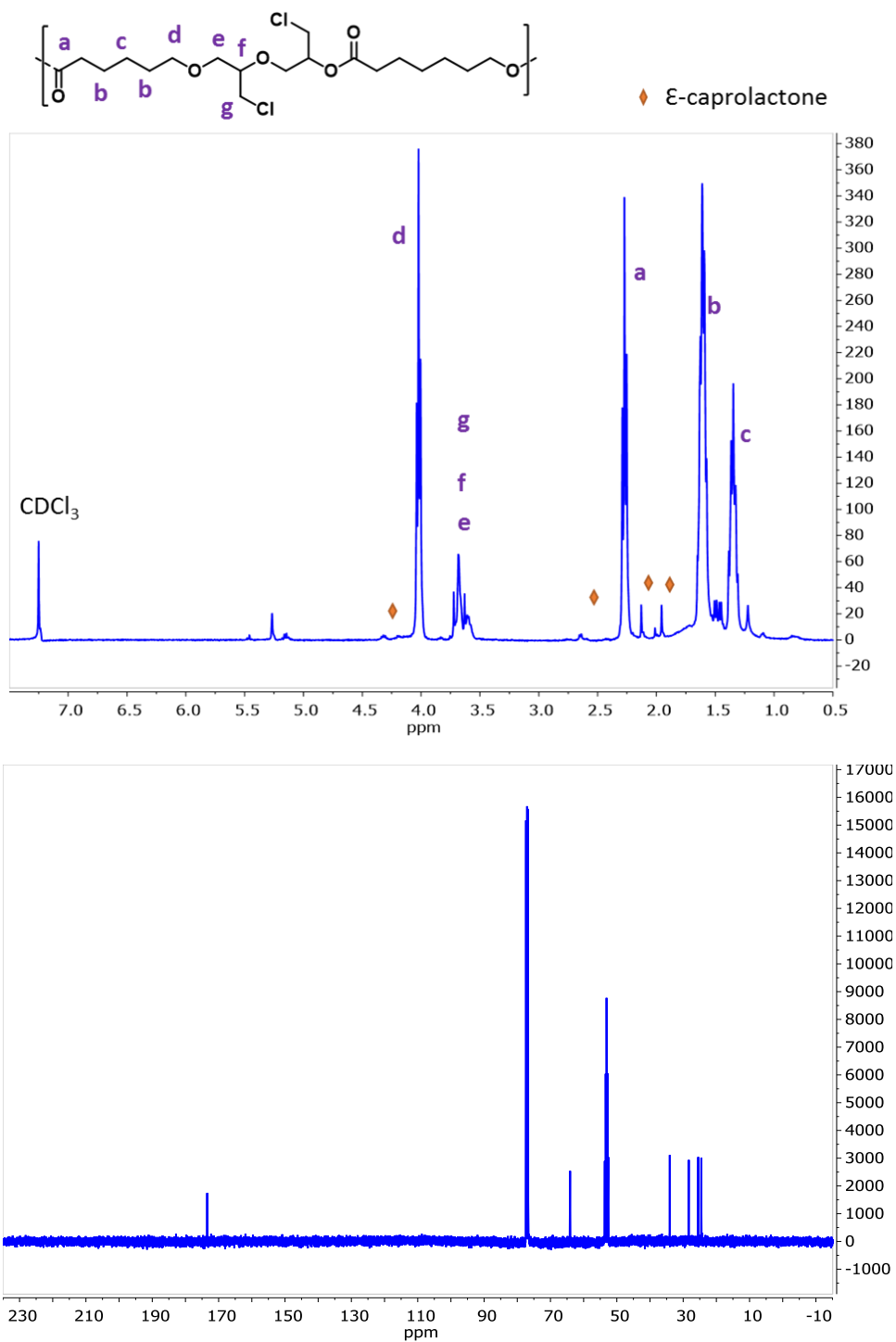


Figure A18  $^1\text{H}$  and  $^{13}\text{C}$  NMR spectra for poly[( $\epsilon$ -caprolactone) $_{0.93}$ -co-(epichlorohydrin) $_{0.07}$ ] in  $\text{CDCl}_3$



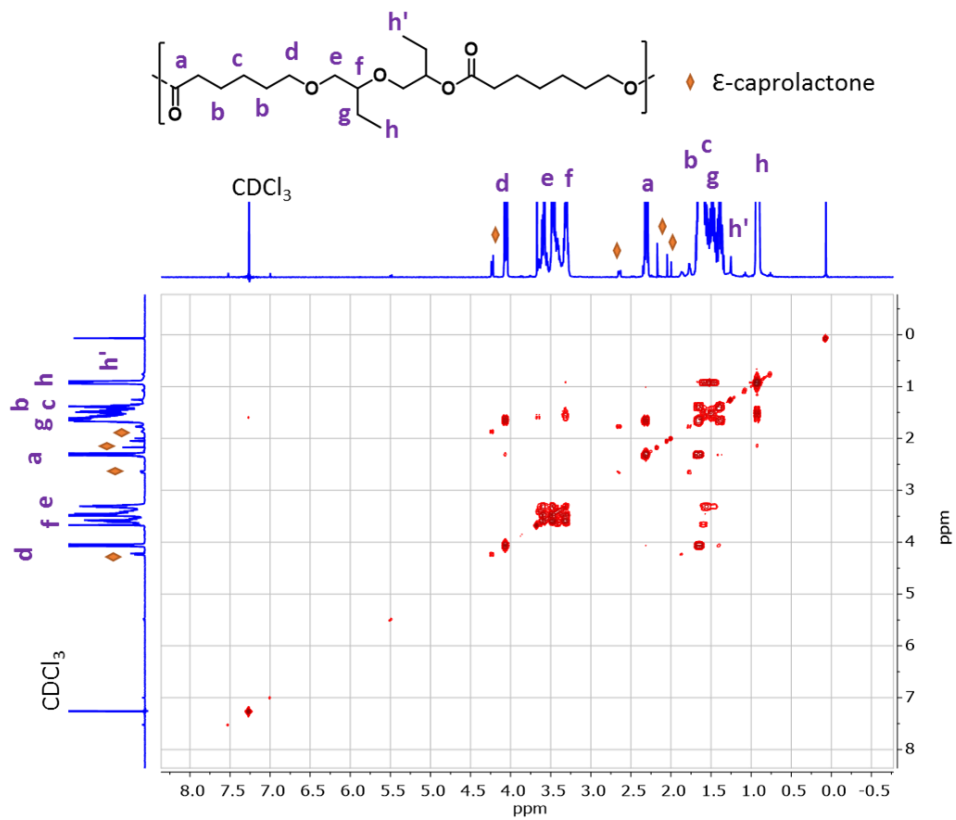


Figure A20 COSY(HH) NMR spectra for poly[( $\epsilon$ -caprolactone)<sub>0.29</sub>-co-(butylene oxide)<sub>0.71</sub>] in CDCl<sub>3</sub>

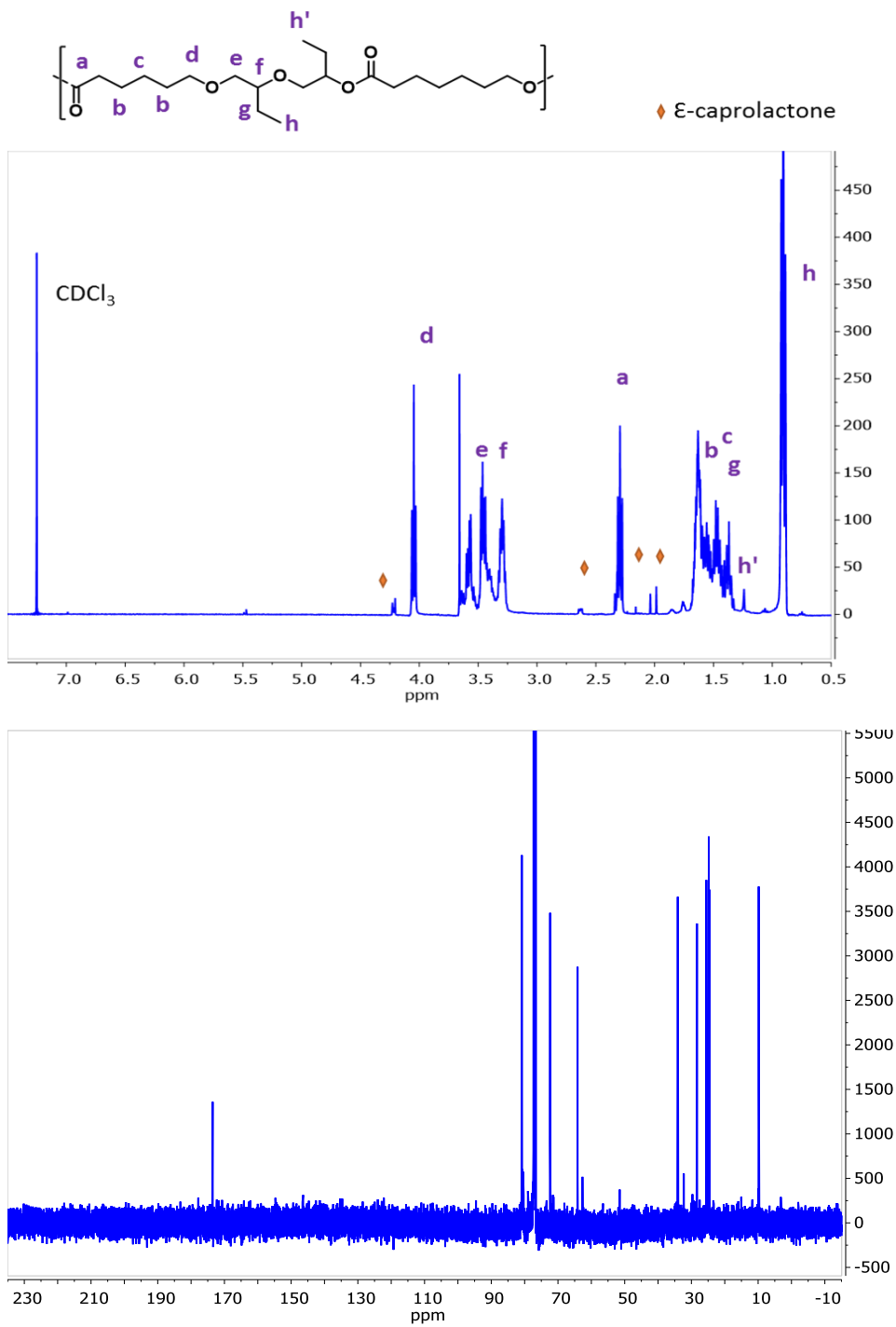


Figure A21  $^1\text{H}$  and  $^{13}\text{C}$  NMR spectra for poly[( $\epsilon$ -caprolactone) $_{0.32}$ -co-(butylene oxide) $_{0.68}$ ] in  $\text{CDCl}_3$

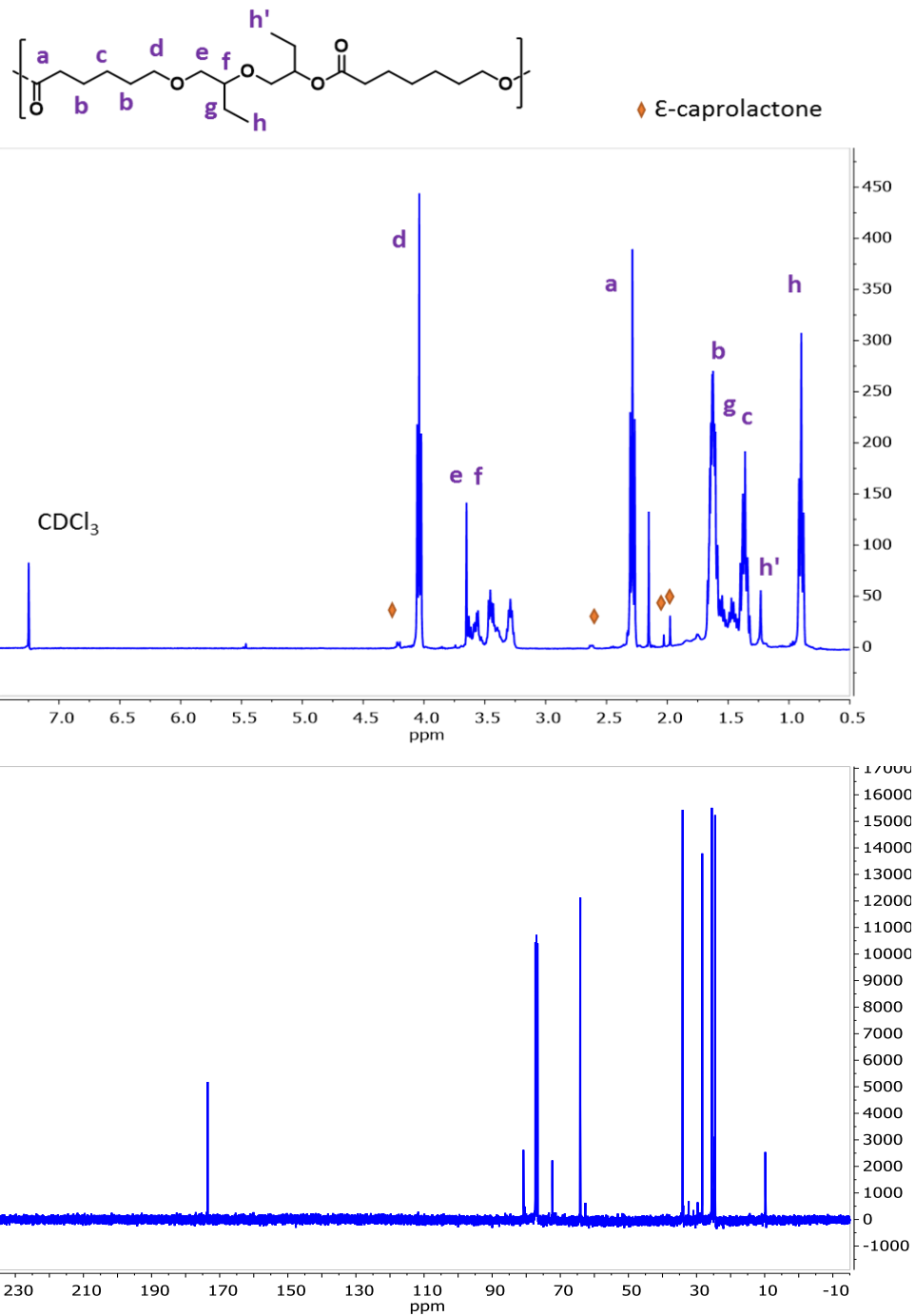


Figure A22  $^1\text{H}$  and  $^{13}\text{C}$  NMR spectra for poly[( $\epsilon$ -caprolactone) $_{0.59}$ -co-(butylene oxide) $_{0.41}$ ] in  $\text{CDCl}_3$

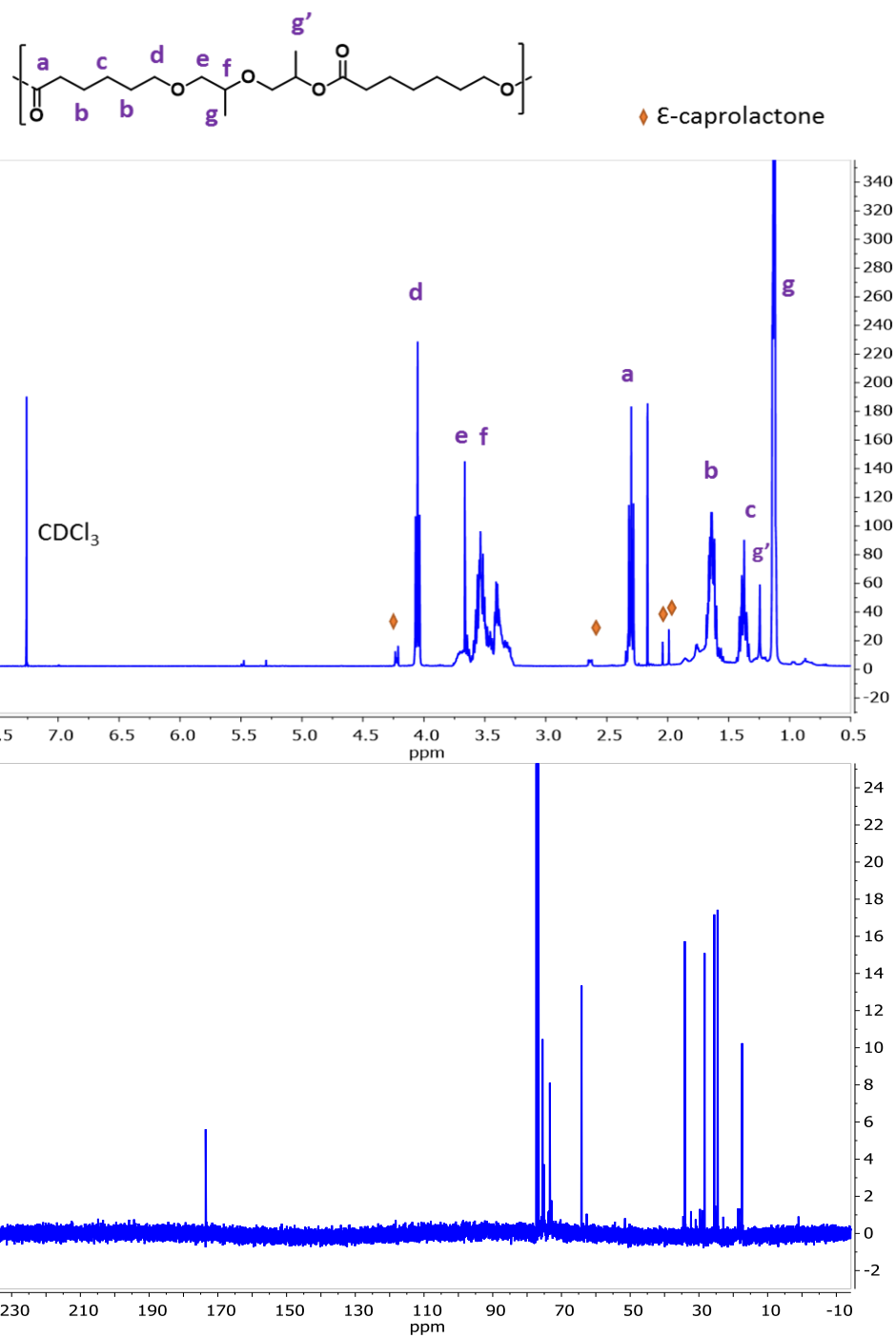


Figure A23  $^1\text{H}$  and  $^{13}\text{C}$  NMR spectra for poly[( $\epsilon$ -caprolactone)<sub>0.28</sub>-co-(propylene oxide)<sub>0.72</sub>] in  $\text{CDCl}_3$

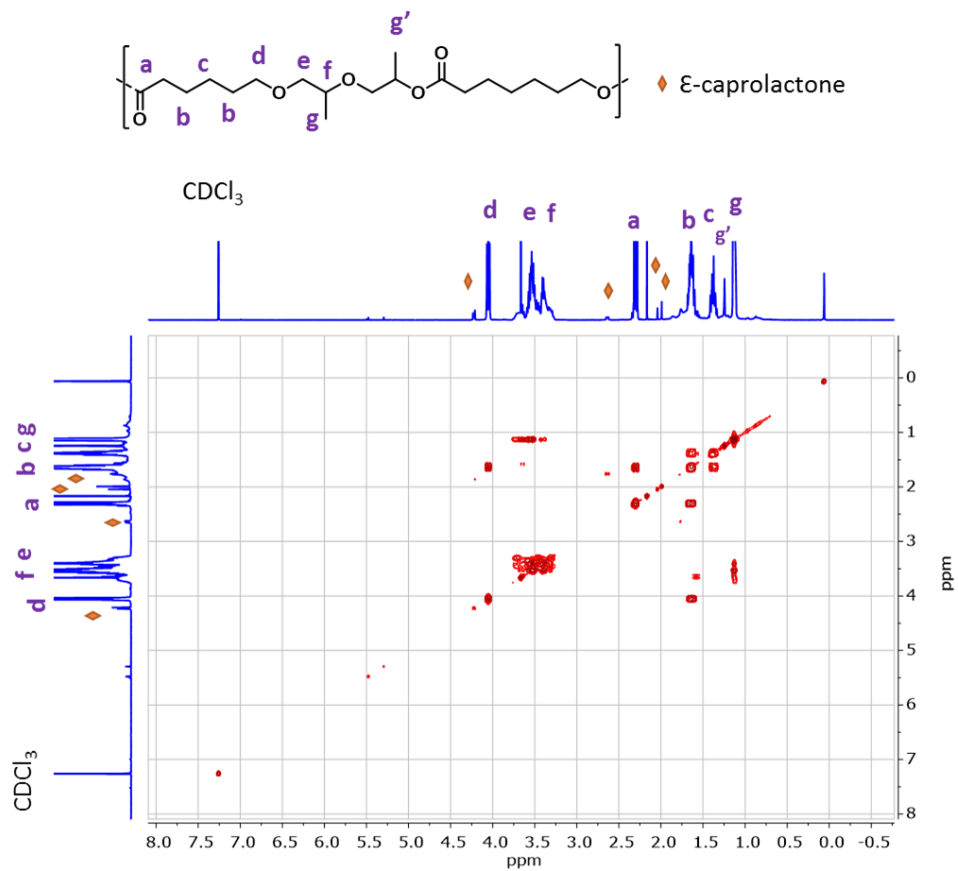


Figure A24 COSY(HH) NMR spectra for poly[( $\epsilon$ -caprolactone)<sub>0.28</sub>-co-(propylene oxide)<sub>0.72</sub>] in  $\text{CDCl}_3$

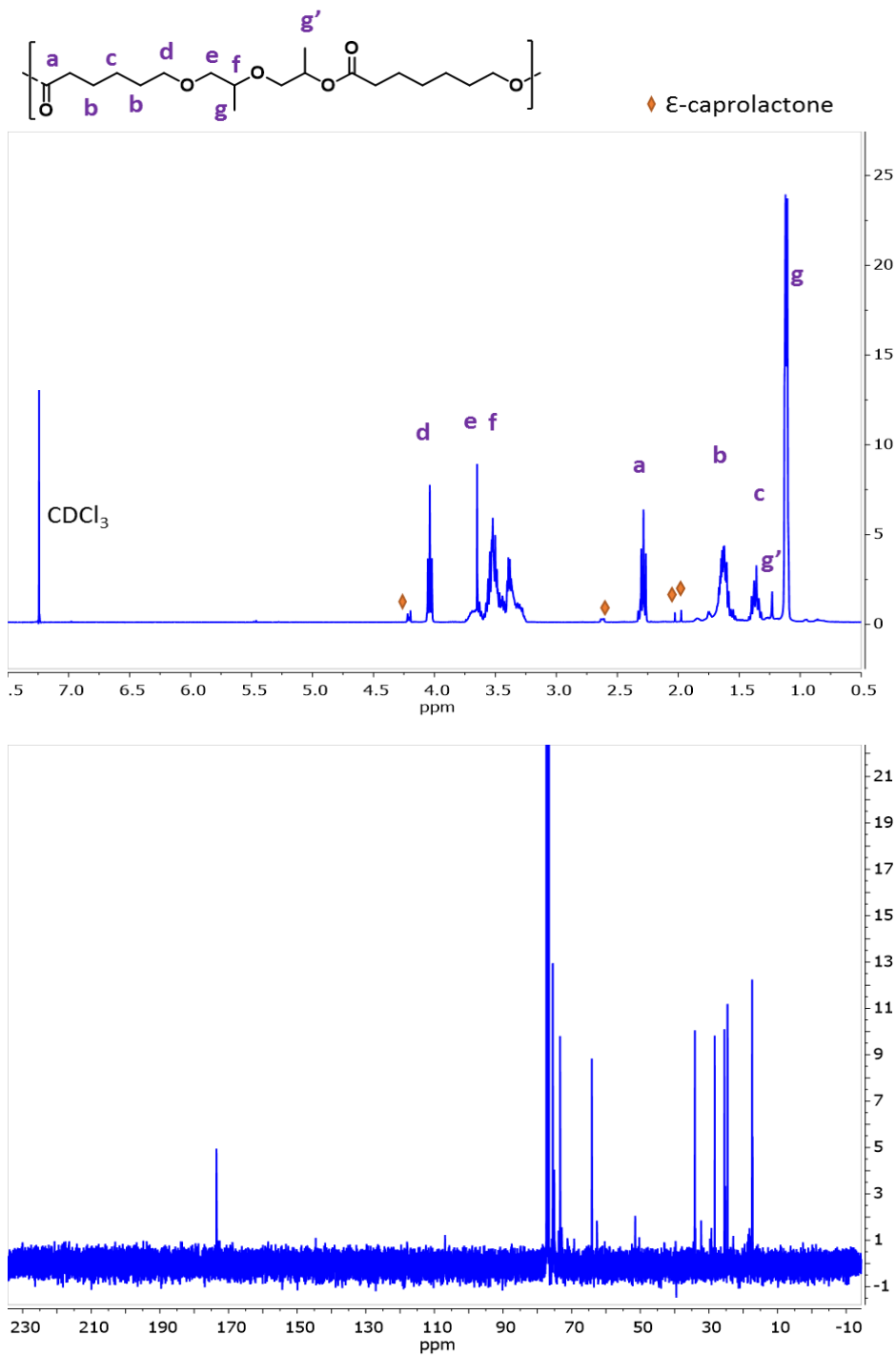


Figure A25  $^1\text{H}$  and  $^{13}\text{C}$  NMR spectra for poly[( $\epsilon$ -caprolactone) $_{0.20}$ -co-(propylene oxide) $_{0.80}$ ] in  $\text{CDCl}_3$

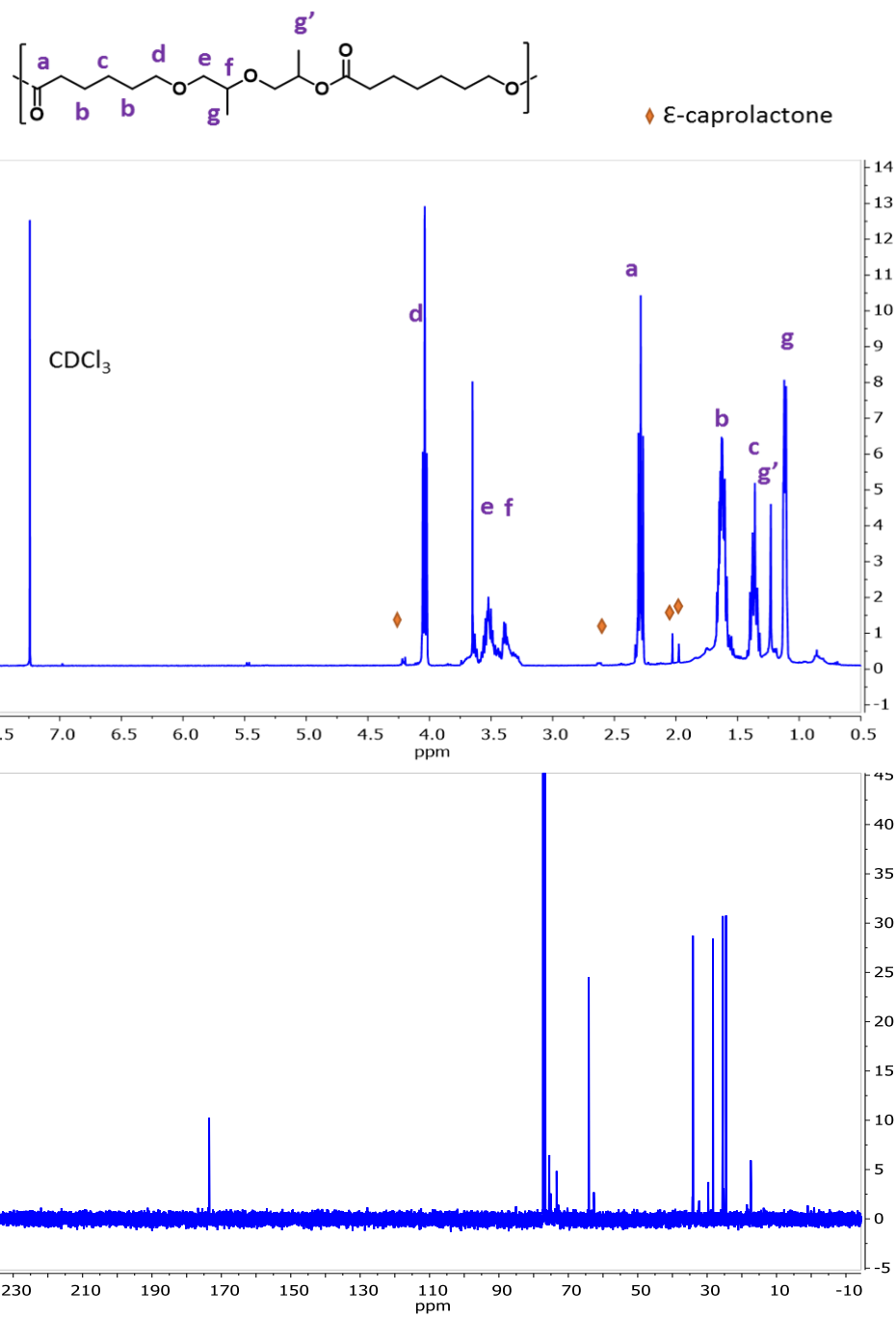


Figure A26  $^1\text{H}$  and  $^{13}\text{C}$  NMR spectra for poly[( $\epsilon$ -caprolactone) $_{0.51}$ -co-(propylene oxide) $_{0.49}$ ] in  $\text{CDCl}_3$

## **Appendix B**

Supporting Information for Chapter 3: Simple bis( $\mu$ -alkoxo-dialkylaluminum)  
initiators for hetero-copolymer synthesis via ring-opening

## METHODS

### Synthesis of a Bis( $\mu$ -alkoxo alkyl aluminum) species 2

A reaction vial was charged with a stir bar and triethylaluminum (12.7 mmol, 12.7 mL) and cooled to  $-78$  °C. 2-methoxyethanol was added drop-wise addition into the reaction vial. The solution was allowed to warm to RT and stirred overnight. The solution was cooled to  $-40$ °C to induce crystallization of the desired product. The resultant crystals were washed three times with anhydrous hexanes and dried *in vacuo*.

### Synthesis of a Bis- $\mu$ -alkoxo alkyl aluminum species 3

A reaction vial was charged with a stir bar and tri-isobutylaluminum (12.7 mmol, 12.7 mL) and cooled to  $-78$  °C. 2-methoxyethanol was added drop-wise addition into the reaction vial. The solution was allowed to warm to RT and stirred overnight. The solution was cooled to  $-40$  °C to induce crystallization of the desired product. The resultant crystals were washed three times with anhydrous hexanes and dried *in vacuo*.

### Synthesis of a Bis- $\mu$ -alkoxo alkyl aluminum species 4

A reaction vial was charged with a stir bar and tri-isopropylaluminum (12.7 mmol, 12.7 mL) and cooled to  $-78$  °C. 2-methoxypropanol was added drop-wise addition into the reaction vial. The solution was allowed to warm to RT and stirred overnight. The solution was cooled to  $-40$  °C to induce crystallization of the desired product. The resultant crystals were washed three times with anhydrous hexanes and dried *in vacuo*.

### Synthesis of a Bis- $\mu$ -alkoxo alkyl aluminum species 5

A reaction vial was charged with a stir bar and tri-isopropylaluminum (12.7 mmol, 12.7 mL) and cooled to  $-78$  °C. 2-(Tetrahydro-2H-pyran-2-yloxy)ethanol was added drop-wise addition into the reaction vial. The solution was allowed to warm to RT and stirred overnight. The solution was cooled to  $-40$  °C to induce crystallization of the desired product. The resultant crystals were washed three times with anhydrous hexanes and dried *in vacuo*.

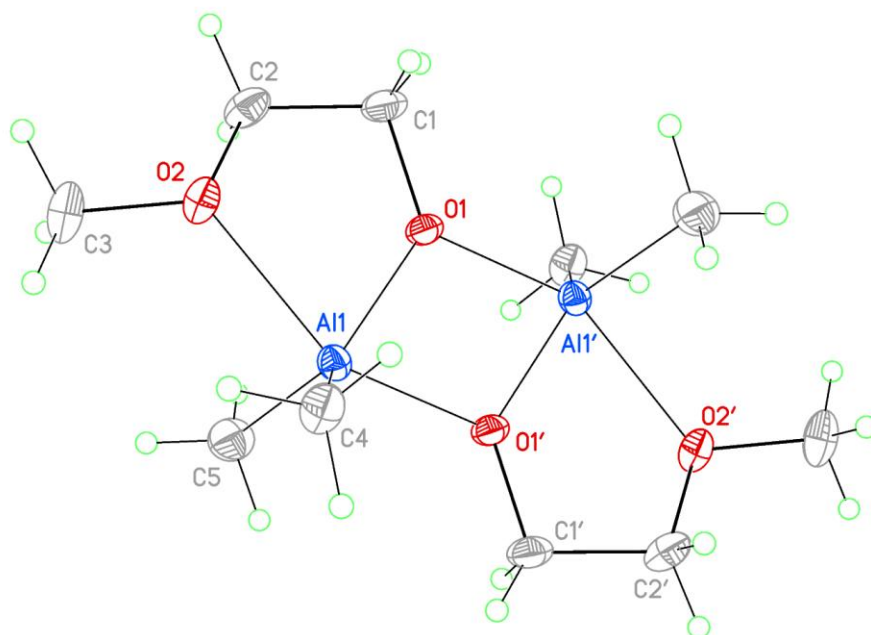


Figure B1 View of Methyl-EtGlycol BOD (species 1) showing the labeling scheme. Displacement ellipsoids are scaled to the 50% probability level. The complex resides around a crystallographic inversion center at  $\frac{1}{2}, \frac{1}{2}, \frac{1}{2}$ . Atoms with labels appended by a ` are related by  $1-x, 1-y, 1-z$ .

Table B1 Crystal data and structure refinement for Ethyl-EtGlycol BOD (species 2).

Empirical formula	C <sub>10</sub> H <sub>26</sub> Al <sub>2</sub> O <sub>4</sub>	
Formula weight	264.27	
Temperature	106(2) K	
Wavelength	0.71073 Å	
Crystal system	monoclinic	
Space group	P 21/n	
Unit cell dimensions	a = 7.3058(7) Å	α = 90°.
	b = 14.1227(12) Å	β = 101.761(3)°.
	c = 7.7679(7) Å	γ = 90°.
Volume	784.65(12) Å <sup>3</sup>	
Z	2	
Density (calculated)	1.119 Mg/m <sup>3</sup>	
Absorption coefficient	0.183 mm <sup>-1</sup>	
F(000)	288	
Crystal size	1.110 x 0.870 x 0.600 mm <sup>3</sup>	
Theta range for data collection	2.885 to 27.483°.	
Index ranges	-9<=h<=6, -18<=k<=18, -10<=l<=9	
Reflections collected	10541	
Independent reflections	1796 [R(int) = 0.0295]	
Completeness to theta = 25.242°	100.0 %	
Absorption correction	Semi-empirical from equivalents	
Max. and min. transmission	1.00 and 0.861	
Refinement method	Full-matrix least-squares on F <sup>2</sup>	
Data / restraints / parameters	1796 / 0 / 76	
Goodness-of-fit on F <sup>2</sup>	1.098	
Final R indices [I>2sigma(I)]	R1 = 0.0257, wR2 = 0.0715	
R indices (all data)	R1 = 0.0304, wR2 = 0.0739	
Extinction coefficient	n/a	
Largest diff. peak and hole	0.299 and -0.178 e.Å <sup>-3</sup>	

Table B2 Atomic coordinates ( $\times 10^4$ ) and equivalent isotropic displacement parameters ( $\text{\AA}^2 \times 10^3$ ) for Ethyl-EtGlycol BOD (species 2).  $U(\text{eq})$  is defined as one third of the trace of the orthogonalized  $U^{ij}$  tensor.

	x	y	z	U(eq)
C1	6967(2)	4480(1)	2779(2)	23(1)
C2	5955(2)	3672(1)	1731(2)	24(1)
C3	2855(2)	3268(1)	293(2)	28(1)
C4	1759(2)	5564(1)	2335(2)	22(1)
C5	2357(2)	3428(1)	4496(2)	26(1)
O1	5927(1)	4730(1)	4065(1)	18(1)
O2	4030(1)	3954(1)	1343(1)	20(1)
Al1	3377(1)	4617(1)	3754(1)	15(1)

Table B3 Bond lengths [ $\text{\AA}$ ] and angles [ $^\circ$ ] for Ethyl-EtGlycol BOD (species 2).

C1-O1	1.4175(12)	C4-H4A	0.98
C1-C2	1.5044(16)	C4-H4B	0.98
C1-H1A	0.99	C4-H4C	0.98
C1-H1B	0.99	C5-A11	1.9710(12)
C2-O2	1.4328(13)	C5-H5A	0.98
C2-H2A	0.99	C5-H5B	0.98
C2-H2B	0.99	C5-H5C	0.98
C3-O2	1.4334(13)	O1-A11	1.8360(8)
C3-H3A	0.98	O1-A11#1	1.9042(8)
C3-H3B	0.98	O2-A11	2.2311(8)
C3-H3C	0.98	A11-O1#1	1.9043(8)
C4-A11	1.9667(11)	A11-A11#1	2.9441(6)
O1-C1-C2	107.19(9)	H5A-C5-H5B	109.5
O1-C1-H1A	110.3	A11-C5-H5C	109.5
C2-C1-H1A	110.3	H5A-C5-H5C	109.5
O1-C1-H1B	110.3	H5B-C5-H5C	109.5
C2-C1-H1B	110.3	C1-O1-A11	124.10(7)
H1A-C1-H1B	108.5	C1-O1-A11#1	131.56(7)
O2-C2-C1	104.89(8)	A11-O1-A11#1	103.82(4)
O2-C2-H2A	110.8	C2-O2-C3	112.38(8)
C1-C2-H2A	110.8	C2-O2-A11	107.95(6)
O2-C2-H2B	110.8	C3-O2-A11	123.75(7)
C1-C2-H2B	110.8	O1-A11-O1#1	76.17(4)
H2A-C2-H2B	108.8	O1-A11-C4	119.50(5)
O2-C3-H3A	109.5	O1#1-A11-C4	100.99(4)
O2-C3-H3B	109.5	O1-A11-C5	118.02(5)
H3A-C3-H3B	109.5	O1#1-A11-C5	101.60(5)
O2-C3-H3C	109.5	C4-A11-C5	121.55(5)
H3A-C3-H3C	109.5	O1-A11-O2	76.24(3)
H3B-C3-H3C	109.5	O1#1-A11-O2	152.37(3)
A11-C4-H4A	109.5	C4-A11-O2	91.24(4)
A11-C4-H4B	109.5	C5-A11-O2	92.62(4)
H4A-C4-H4B	109.5	O1-A11-A11#1	38.91(2)
A11-C4-H4C	109.5	O1#1-A11-A11#1	37.27(2)
H4A-C4-H4C	109.5	C4-A11-A11#1	115.49(4)
H4B-C4-H4C	109.5	C5-A11-A11#1	115.02(4)
A11-C5-H5A	109.5	O2-A11-A11#1	115.13(3)
A11-C5-H5B	109.5		

Symmetry transformations used to generate equivalent atoms:

#1 -x+1,-y+1,-z+1

Table B4 Anisotropic displacement parameters ( $\text{\AA}^2 \times 10^3$ ) for Ethyl-EtGlycol BOD (species 2). The anisotropic displacement factor exponent takes the form:  $-2\pi^2 [ h^2 a^{*2} U^{11} + \dots + 2 h k a^* b^* U^{12} ]$

	U11	U22	U33	U23	U13	U12
C1	20(1)	31(1)	21(1)	-3(1)	10(1)	2(1)
C2	26(1)	25(1)	21(1)	-4(1)	7(1)	8(1)
C3	37(1)	22(1)	22(1)	-6(1)	-4(1)	-2(1)
C4	23(1)	21(1)	21(1)	-2(1)	0(1)	4(1)
C5	31(1)	21(1)	30(1)	1(1)	12(1)	-2(1)
O1	14(1)	27(1)	14(1)	-5(1)	4(1)	1(1)
O2	23(1)	17(1)	17(1)	-3(1)	0(1)	2(1)
Al1	13(1)	16(1)	15(1)	0(1)	1(1)	0(1)

Table B5 Hydrogen coordinates ( $\times 10^4$ ) and isotropic displacement parameters ( $\text{\AA}^2 \times 10^3$ ) for Ethyl-EtGlycol BOD (species 2).

	x	y	z	U(eq)
H1A	8247	4284	3352	27
H1B	7056	5026	2002	27
H2A	6423	3573	636	28
H2B	6120	3079	2425	28
H3A	3240	3194	-836	43
H3B	1552	3482	88	43
H3C	2969	2659	910	43
H4A	2519	6102	2101	34
H4B	816	5782	2978	34
H4C	1137	5278	1219	34
H5A	3380	2982	4905	40
H5B	1480	3151	3498	40
H5C	1702	3558	5453	40

Table B6 Torsion angles [°] for Ethyl-EtGlycol BOD (species 2).

---

O1-C1-C2-O2	46.06(11)
C2-C1-O1-Al1	-31.22(12)
C2-C1-O1-Al1#1	158.40(7)
C1-C2-O2-C3	178.35(9)
C1-C2-O2-Al1	-41.74(9)
C1-O1-Al1-O1#1	-172.60(10)
Al1#1-O1-Al1-O1#1	0.003(1)
C1-O1-Al1-C4	-77.65(9)
Al1#1-O1-Al1-C4	94.95(5)
C1-O1-Al1-C5	91.46(9)
Al1#1-O1-Al1-C5	-95.94(5)
C1-O1-Al1-O2	5.87(8)
Al1#1-O1-Al1-O2	178.47(4)
C1-O1-Al1-Al1#1	-172.60(10)

---

Symmetry transformations used to generate equivalent atoms:

#1 -x+1,-y+1,-z+1

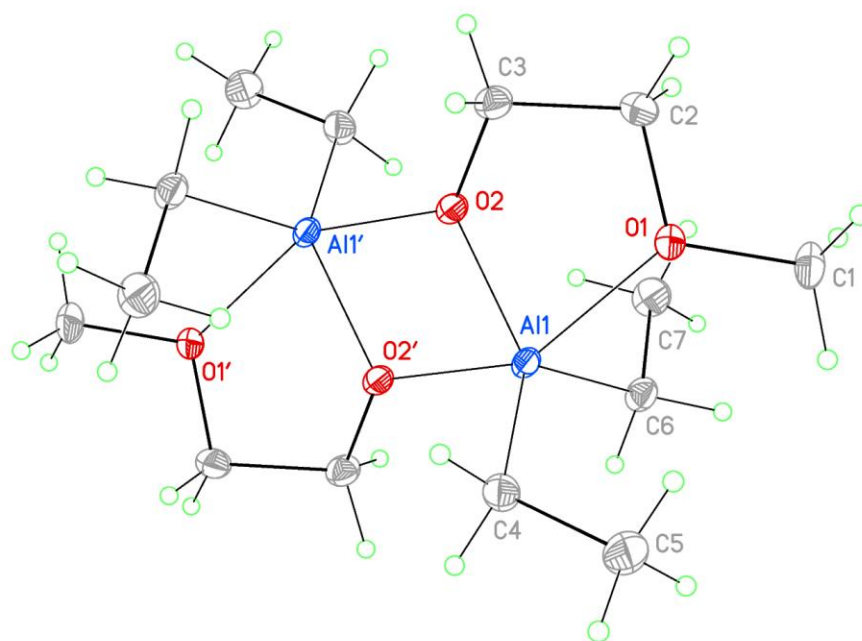


Figure B2 View of Ethyl-EtGlycol BOD (species 2). showing the atom labeling scheme. Displacement ellipsoids are scaled to the 50% probability level. The complex resides around a crystallographic inversion center at  $\frac{1}{2}, \frac{1}{2}, \frac{1}{2}$ . Atoms with labels appended by a ' are related by  $1-x, 1-y, 1-z$ .

Table B7 Crystal data and structure refinement for Ethyl-EtGlycol BOD (species 2).

Empirical formula	C <sub>14</sub> H <sub>34</sub> Al <sub>2</sub> O <sub>4</sub>	
Formula weight	320.37	
Temperature	100(2) K	
Wavelength	0.71073 Å	
Crystal system	monoclinic	
Space group	P 21/n	
Unit cell dimensions	a = 8.9134(8) Å	α = 90°.
	b = 7.5787(6) Å	β = 106.855(2)°.
	c = 14.5088(12) Å	γ = 90°.
Volume	937.99(14) Å <sup>3</sup>	
Z	2	
Density (calculated)	1.134 Mg/m <sup>3</sup>	
Absorption coefficient	0.164 mm <sup>-1</sup>	
F(000)	352	
Crystal size	1.170 x 0.650 x 0.480 mm <sup>3</sup>	
Theta range for data collection	2.413 to 27.571°.	
Index ranges	-11 ≤ h ≤ 11, -9 ≤ k ≤ 8, -18 ≤ l ≤ 11	
Reflections collected	13048	
Independent reflections	2152 [R(int) = 0.0317]	
Completeness to theta = 25.242°	100.0 %	
Absorption correction	Semi-empirical from equivalents	
Max. and min. transmission	1.00 and 0.858	
Refinement method	Full-matrix least-squares on F <sup>2</sup>	
Data / restraints / parameters	2152 / 0 / 94	
Goodness-of-fit on F <sup>2</sup>	1.038	
Final R indices [I > 2σ(I)]	R1 = 0.0259, wR2 = 0.0693	
R indices (all data)	R1 = 0.0299, wR2 = 0.0714	
Extinction coefficient	n/a	
Largest diff. peak and hole	0.330 and -0.165 e.Å <sup>-3</sup>	

Table B8 Atomic coordinates ( $\times 10^4$ ) and equivalent isotropic displacement parameters ( $\text{\AA}^2 \times 10^3$ ) for Ethyl-EtGlycol BOD (species 2).  $U(\text{eq})$  is defined as one third of the trace of the orthogonalized  $U^{ij}$  tensor.

	x	y	z	U(eq)
C1	3677(1)	9053(2)	6813(1)	20(1)
C2	5999(1)	8668(1)	6338(1)	18(1)
C3	6500(1)	7888(1)	5516(1)	16(1)
C4	1902(1)	6682(1)	4344(1)	16(1)
C5	740(1)	7903(2)	4625(1)	24(1)
C6	3452(1)	4651(1)	6525(1)	15(1)
C7	4973(1)	4099(2)	7286(1)	21(1)
O1	4330(1)	8413(1)	6079(1)	15(1)
O2	5735(1)	6236(1)	5290(1)	13(1)
All	3740(1)	5769(1)	5354(1)	11(1)

Table B9 Bond lengths [ $\text{\AA}$ ] and angles [ $^\circ$ ] for Ethyl-EtGlycol BOD (species 2).

C1-O1	1.4381(12)	C5-H5A	0.98
C1-H1A	0.98	C5-H5B	0.98
C1-H1B	0.98	C5-H5C	0.98
C1-H1C	0.98	C6-C7	1.5377(14)
C2-O1	1.4377(12)	C6-Al1	1.9808(10)
C2-C3	1.5089(14)	C6-H6A	0.99
C2-H2A	0.99	C6-H6B	0.99
C2-H2B	0.99	C7-H7A	0.98
C3-O2	1.4177(12)	C7-H7B	0.98
C3-H3A	0.99	C7-H7C	0.98
C3-H3B	0.99	O1-Al1	2.2535(8)
C4-C5	1.5303(15)	O2-Al1	1.8419(7)
C4-Al1	1.9791(10)	O2-Al1#1	1.9118(8)
C4-H4A	0.99	Al1-O2#1	1.9118(8)
C4-H4B	0.99	Al1-Al1#1	2.9661(6)
O1-C1-H1A	109.5	C5-C4-Al1	119.56(7)
O1-C1-H1B	109.5	C5-C4-H4A	107.4
H1A-C1-H1B	109.5	Al1-C4-H4A	107.4
O1-C1-H1C	109.5	C5-C4-H4B	107.4
H1A-C1-H1C	109.5	Al1-C4-H4B	107.4
H1B-C1-H1C	109.5	H4A-C4-H4B	107.0
O1-C2-C3	105.21(8)	C4-C5-H5A	109.5
O1-C2-H2A	110.7	C4-C5-H5B	109.5
C3-C2-H2A	110.7	H5A-C5-H5B	109.5
O1-C2-H2B	110.7	C4-C5-H5C	109.5
C3-C2-H2B	110.7	H5A-C5-H5C	109.5
H2A-C2-H2B	108.8	H5B-C5-H5C	109.5
O2-C3-C2	107.23(8)	C7-C6-Al1	115.22(7)
O2-C3-H3A	110.3	C7-C6-H6A	108.5
C2-C3-H3A	110.3	Al1-C6-H6A	108.5
O2-C3-H3B	110.3	C7-C6-H6B	108.5
C2-C3-H3B	110.3	Al1-C6-H6B	108.5
H3A-C3-H3B	108.5	H6A-C6-H6B	107.5

C6-C7-H7A	109.5	O2-A11-C4	119.98(4)
C6-C7-H7B	109.5	O2#1-A11-C4	100.54(4)
H7A-C7-H7B	109.5	O2-A11-C6	119.49(4)
C6-C7-H7C	109.5	O2#1-A11-C6	100.97(4)
H7A-C7-H7C	109.5	C4-A11-C6	119.96(4)
H7B-C7-H7C	109.5	O2-A11-O1	75.79(3)
C2-O1-C1	111.84(8)	O2#1-A11-O1	151.40(3)
C2-O1-A11	108.96(6)	C4-A11-O1	93.79(4)
C1-O1-A11	123.80(6)	C6-A11-O1	92.89(4)
C3-O2-A11	124.36(6)	O2-A11-A11#1	38.63(2)
C3-O2-A11#1	130.22(6)	O2#1-A11-A11#1	36.98(2)
A11-O2-A11#1	104.39(3)	C4-A11-A11#1	115.36(3)
		C6-A11-A11#1	115.36(3)
O2-A11-O2#1	75.61(3)	O1-A11-A11#1	114.43(2)

---

Symmetry transformations used to generate equivalent atoms:

#1 -x+1,-y+1,-z+1

Table B10 Anisotropic displacement parameters ( $\text{\AA}^2 \times 10^3$ ) for Ethyl-EtGlycol BOD (species 2).  
 The anisotropic displacement factor exponent takes the form:  $-2\pi^2 [ h^2 a^{*2} U^{11} + \dots + 2 h k a^* b^* U^{12} ]$

	U11	U22	U33	U23	U13	U12
C1	22(1)	23(1)	17(1)	-6(1)	10(1)	2(1)
C2	14(1)	19(1)	20(1)	-6(1)	4(1)	-3(1)
C3	15(1)	15(1)	20(1)	-2(1)	7(1)	-3(1)
C4	14(1)	19(1)	14(1)	-1(1)	2(1)	3(1)
C5	15(1)	31(1)	23(1)	-3(1)	3(1)	7(1)
C6	15(1)	19(1)	14(1)	2(1)	6(1)	0(1)
C7	20(1)	26(1)	16(1)	4(1)	4(1)	2(1)
O1	13(1)	19(1)	13(1)	-4(1)	5(1)	0(1)
O2	11(1)	13(1)	16(1)	-2(1)	6(1)	-1(1)
Al1	9(1)	15(1)	10(1)	1(1)	4(1)	1(1)

Table B11 Hydrogen coordinates ( $\times 10^4$ ) and isotropic displacement parameters ( $\text{\AA}^2 \times 10^3$ ) for Ethyl-EtGlycol BOD (species 2).

	x	y	z	U(eq)
H1A	4196	8471	7426	30
H1B	2552	8795	6630	30
H1C	3838	10331	6885	30
H2A	6522	8056	6949	21
H2B	6262	9939	6413	21
H3A	6197	8680	4950	19
H3B	7651	7728	5708	19
H4A	2302	7318	3867	19
H4B	1306	5651	4008	19
H5A	355	7330	5118	35
H5B	-145	8151	4056	35
H5C	1264	9011	4880	35
H6A	2879	5485	6826	18
H6B	2785	3592	6329	18
H7A	5594	3346	6987	31
H7B	4715	3445	7803	31
H7C	5580	5153	7554	31

Table B12 Torsion angles [°] for Ethyl-EtGlycol BOD (species 2).

---

O1-C2-C3-O2	-45.31(11)
C3-C2-O1-C1	178.40(8)
C3-C2-O1-A11	37.92(9)
C2-C3-O2-A11	35.41(11)
C2-C3-O2-A11#1	-158.07(7)
C3-O2-A11-O2#1	169.42(9)
A11#1-O2-A11-O2#1	0.001(1)
C3-O2-A11-C4	75.40(8)
A11#1-O2-A11-C4	-94.02(5)
C3-O2-A11-C6	-95.96(8)
A11#1-O2-A11-C6	94.62(5)
C3-O2-A11-O1	-10.75(7)
A11#1-O2-A11-O1	179.84(4)
C3-O2-A11-A11#1	169.42(9)

---

Symmetry transformations used to generate equivalent atoms:

#1 -x+1,-y+1,-z+1

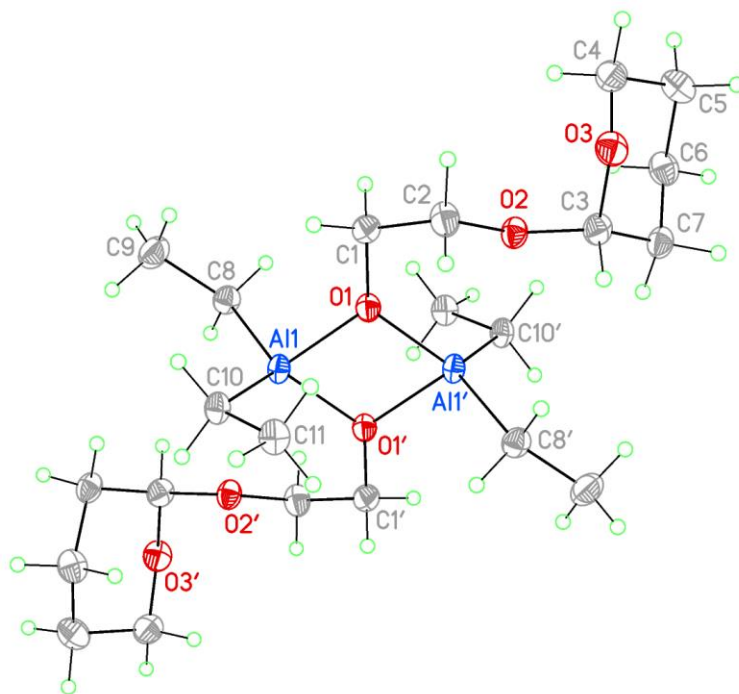


Figure B3 View of Ethyl-THP BOD (species 5) showing the heteroatom labeling scheme. Displacement ellipsoids are scaled to the 50% probability level. The complex sits around a crystallographic inversion center at  $\frac{1}{2}, \frac{1}{2}, \frac{1}{2}$ . Atoms with labels appended by a ' are related by  $1-x, 1-y, 1-z$ .

Table B13 Crystal data and structure refinement for Ethyl-THP BOD (species 5).

Empirical formula	C <sub>22</sub> H <sub>46</sub> Al <sub>2</sub> O <sub>6</sub>
Formula weight	460.55
Temperature	100(2) K
Wavelength	1.54184 Å
Crystal system	monoclinic
Space group	P 21/c
Unit cell dimensions	a = 9.50410(10) Å      α = 90°. b = 16.0805(2) Å      β = 92.1070(10)°. c = 8.49550(10) Å      γ = 90°.
Volume	1297.50(3) Å <sup>3</sup>
Z	2
Density (calculated)	1.179 Mg/m <sup>3</sup>
Absorption coefficient	1.275 mm <sup>-1</sup>
F(000)	504
Crystal size	0.560 x 0.190 x 0.150 mm <sup>3</sup>
Theta range for data collection	4.656 to 73.499°.
Index ranges	-11 ≤ h ≤ 11, -19 ≤ k ≤ 19, -10 ≤ l ≤ 9
Reflections collected	11729
Independent reflections	2581 [R(int) = 0.0200]
Completeness to theta = 67.684°	100.0 %
Absorption correction	Semi-empirical from equivalents
Max. and min. transmission	1.00 and 0.714
Refinement method	Full-matrix least-squares on F <sup>2</sup>
Data / restraints / parameters	2581 / 0 / 138
Goodness-of-fit on F <sup>2</sup>	1.061
Final R indices [I > 2σ(I)]	R1 = 0.0318, wR2 = 0.0802
R indices (all data)	R1 = 0.0322, wR2 = 0.0804
Extinction coefficient	n/a
Largest diff. peak and hole	0.292 and -0.247 e.Å <sup>-3</sup>

Table B14 Atomic coordinates ( $\times 10^4$ ) and equivalent isotropic displacement parameters ( $\text{\AA}^2 \times 10^3$ ) for Ethyl-THP BOD (species 5).  $U(\text{eq})$  is defined as one third of the trace of the orthogonalized  $U^{ij}$  tensor.

	x	y	z	U(eq)
C1	4754(1)	6490(1)	6114(2)	23(1)
C2	5294(1)	6537(1)	7793(2)	26(1)
C3	7359(1)	6208(1)	9352(1)	23(1)
C4	8121(2)	7617(1)	9334(2)	28(1)
C5	9657(2)	7371(1)	9281(2)	31(1)
C6	9792(1)	6536(1)	8444(2)	27(1)
C7	8852(1)	5896(1)	9199(1)	23(1)
C8	4014(1)	5781(1)	2021(1)	22(1)
C9	2857(2)	6430(1)	1685(2)	33(1)
C10	1926(1)	5041(1)	4908(1)	21(1)
C11	1961(1)	4834(1)	6676(2)	24(1)
Al1	3783(1)	5134(1)	3972(1)	18(1)
O1	4906(1)	5666(1)	5537(1)	19(1)
O2	6715(1)	6236(1)	7804(1)	21(1)
O3	7303(1)	6991(1)	10088(1)	26(1)

Table B15 Bond lengths [ $\text{\AA}$ ] and angles [ $^\circ$ ] for Ethyl-THP BOD (species 5).

C1-O1	1.4222(14)	C6-H6B	0.99
C1-C2	1.5001(18)	C7-H7A	0.99
C1-H1A	0.99	C7-H7B	0.99
C1-H1B	0.99	C8-C9	1.5357(18)
C2-O2	1.4340(15)	C8-Al1	1.9756(12)
C2-H2A	0.99	C8-H8A	0.99
C2-H2B	0.99	C8-H8B	0.99
C3-O3	1.4072(15)	C9-H9A	0.98
C3-O2	1.4310(15)	C9-H9B	0.98
C3-C7	1.5153(17)	C9-H9C	0.98
C3-H3	1.00	C10-C11	1.5376(17)
C4-O3	1.4375(17)	C10-Al1	1.9682(12)
C4-C5	1.515(2)	C10-H10A	0.99
C4-H4A	0.99	C10-H10B	0.99
C4-H4B	0.99	C11-H11A	0.98
C5-C6	1.5274(19)	C11-H11B	0.98
C5-H5A	0.99	C11-H11C	0.98
C5-H5B	0.99	Al1-O1#1	1.8280(9)
C6-C7	1.5202(19)	Al1-O1	1.8804(9)
C6-H6A	0.99	O1-Al1#1	1.8280(9)
O1-C1-C2	109.81(10)	H2A-C2-H2B	108.7
O1-C1-H1A	109.7	O3-C3-O2	110.98(10)
C2-C1-H1A	109.7	O3-C3-C7	112.67(11)
O1-C1-H1B	109.7	O2-C3-C7	107.57(10)
C2-C1-H1B	109.7	O3-C3-H3	108.5
H1A-C1-H1B	108.2	O2-C3-H3	108.5
O2-C2-C1	106.16(10)	C7-C3-H3	108.5
O2-C2-H2A	110.5	O3-C4-C5	111.59(11)
C1-C2-H2A	110.5	O3-C4-H4A	109.3
O2-C2-H2B	110.5	C5-C4-H4A	109.3
C1-C2-H2B	110.5	O3-C4-H4B	109.3

C5-C4-H4B	109.3	H9A-C9-H9B	109.5
H4A-C4-H4B	108.0	C8-C9-H9C	109.5
C4-C5-C6	109.92(11)	H9A-C9-H9C	109.5
C4-C5-H5A	109.7	H9B-C9-H9C	109.5
C6-C5-H5A	109.7	C11-C10-A11	115.05(8)
C4-C5-H5B	109.7	C11-C10-H10A	108.5
C6-C5-H5B	109.7	A11-C10-H10A	108.5
H5A-C5-H5B	108.2	C11-C10-H10B	108.5
C7-C6-C5	109.78(11)	A11-C10-H10B	108.5
C7-C6-H6A	109.7	H10A-C10-H10B	107.5
C5-C6-H6A	109.7	C10-C11-H11A	109.5
C7-C6-H6B	109.7	C10-C11-H11B	109.5
C5-C6-H6B	109.7	H11A-C11-H11B	109.5
H6A-C6-H6B	108.2	C10-C11-H11C	109.5
C3-C7-C6	112.23(11)	H11A-C11-H11C	109.5
C3-C7-H7A	109.2	H11B-C11-H11C	109.5
C6-C7-H7A	109.2	O1#1-A11-O1	78.11(4)
C3-C7-H7B	109.2	O1#1-A11-C10	117.91(5)
C6-C7-H7B	109.2	O1-A11-C10	104.06(5)
H7A-C7-H7B	107.9	O1#1-A11-C8	117.76(5)
C9-C8-A11	114.38(9)	O1-A11-C8	106.05(5)
C9-C8-H8A	108.7	C10-A11-C8	120.54(5)
A11-C8-H8A	108.7	C1-O1-A11#1	130.84(7)
C9-C8-H8B	108.7	C1-O1-A11	127.25(7)
A11-C8-H8B	108.7	A11#1-O1-A11	101.89(4)
H8A-C8-H8B	107.6	C3-O2-C2	112.82(9)
C8-C9-H9A	109.5	C3-O3-C4	113.53(10)
C8-C9-H9B	109.5		

---

Symmetry transformations used to generate equivalent atoms:

#1 -x+1,-y+1,-z+1

Table B16 Anisotropic displacement parameters ( $\text{\AA}^2 \times 10^3$ ) for Ethyl-THP BOD (species 5). The anisotropic displacement factor exponent takes the form:  $-2\pi^2 [ h^2 a^{*2} U^{11} + \dots + 2 h k a^* b^* U^{12} ]$

	U11	U22	U33	U23	U13	U12
C1	24(1)	20(1)	26(1)	-1(1)	-3(1)	3(1)
C2	22(1)	29(1)	26(1)	-7(1)	-2(1)	6(1)
C3	28(1)	24(1)	16(1)	0(1)	0(1)	1(1)
C4	36(1)	23(1)	24(1)	-4(1)	-4(1)	3(1)
C5	32(1)	31(1)	30(1)	-6(1)	0(1)	-5(1)
C6	26(1)	32(1)	24(1)	-4(1)	1(1)	0(1)
C7	26(1)	25(1)	18(1)	-1(1)	-3(1)	5(1)
C8	23(1)	24(1)	19(1)	3(1)	2(1)	0(1)
C9	30(1)	30(1)	38(1)	13(1)	-1(1)	2(1)
C10	17(1)	26(1)	18(1)	1(1)	1(1)	2(1)
C11	22(1)	30(1)	19(1)	0(1)	3(1)	1(1)
Al1	15(1)	24(1)	15(1)	2(1)	0(1)	2(1)
O1	18(1)	21(1)	18(1)	-2(1)	-1(1)	2(1)
O2	22(1)	24(1)	18(1)	-2(1)	-2(1)	4(1)
O3	29(1)	27(1)	22(1)	-6(1)	0(1)	4(1)

Table B17 Hydrogen coordinates (  $\times 10^4$ ) and isotropic displacement parameters ( $\text{\AA}^2 \times 10^3$ ) for Ethyl-THP BOD (species 5).

	x	y	z	U(eq)
H1A	3750	6653	6046	28
H1B	5288	6880	5460	28
H2A	5269	7118	8178	31
H2B	4713	6188	8476	31
H3	6834	5799	9996	27
H4A	8043	8148	9914	34
H4B	7740	7706	8247	34
H5A	10067	7329	10367	37
H5B	10184	7802	8715	37
H6A	9513	6599	7316	33
H6B	10783	6347	8517	33
H7A	8836	5383	8554	28
H7B	9252	5753	10257	28
H8A	4936	6068	2091	26
H8B	4032	5390	1120	26
H9A	3042	6721	700	49
H9B	2849	6831	2552	49
H9C	1941	6151	1587	49
H10A	1418	5573	4743	25
H10B	1380	4603	4337	25
H11A	2444	4302	6855	36
H11B	996	4795	7038	36
H11C	2466	5274	7262	36

Table B18 Torsion angles [°] for Ethyl-THP BOD (species 5).

---

O1-C1-C2-O2	55.34(13)
O3-C4-C5-C6	56.83(14)
C4-C5-C6-C7	-52.99(15)
O3-C3-C7-C6	-51.48(14)
O2-C3-C7-C6	71.14(13)
C5-C6-C7-C3	50.50(14)
C2-C1-O1-Al1#1	-31.08(15)
C2-C1-O1-Al1	151.15(8)
O1#1-Al1-O1-C1	178.27(11)
C10-Al1-O1-C1	-65.60(10)
C8-Al1-O1-C1	62.50(10)
O1#1-Al1-O1-Al1#1	-0.001(1)
C10-Al1-O1-Al1#1	116.13(5)
C8-Al1-O1-Al1#1	-115.77(5)
O3-C3-O2-C2	-55.39(13)
C7-C3-O2-C2	-179.06(10)
C1-C2-O2-C3	-177.40(10)
O2-C3-O3-C4	-65.58(13)
C7-C3-O3-C4	55.12(13)
C5-C4-O3-C3	-58.45(14)

---

Symmetry transformations used to generate equivalent atoms:

#1 -x+1,-y+1,-z+1

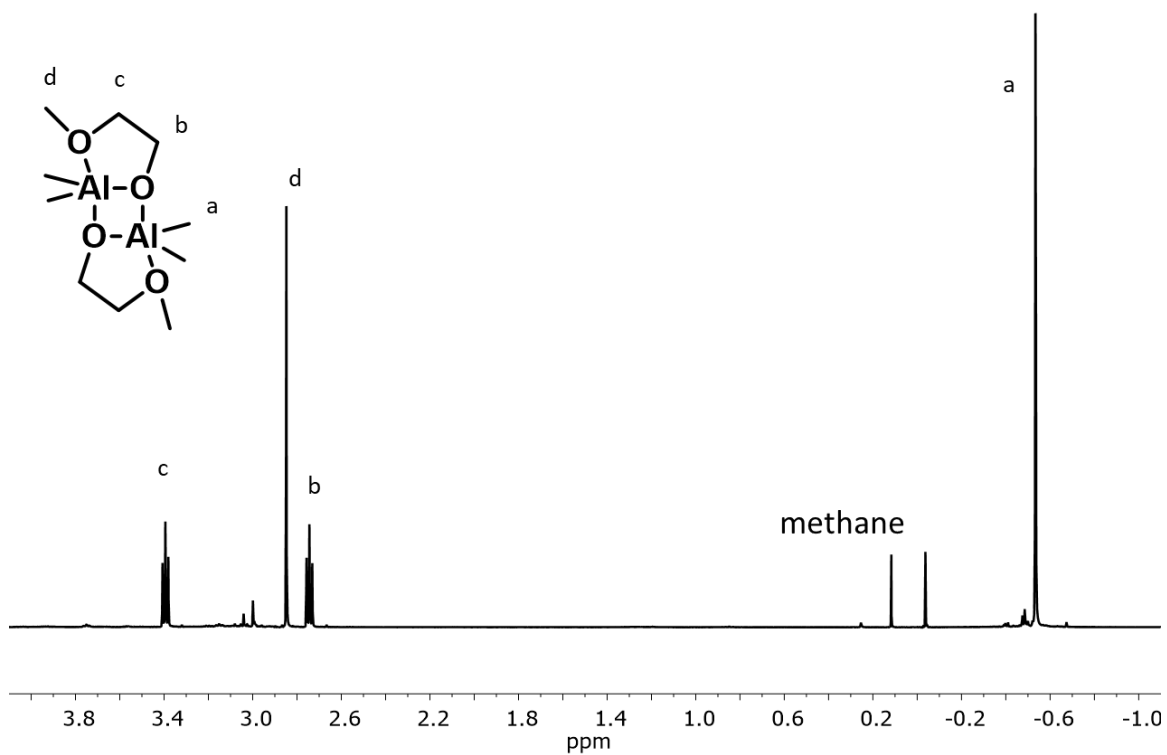


Figure B4  $^1\text{H}$  NMR spectrum Methyl-EtGlycol BOD (species 1) initiator (benzene, 400 MHz)

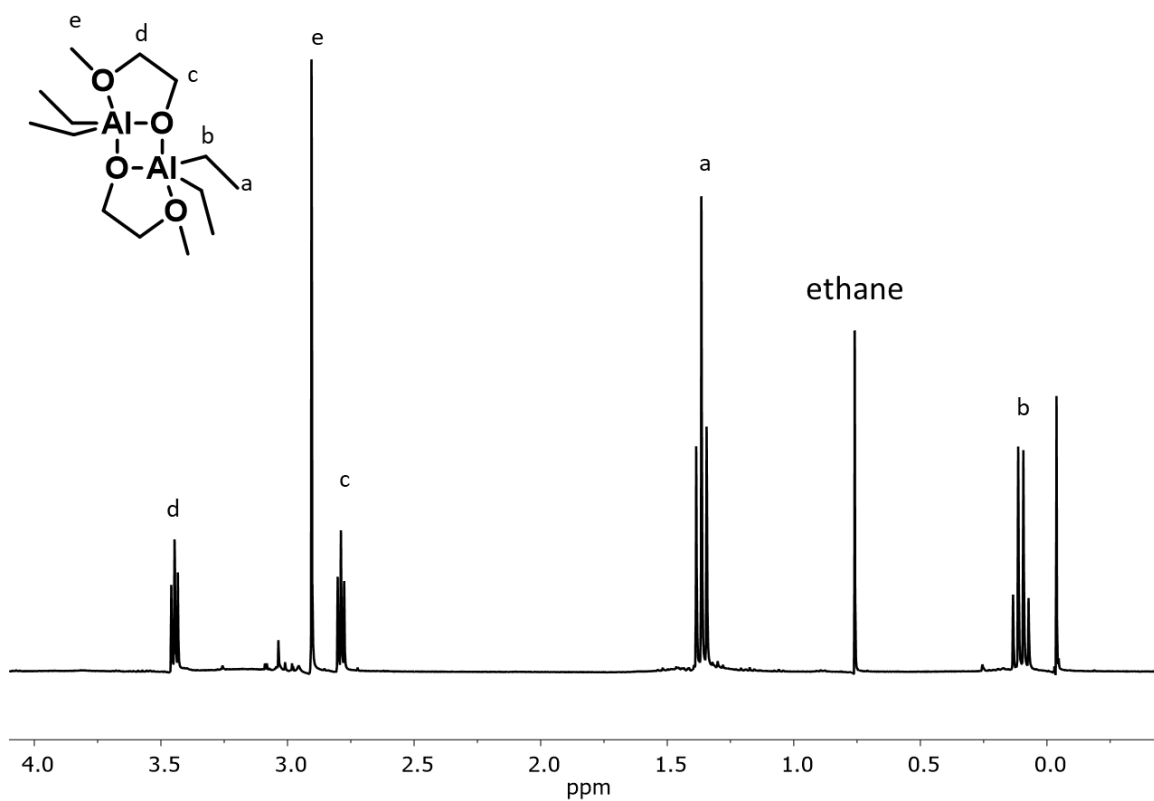


Figure B5  $^1\text{H}$  NMR spectrum Ethyl-EtGlycol BOD (species 2) initiator (benzene, 400 MHz)

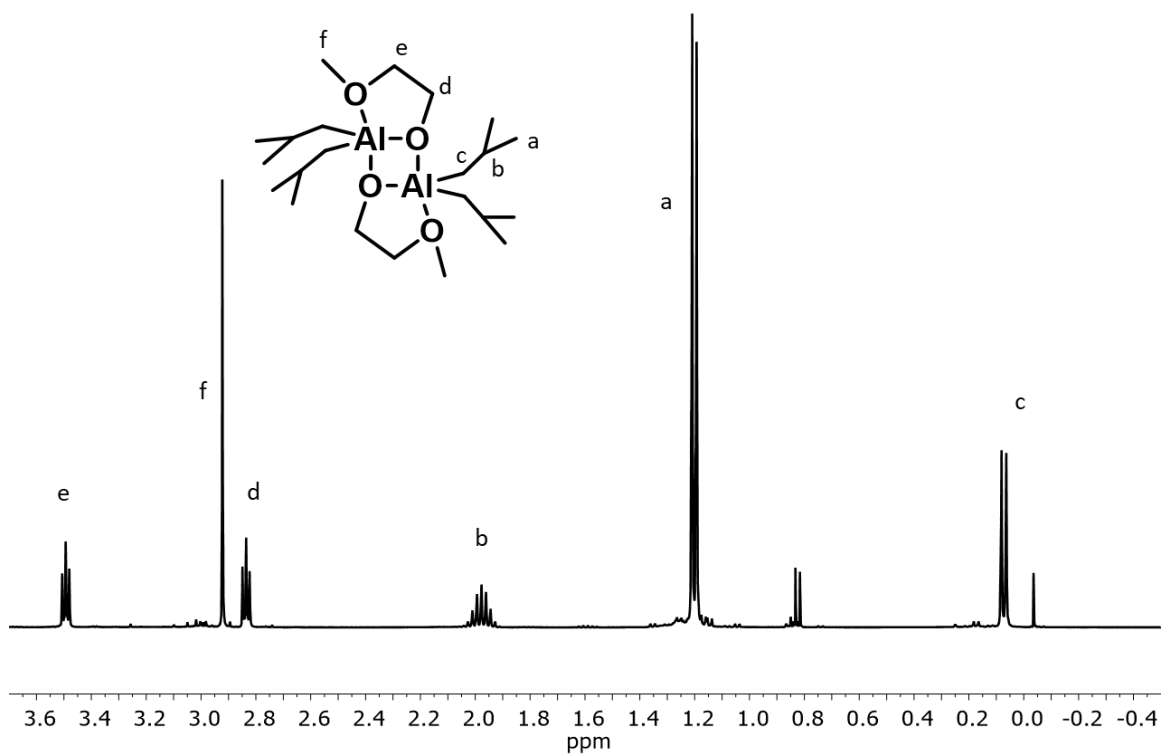


Figure B6  $^1\text{H}$  NMR spectrum Isobutyl-EtGlycol BOD (species 3) initiator (benzene, 400 MHz)

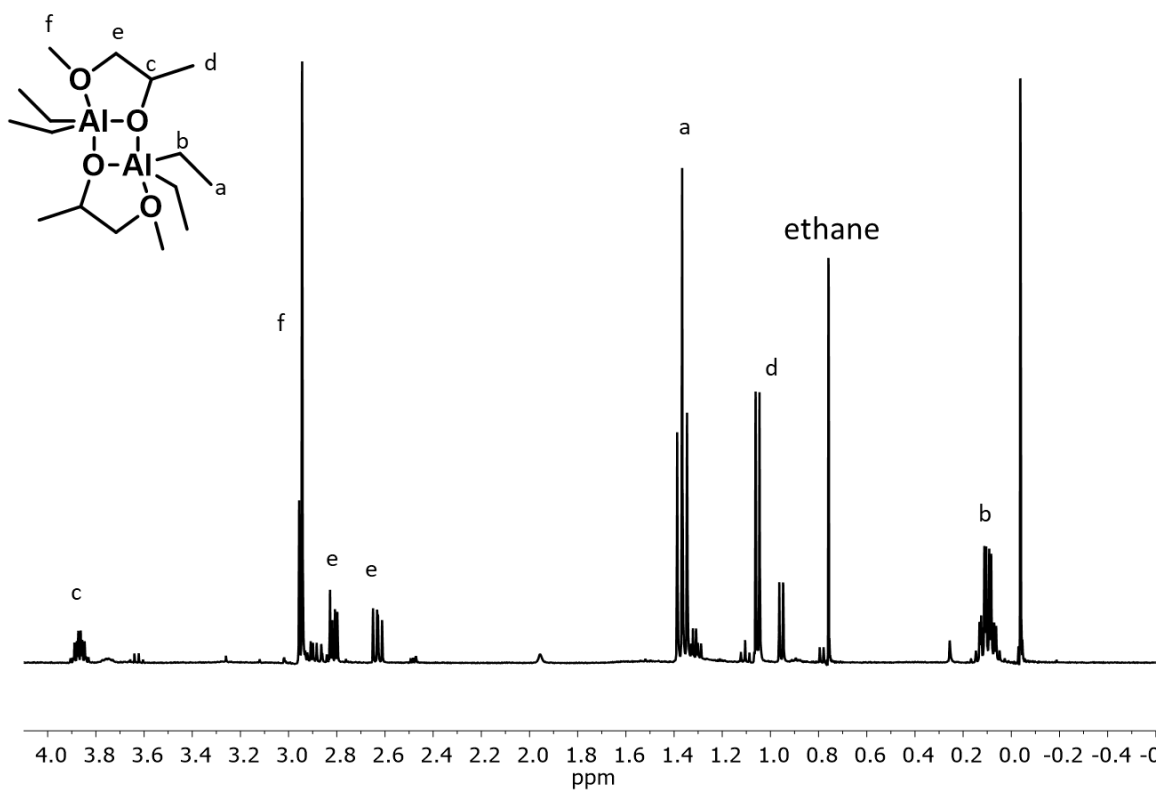


Figure B7  $^1\text{H}$  NMR spectrum Ethyl-PropGlycol BOD (species 4) initiator (benzene, 400 MHz)

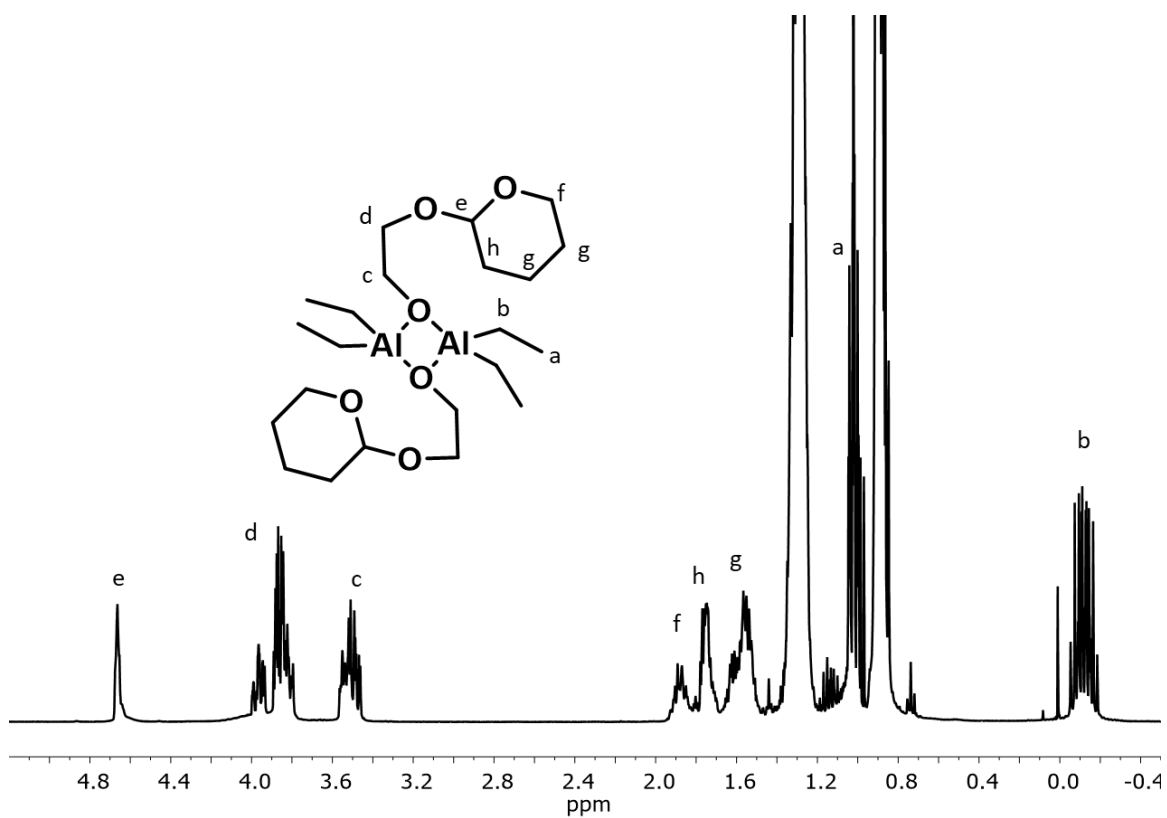


Figure B8  $^1\text{H}$  NMR spectrum Ethyl-THP BOD (species 5) initiator ( $\text{CDCl}_3$ , 400 MHz)

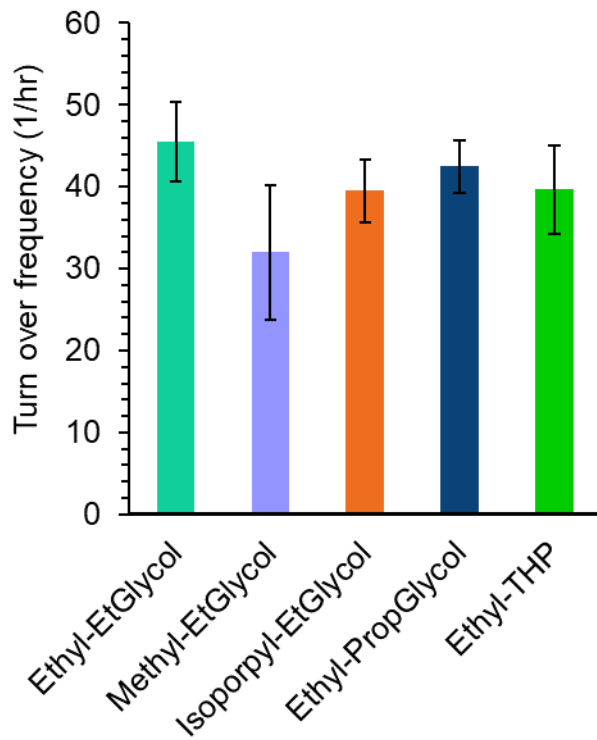


Figure B9 Kinetic study on the performance on initiators on the rate of lactide polymerization.

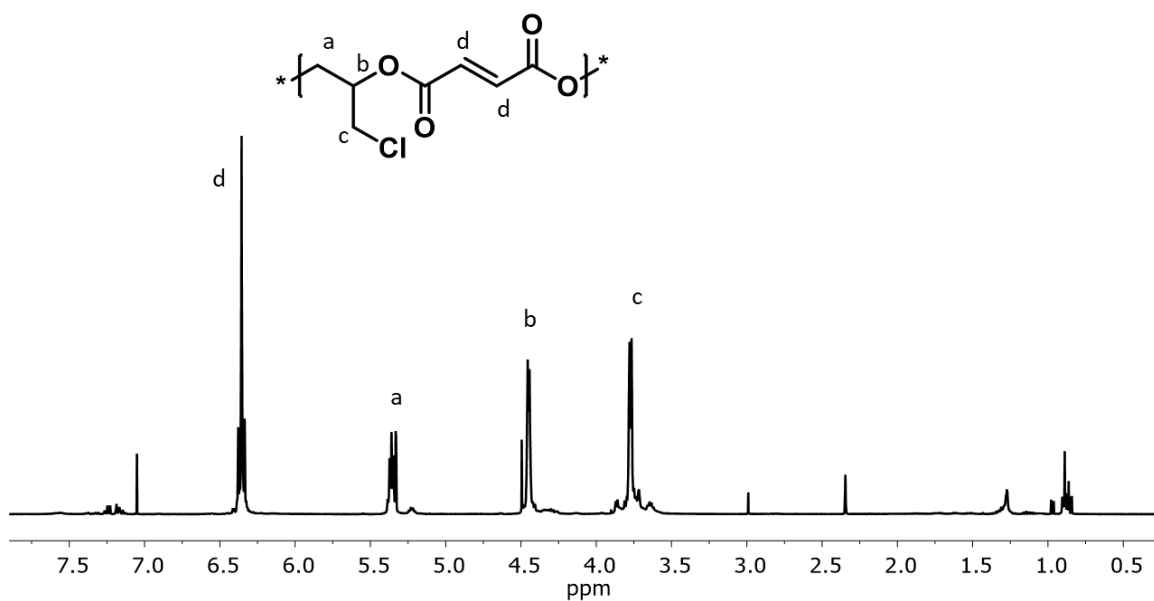


Figure B10  $^1\text{H}$  NMR spectrum of poly(maleic anhydride-co-epichlorohydrin) created with BOD initiator ( $\text{CD}_1\text{Cl}_3$ , 400 MHz)

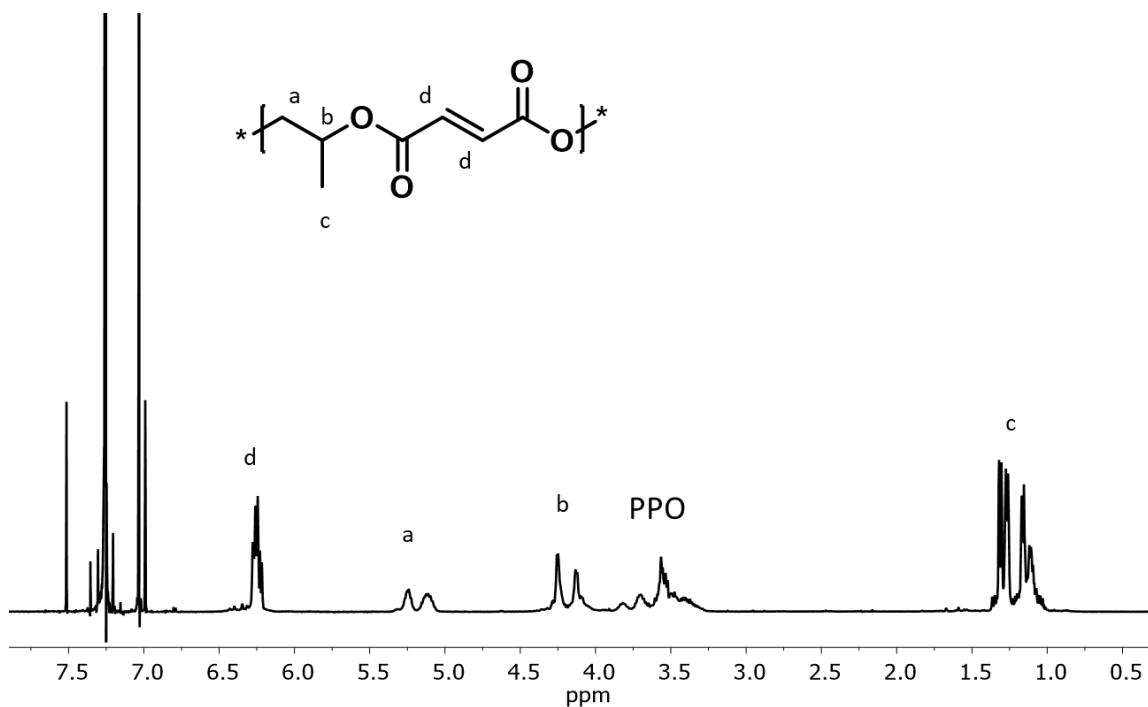


Figure B11 <sup>1</sup>H NMR spectrum of poly(maleic anhydride-co-propylene oxide) created with BOD initiator (CD<sub>1</sub>Cl<sub>3</sub>, 400 MHz). This polymerization had excess propylene oxide leading to some homopolymerization.

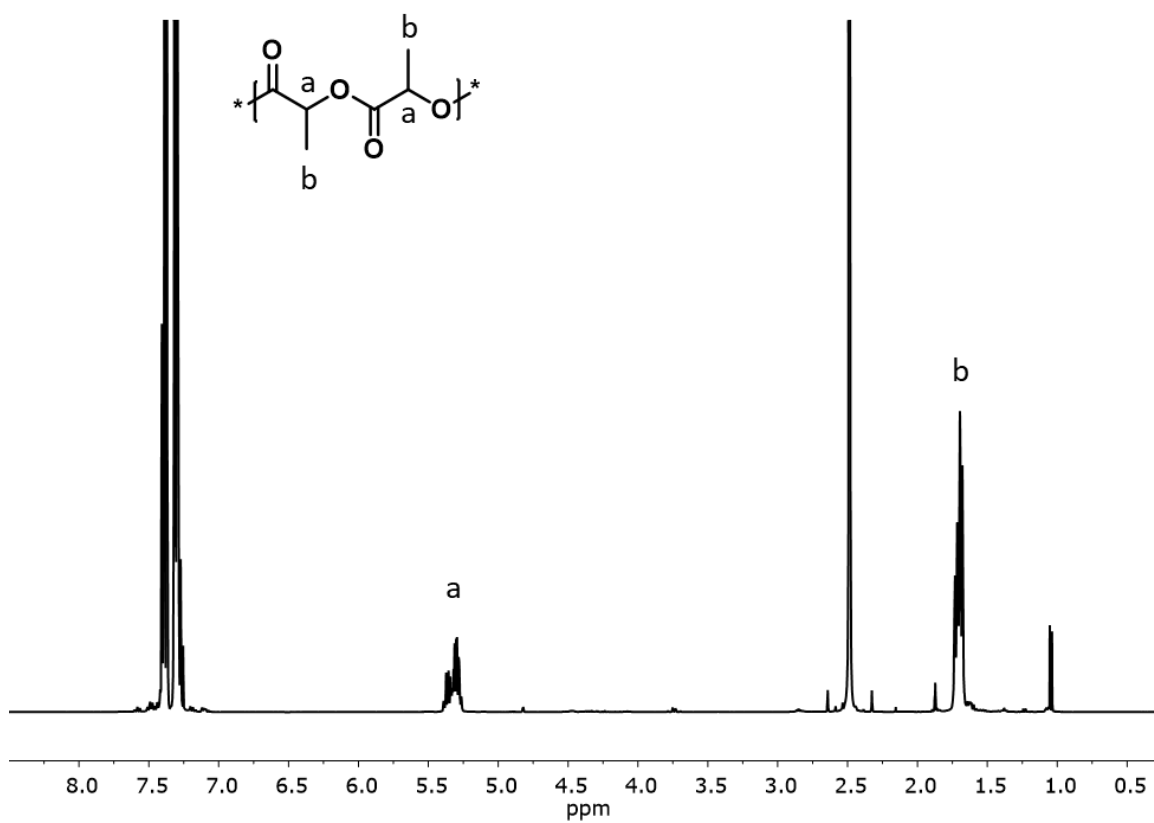


Figure B12  $^1\text{H}$  NMR spectrum of poly(DL-lactide) created with MOD initiator( $\text{CD}_1\text{Cl}_3$ , 400 MHz)

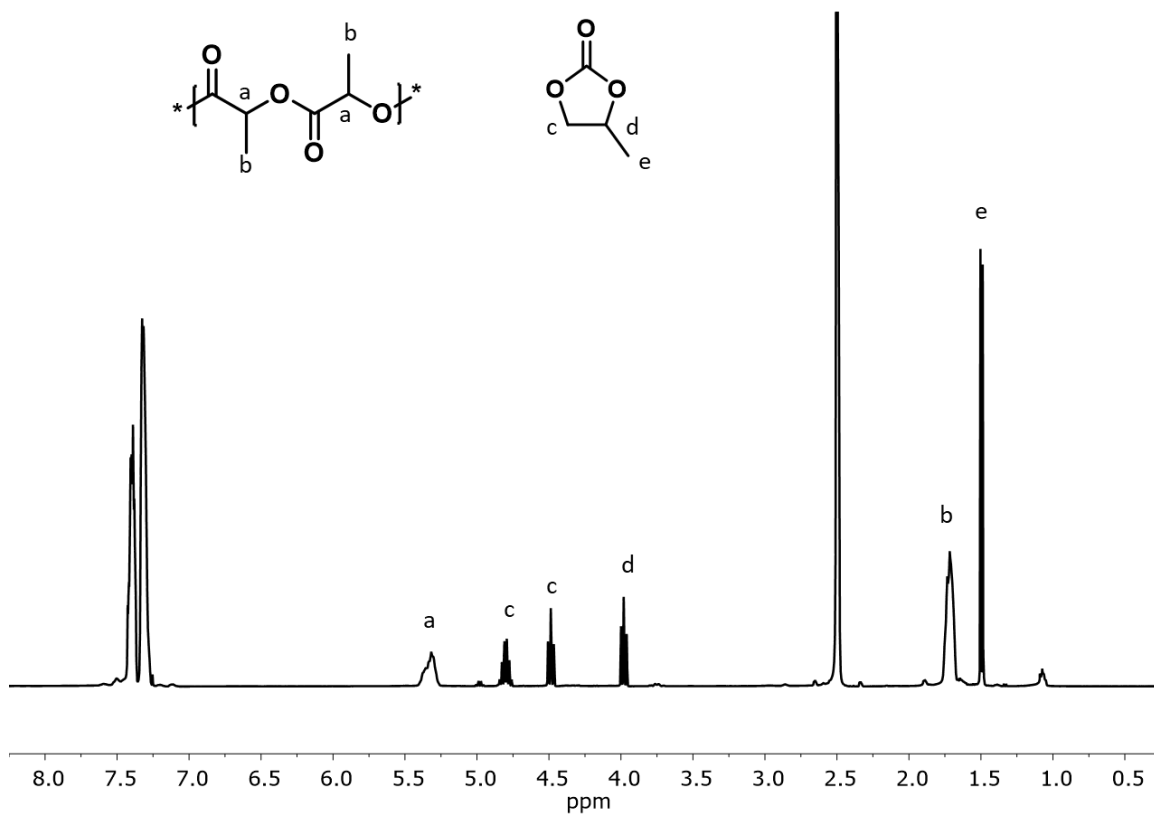


Figure B13 <sup>1</sup>H NMR spectrum of poly(DL-lactide) created with MOD initiator from an attempted copolymerization involving propylene carbonate and lactide (CDCl<sub>3</sub>, 400 MHz)

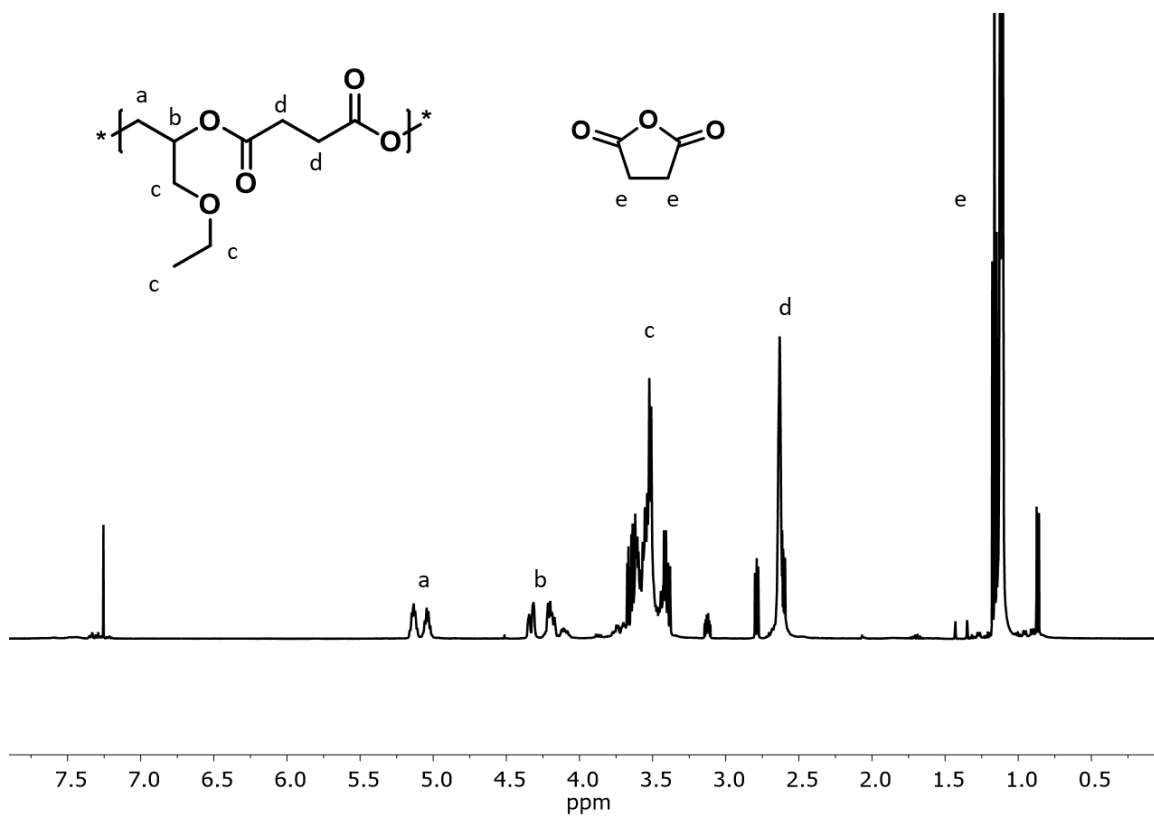


Figure B14 <sup>1</sup>H NMR spectrum of poly(succinic anhydride-co-ethyl glycidyl ether) created with MOD initiator (CD<sub>1</sub>Cl<sub>3</sub>, 400 MHz)

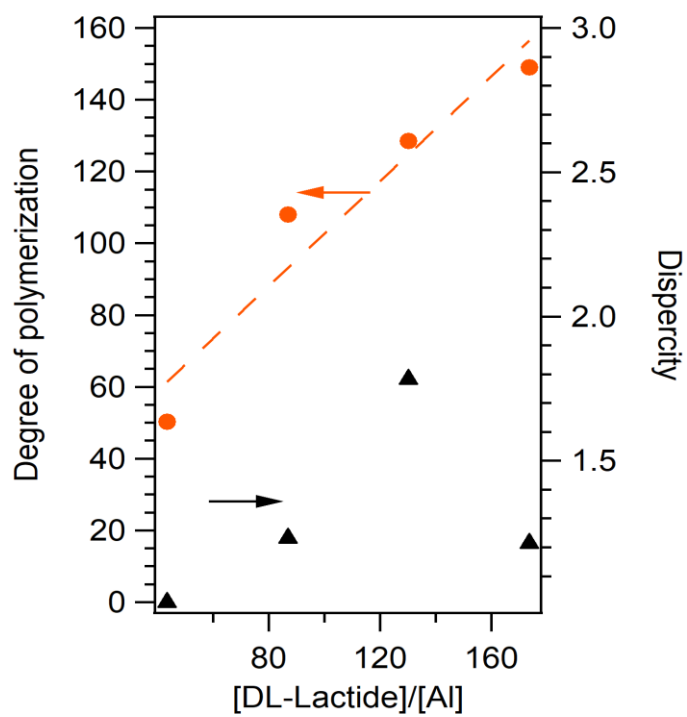


Figure B15 Control of molecular weight with the MOD via homopolymerization of DL-lactide

## **Appendix C**

Supporting Information for Chapter 4: Biologically derived monomers for  
synthesis of functionable material

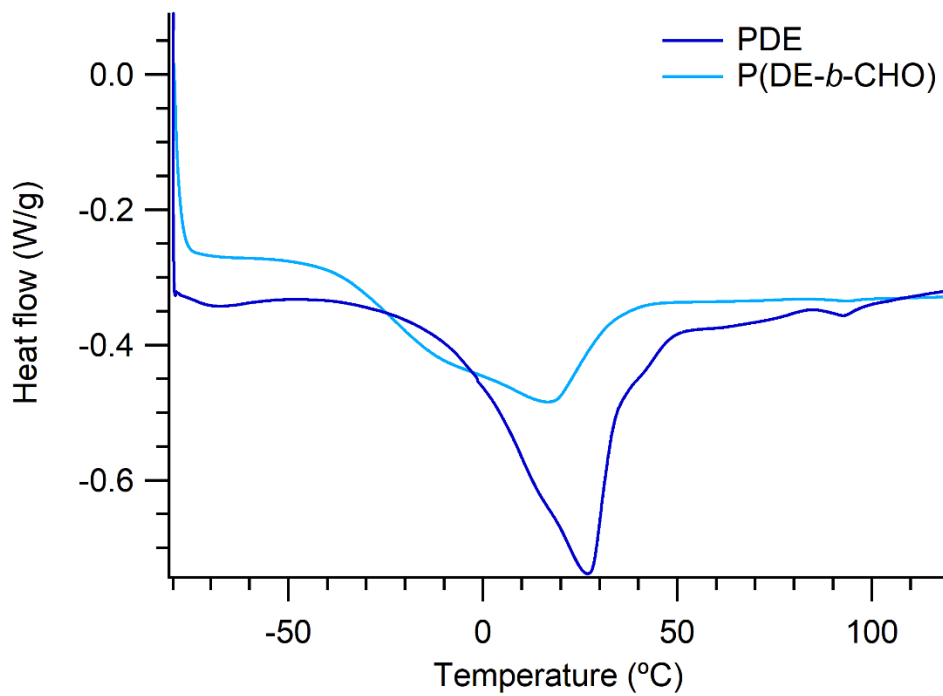


Figure C1 DSC characterization of linear homopolymer and the crosslinked polymer created after. The crystalline peak width shifts in location and shape upon further polymerization.

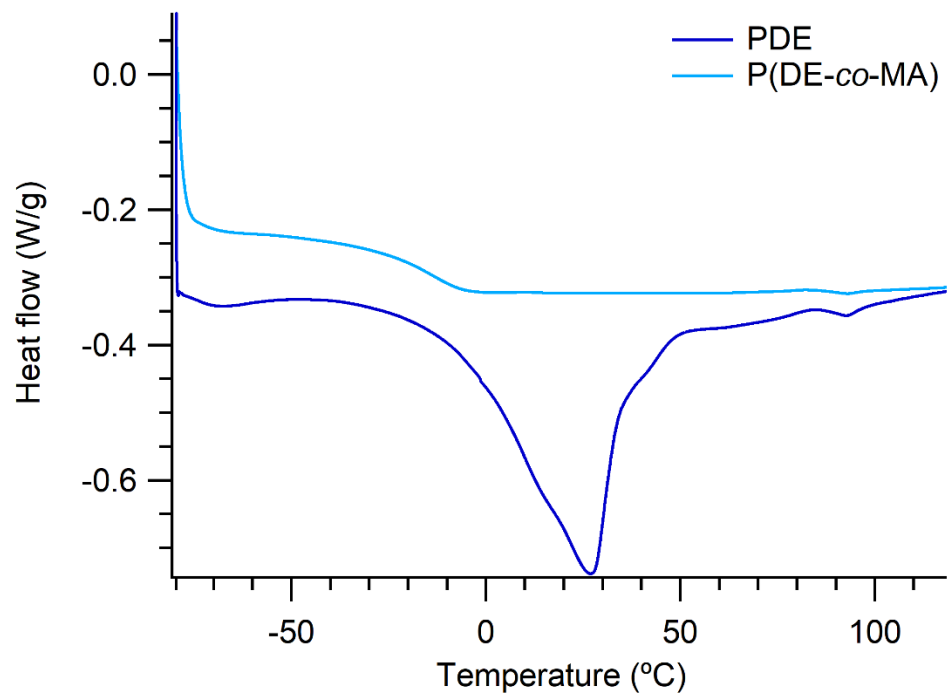


Figure C2 DSC characterization of linear homopolymer and the crosslinked alternating copolymer created. The crystalline peak width shifts in location and shape upon further polymerization.

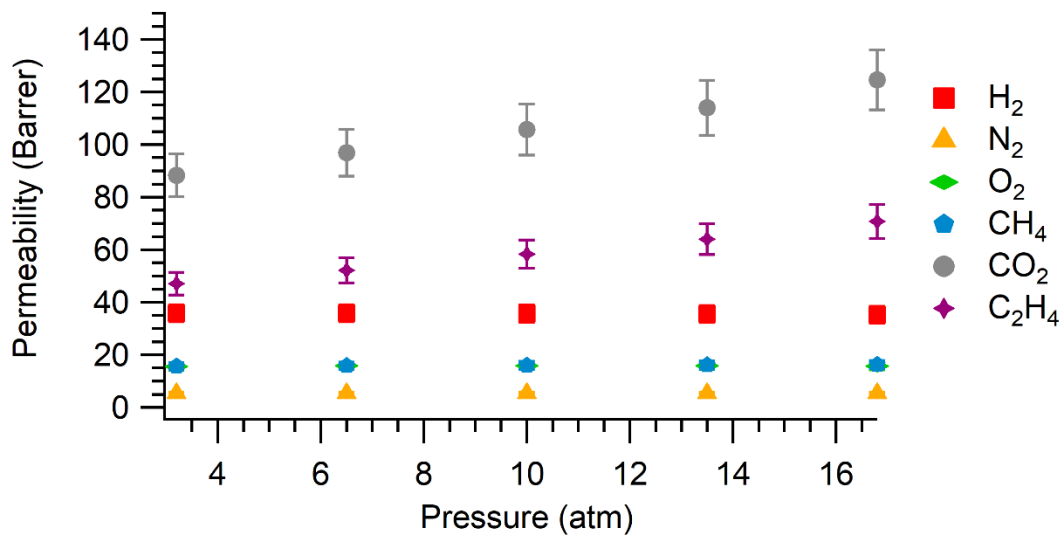


Figure C3 Pure gas permeability as a function of upstream pressure at 35 °C in crosslinked P(MA-co-DE)

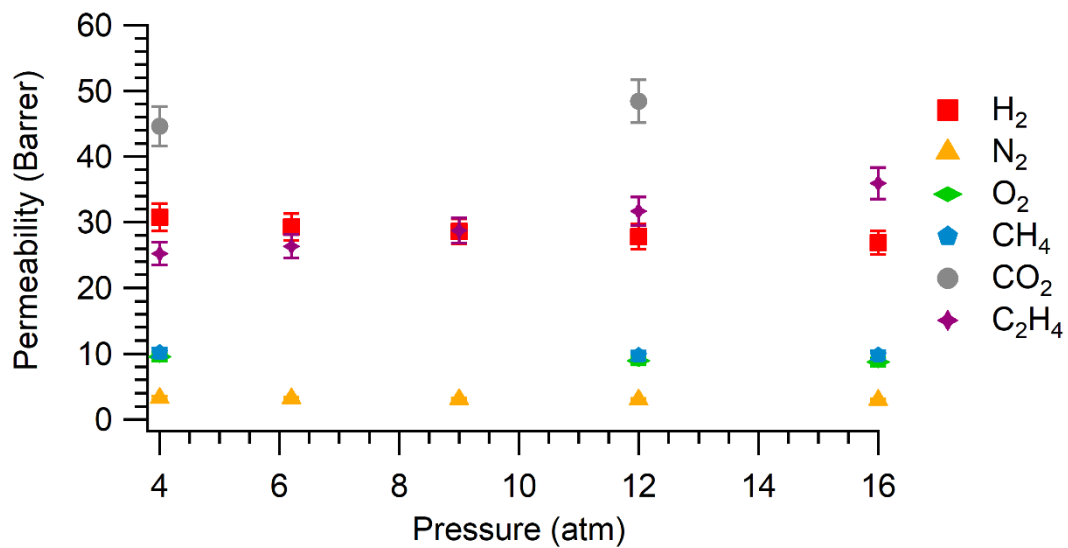


Figure C4 Pure gas permeability as a function of upstream pressure at 35 °C in crosslinked P(DE-b-CHO)

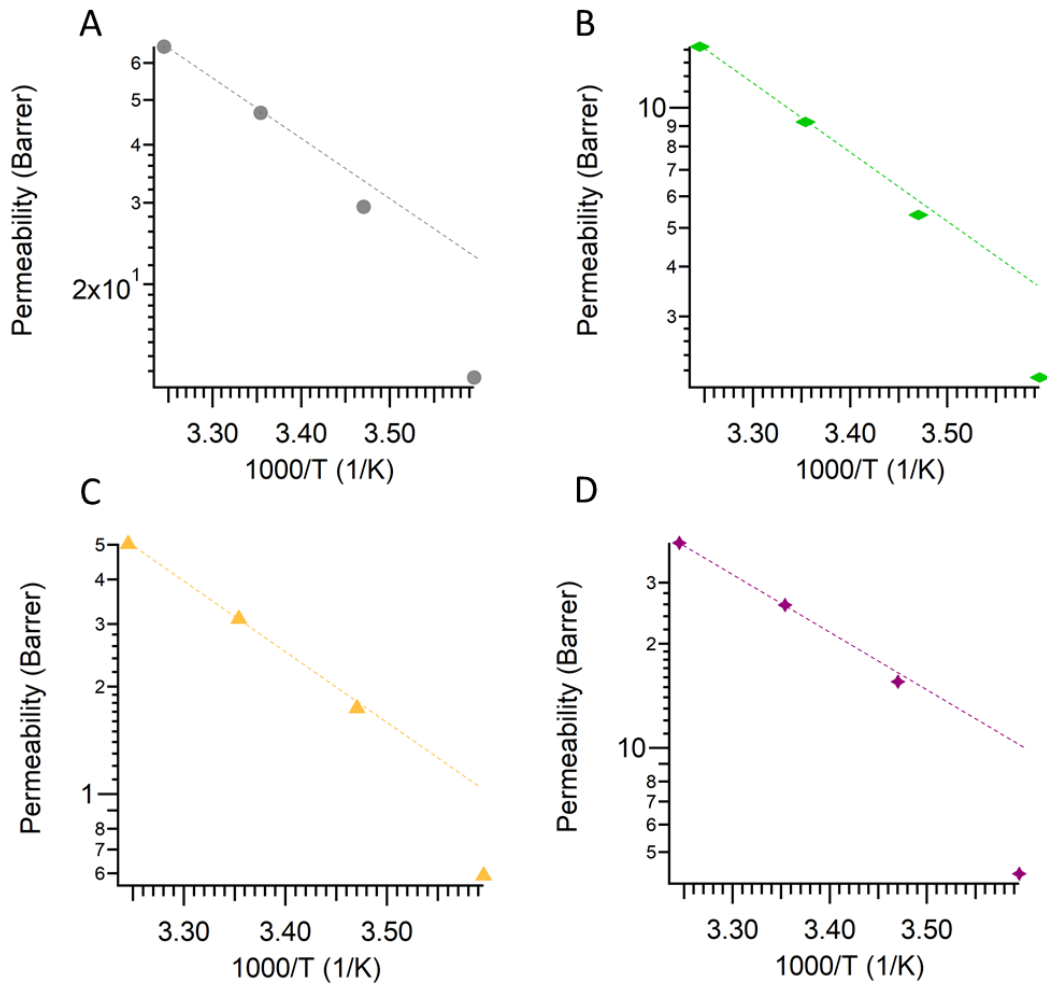


Figure C5 Pure gas permeability as a function of temperature at 2 atm in crosslinked P(DE-b-CHO) film. The deviation from the fit showcases the deviation from Arrhenius behavior due to crystallization.

## **Appendix D**

Supporting Information for Chapter 5: Impact of polyether polarity on ionic conductivity

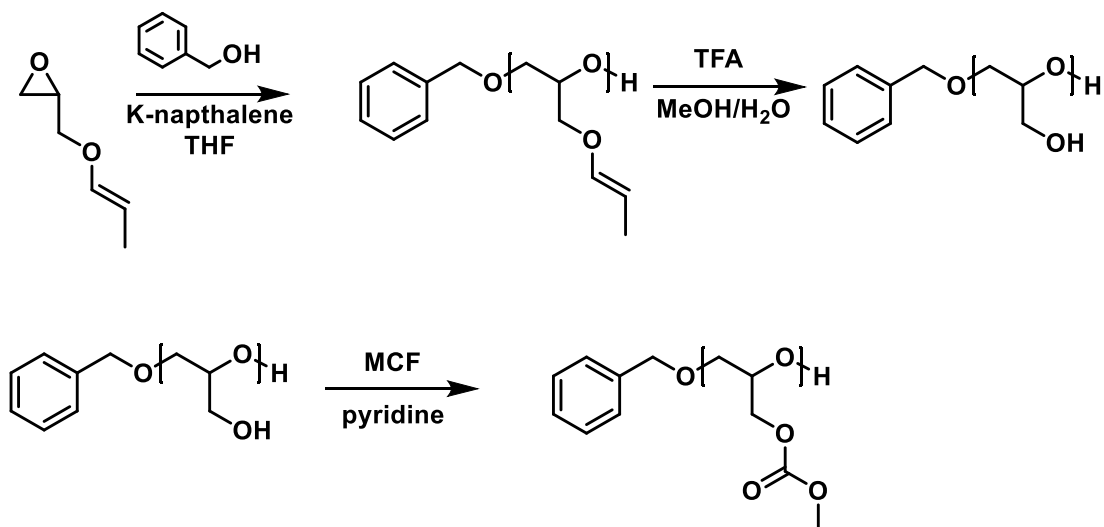
## METHODS

### Polymer 1 synthesis

Allyl glycidyl ether was isomerized according to the procedure described in Crivello et al.<sup>203</sup> The resulting propenyl glycidyl ether was purified via distillation prior to polymerization. Polymerization of propenyl glycidyl ether was initiated with benzyl alcohol and potassium naphthalenide as described previously.<sup>204</sup> The resulting polymer was precipitated in hexanes and dried *in vacuo*.

The resulting poly(propenyl glycidyl ether) was hydrolyzed to polyglycerol by suspending the polymer in a mixture of 5:0.5:0.1 mL of methanol, water, and trifluoroacetic acid per 1 gram of polymer. The polyglycerol was purified via dialysis and dried *in vacuo*.

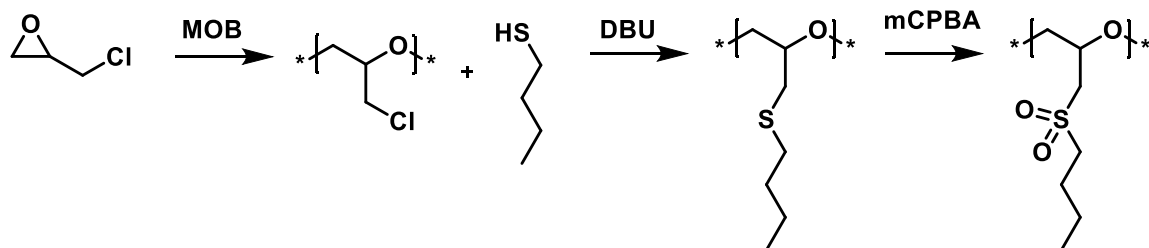
Polyglycidol was further reacted with methyl chloroformate (MCF) to create the final polymer **1**. For every alcohol functionality, 1.2 mole excess of methyl chloroformate was added. Similarly, an excess of pyridine was added in order to quench the forming hydrochloric acid. The polyglycidol was dried *in vacuo* and dissolved in pyridine. The solution was cooled in an ice bath while the MCF was added. The reaction was terminated and purified with a solution of sodium bicarbonate.



Scheme D1 Synthesis scheme of polymer 1

## Polymer synthesis 2

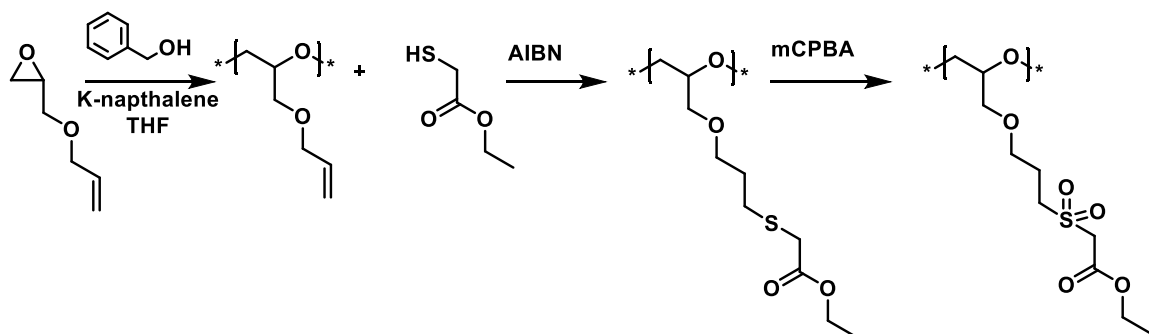
Epichlorohydrin was used out of the bottle. Polyepichlorohydrin was synthesized with a MOB catalyst developed in the Lynd group. The procedure used is described in a publication from the Lynd group.<sup>149</sup> Polyepichlorohydrin was further modified by n-butane thiol added in triple molar excess in the presence of 1 molar equivalence of 1,8-Diazabicyclo[5.4.0]undec-7-ene (DBU) in comparison to epichlorohydrin repeat unit. The resulting polymer was further oxidized via meta-Chloroperoxybenzoic acid (mCPBA) in dichloromethane.



Scheme D2 Synthesis scheme of polymer 2

### Polymer synthesis 3

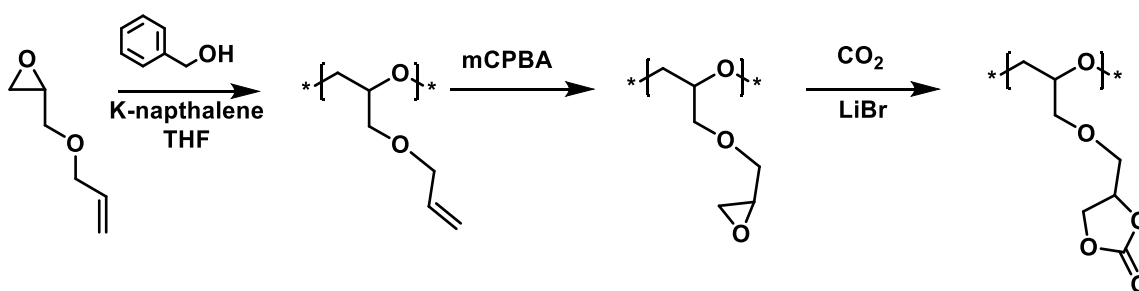
Polymerization of allyl glycidyl ether was initiated with benzyl alcohol and potassium naphthalene as described previously.<sup>204</sup> The resulting polymer was precipitated in hexanes and dried in vacuo. Next a thiol-ene click reaction was done with 3 times molar excess of ethyl 2-mercaptoacetate and 1 mol % AIBN at elevated temperature in NN-dimethylformamide. The resulting polymer was further oxidized via meta-Chloroperoxybenzoic acid (mCPBA) in dichloromethane.



Scheme D3 Synthetic scheme of polymer 3

## Polymer synthesis 4

Polymerization of allyl glycidyl ether was initiated with benzyl alcohol and potassium naphthalene as described previously.<sup>204</sup> The resulting polymer was precipitated in hexanes and dried *in vacuo*. Poly allyl glycidyl ether was further epoxidized via meta-Chloroperoxybenzoic acid (mCPBA) in dichloromethane. The resulting polymer was carbonated using a method described in Brocas *et al.*<sup>205</sup>



Scheme D4 Synthetic scheme of polymer 4

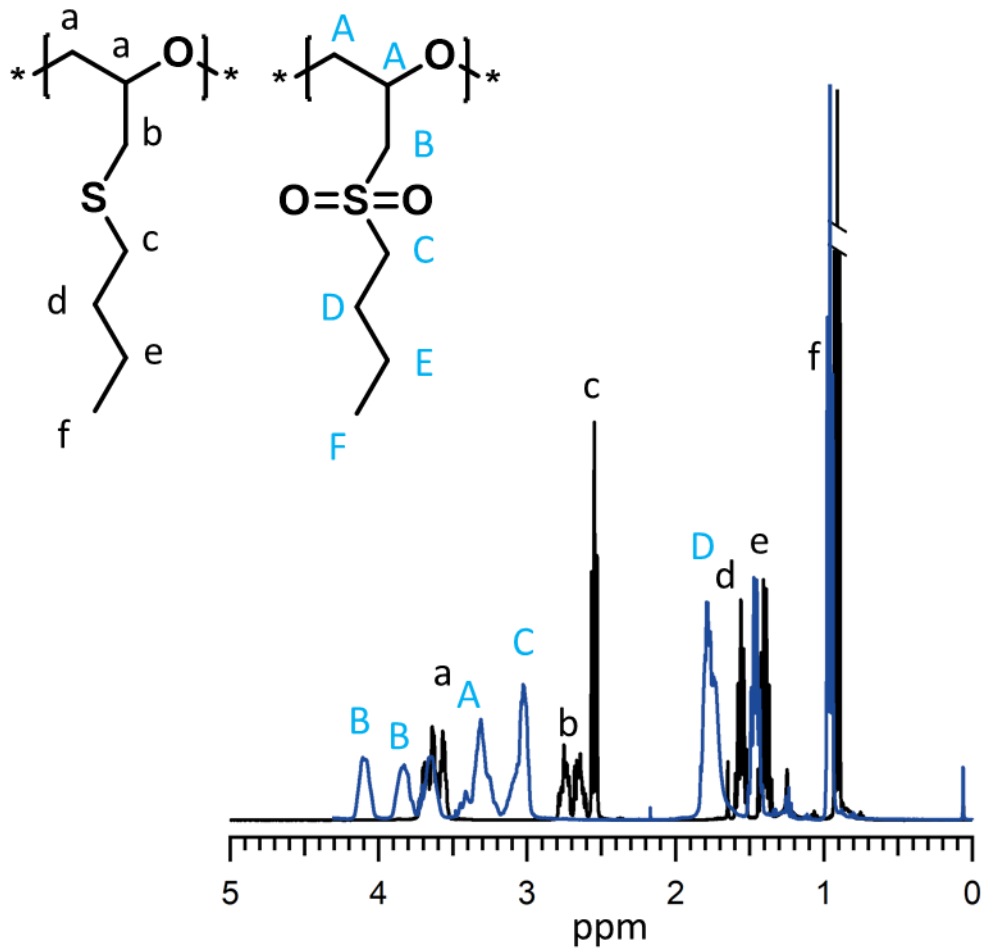


Figure D1  $^1\text{H}$  NMR characterization of synthesis steps in creation of polymer 2

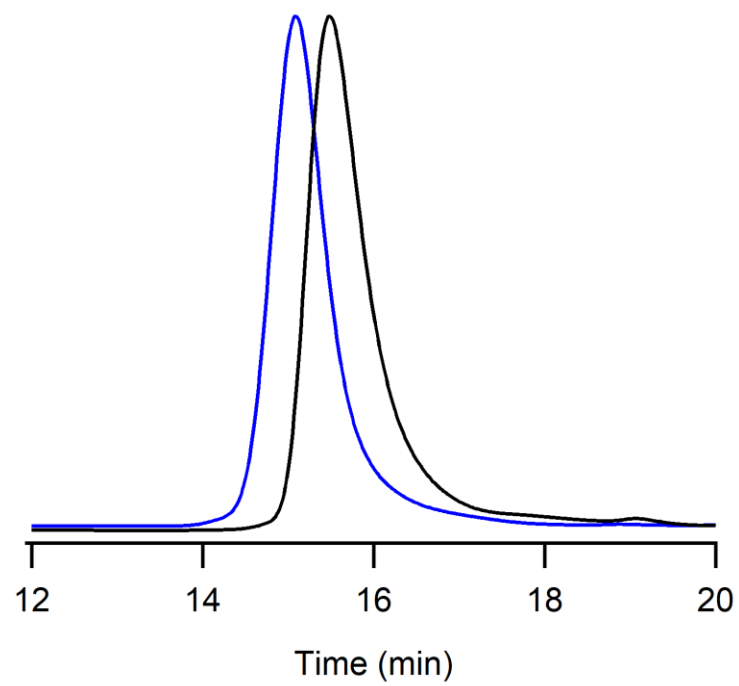


Figure D2 GPC characterization of polymers used in the creation of polymer **2** to show oxidation related molecular weight increase.

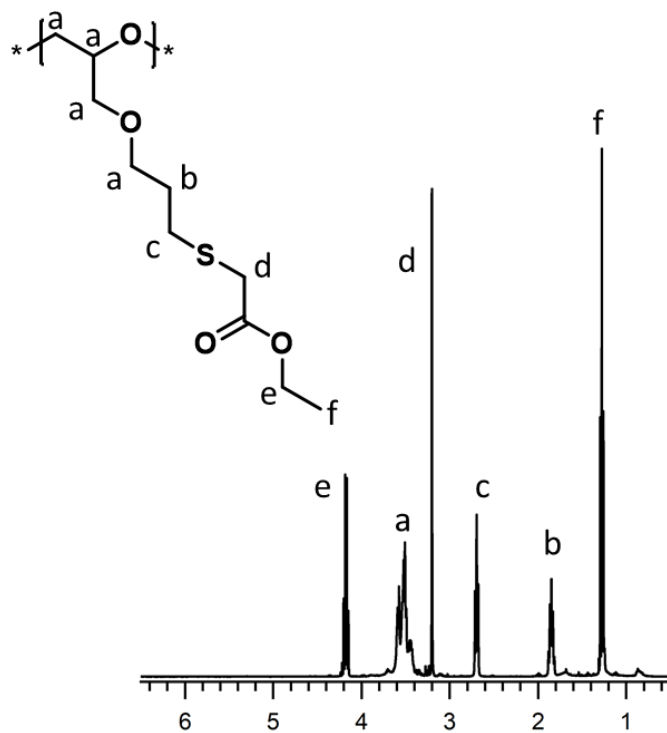


Figure D3 <sup>1</sup>H NMR of the modified poly allyl glycidyl ether created in the first step of synthesized of polymer **3**

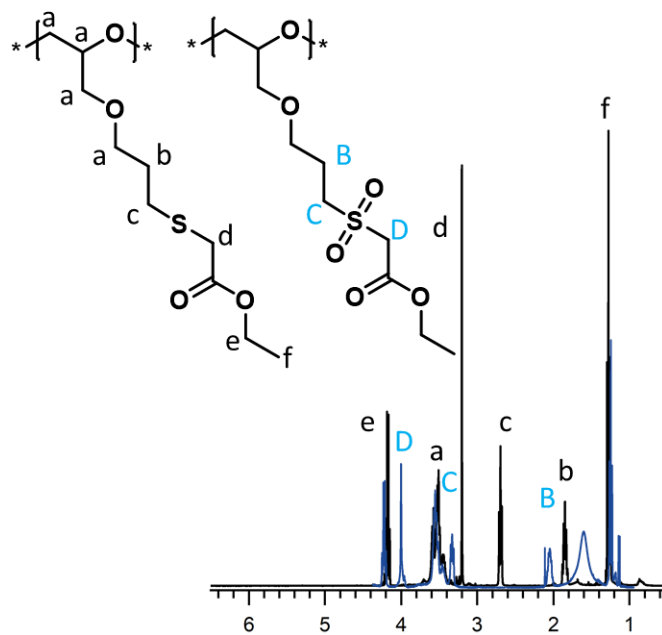


Figure D4  $^1\text{H}$  NMR of the oxidation of to produce polymer **3**

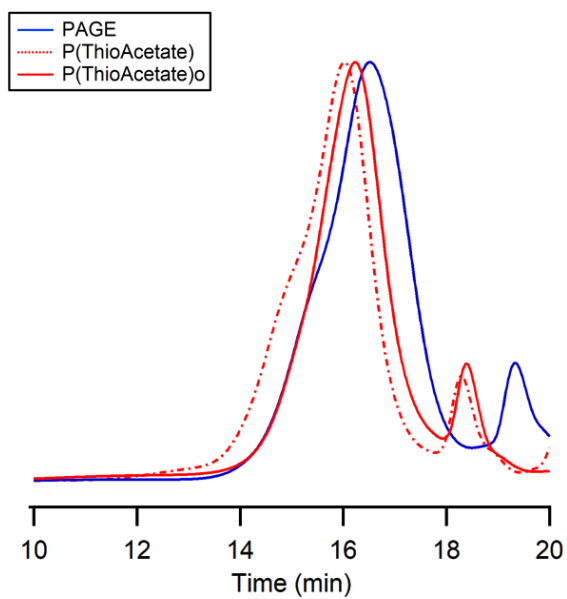


Figure D5 GPC characterization of polymers used in the creation of polymer **3**

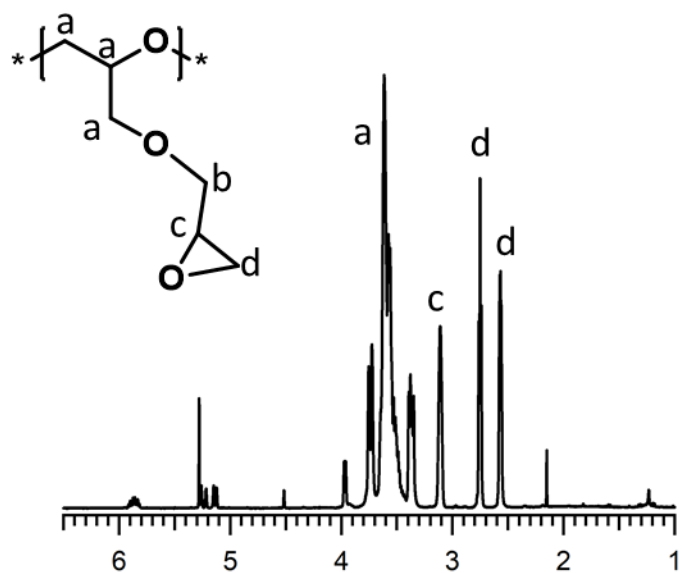


Figure D6 <sup>1</sup>H NMR of the modified poly allyl glycidyl ether created in the first step of synthesized of polymer **4**

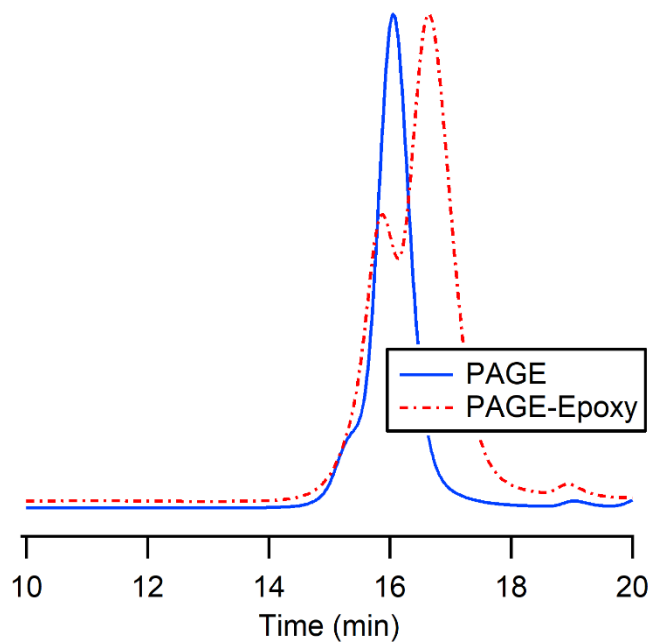


Figure D7 GPC characterization of polymers used in the creation of polymer **4**

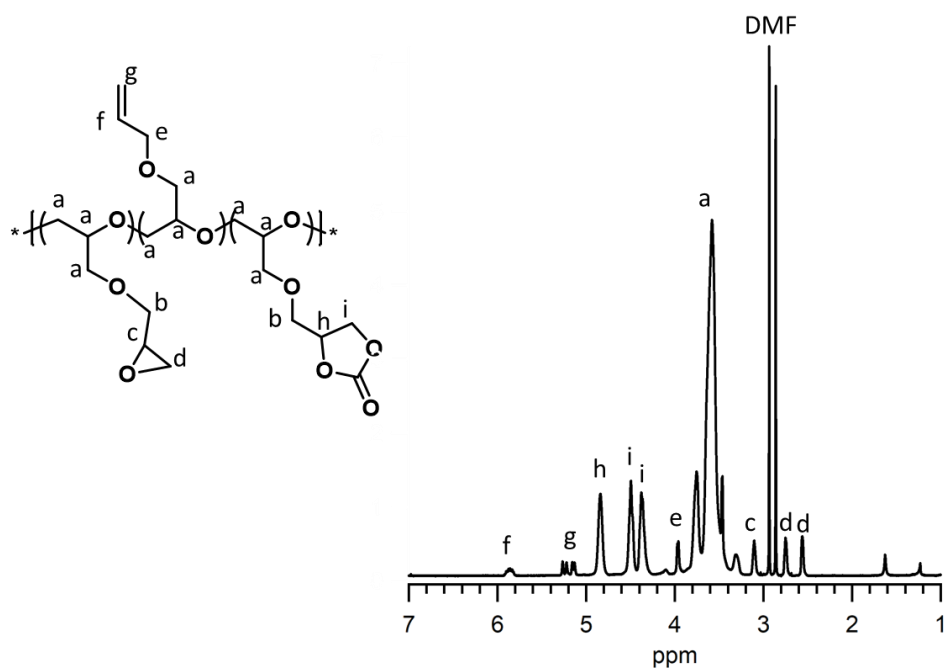


Figure D8 <sup>1</sup>H NMR of the synthesized of polymer 4

## **Appendix E**

Supporting Information for Chapter 5: Hydrophobic or Hydrophilic:  
Formation of Polydopamine on surfaces



OFFICE OF RESEARCH SUPPORT  
THE UNIVERSITY OF TEXAS AT AUSTIN

P.O. Box 7426, Austin, Texas 78713 · Mail Code A3200  
(512) 471-8871 · FAX (512) 471-8873

FWA # 00002030

Date: 01/10/18  
PI: Malgorzata Chwatko  
Dept: Engineering, Chemical  
Title: Polydopamine: A Neat Polymer to Teaching Polymerization  
as a Supplement to Current Instruction  
RE: Non-Human Subjects Research Determination

Dear Malgorzata Chwatko:

The Office of Research Support (ORS) reviewed the above protocol submission request and determined it did not meet the criteria for human subjects research as defined in the Common Rule (45 CFR 46) or FDA Regulations (21 CFR 56). IRB review and oversight is not required because the activities involve:

- No human interactions
- Classroom activities used to teach methodology and technique
- Program evaluation where results are not generalized to other services or programs
- Secondary use of de-identified data set (no direct or links to identifiers)
- Obtaining information that is not about living individuals
- Obtaining information from publicly available sets
- Biographical research that is not generalizable beyond the individual
- Archival research using existing literature
- Other (Explain):

At this time you are free to begin your research as IRB approval is not necessary. You should retain this letter with the respective research documents as evidence that IRB review and oversight is not required.

If you have any questions contact the ORS by phone at (512) 471-8871 or via e-mail at [orsc@uts.cc.utexas.edu](mailto:orsc@uts.cc.utexas.edu).

Sincerely,

A handwritten signature in cursive script that reads "James P. Wilson".

James Wilson, Ph.D.  
Institutional Review Board Chair

Figure E1 IRB review of the experimental protocol used in the study

## **TEACHER HANDOUT**

**Purpose:** The students will create polymers on a surface of Teflon and will explore water properties of the materials.

### **Materials:**

1. Teflon sheet
2. Dopamine
3. CAPS
4. Citric acid buffer
5. Tris HCl
6. pH paper

### **Preparation**

Teflon sheet should be prewetted in a 50 w% IPA solution for 10 minutes, followed by a water wash. Microgram sensitive scales are beneficial for this experiment and should be set out at student workstations.

Solution A is a 10mM CAPS Solution B is 10 mM Tris HCl buffer and Solution C is 10mM Citric Acid buffer. Solution A should be adjusted to be at a pH of 10. Solution B should be adjusted to a pH of 8. Lastly, solution C should be adjusted to a pH of 4.

Special note: each solution can also have 10 mM ammonium persulfate in order to decrease the reaction time from 18-24h to 15 minutes.

## STUDENT HANDOUT

Polymers are all around us! They can serve many functions by the variety of properties they can offer. Polymer coatings are of central importance for many applications as well by being able to change just the surface properties of the material.



Figure: Image from Q Wei et al. Material Horizons, 2015

By observing the natural world, it was found that mussels produce a sticky polymer that allows them to stick to many surfaces. In our laboratory experiment we will create this polymer using different techniques.

### Procedure:

1. Measure and record the solution pH of the three flasks in front of you
2. Cut out 3 samples of plastic, all the same size. Weigh the samples and record their weight
3. Place the three samples in three different beakers
4. Add 50 mL of solution A to beaker A, 50 mL solution B to beaker B and 50 mL of solution C to beaker C
5. Next calculate how much dopamine do you need to add to each beaker to achieve a 2 mg/ml concentration. Add the calculated amount to each beaker
6. Leave overnight unless otherwise instructed
7. Next day remove the samples
8. Allow to dry (takes a 15ish minutes), weigh samples
9. Place a droplet of water on sample and precursor. What happened?

### Questions:

1. Why does the pH of the solution impact polymerization?
2. In which conditions did the polymerization proceed the furthest?
3. If the CO<sub>2</sub> concentration in the air goes up what impact could that have on the mussels producing polymer?

## **PRE-ASSESSMENT**

- 1) What is a polymer ??
- 2) What are some common uses for polymers ?
- 3) Circle all terms that are macromolecules:

Polymer

Protein

Plastic

carbon dioxide

water

- 4) Define pH and pKa ??
- 5) Define hydrophilic and hydrophobic
- 6) Does the body interact better with hydrophilic or hydrophobic things?

**POST ASSESSMENT:**

- 1) What is a polymer ??
- 2) Why are some common uses for polymers ?
- 3) Circle all terms that are macromolecules:

Polymer                      Protein                      Plastic                      carbon dioxide                      water

- 4) Define pH and pKa ??
- 5) Define hydrophilic and hydrophobic
- 6) Does the body interact better with hydrophilic or hydrophobic things

**Rate the following statements from 1 to 4** with the following ranking : Strongly Disagree = 1, Disagree = 2, Agree = 3, Strongly Agree = 4

- a) The activity was about the right length
- b) This activity increased my interest in going to college
- c) This activity increased my interest in a degree or career related to science and engineering
- d) This activity should be offered again

Comments! What did you like or not like about this activity? If we do it again what should be changed?

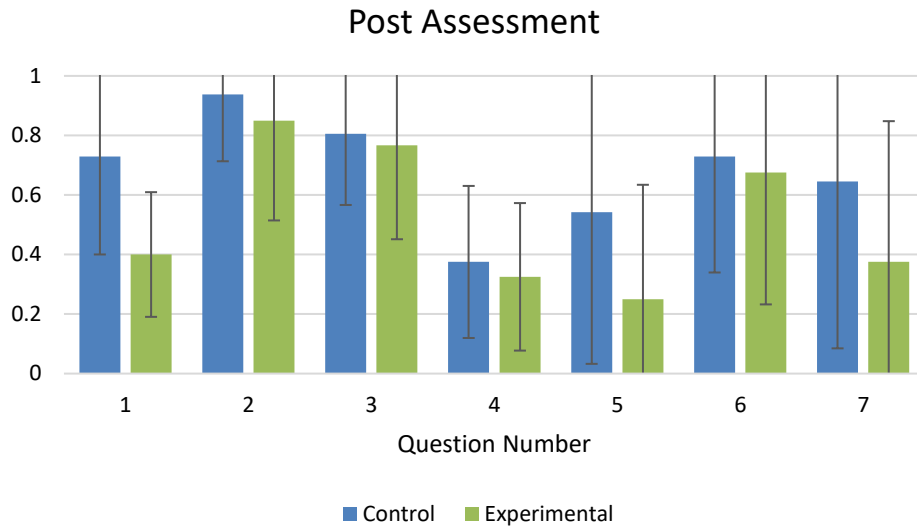


Figure E2 Complete post assessment results from the study

## References

- 1 D. K. Schneiderman and M. A. Hillmyer, *Macromolecules*, 2017, **50**, 3733–3749.
- 2 E. Blasco, M. B. Sims, A. S. Goldmann, B. S. Sumerlin and C. Barner-Kowollik, *Macromolecules*, 2017, **50**, 5215–5252.
- 3 J. H. Park and G. C. Rutledge, *Macromolecules*, 2017, **50**, 5627–5642.
- 4 C. M. Bates and F. S. Bates, *Macromolecules*, 2017, **50**, 3–22.
- 5 G. D. Bittner, C. Z. Yang and M. A. Stoner, *Environ. Heal. A Glob. Access Sci. Source*, , DOI:10.1186/1476-069X-13-41.
- 6 B. Mertens, E. Van Hoeck, M. N. Blaude, C. Simon, M. Onghena, T. Vandermarken, K. Van Langenhove, H. Demaegdt, K. Vandermeiren, A. Covaci, M. L. Scippo, M. Elskens and J. Van Loco, *Food Chem. Toxicol.*, 2016, **97**, 108–119.
- 7 M. K. Sarath Josh, S. Pradeep, S. Balachandran, R. Sudha Devi, K. S. Vijayalakshmi Amma and S. Benjamin, *J. Polym. Res.*, , DOI:10.1007/s10965-012-9915-4.
- 8 E. Fries, J. H. Dekiff, J. Willmeyer, M. T. Nuelle, M. Ebert and D. Remy, *Environ. Sci. Process. Impacts*, 2013, **15**, 1949–1956.
- 9 M. Manikkam, R. Tracey, C. Guerrero-Bosagna and M. K. Skinner, *PLoS One*, , DOI:10.1371/journal.pone.0055387.
- 10 A. M. Nelson and T. E. Long, *Polym. Int.*, 2012, **61**, 1485–1491.
- 11 L. Mcneill and R. Moore, *Int. J. Consum. Stud.*, 2015, **39**, 212–222.
- 12 D. Hanss and G. Böhm, *Int. J. Consum. Stud.*, 2012, **36**, 678–687.
- 13 P. Sörqvist, A. Haga, L. Langeborg, M. Holmgren, M. Wallinder, A. Nörtl, P. B. Seager and J. E. Marsh, *Food Qual. Prefer.*, 2015, **43**, 1–9.
- 14 K. G. Grunert, S. Hieke and J. Wills, *Food Policy*, , DOI:10.1016/j.foodpol.2013.12.001.
- 15 J. Rokka and L. Uusitalo, *Int. J. Consum. Stud.*, 2008, **32**, 516–525.
- 16 L. Magnier and J. Schoormans, *J. Environ. Psychol.*, 2015, **44**, 53–62.

- 17 H. Nakajima, P. Dijkstra and K. Loos, *Polymers (Basel)*., 2017, **9**, 523.
- 18 K. Yao and C. Tang, *Macromolecules*, 2013, **46**, 1689–1712.
- 19 R. Muellhaupt, *Macromol. Chem. Phys.*, 2013, **214**, 159–174.
- 20 R. Noyori, *Chem. Commun.*, 2005, 1807–1811.
- 21 M. Poliakoff, J. M. Fitzpatrick, T. R. Farren and P. T. Anastas, *Science*, 2002, **297**, 807–810.
- 22 S. Miao, P. Wang, Z. Su and S. Zhang, *Acta Biomater.*, 2014, **10**, 1692–1704.
- 23 R. Geyer, J. R. Jambeck and K. L. Law, *Sci. Adv.*, 2017, **3**, e1700782.
- 24 J. R. Jambeck, R. Geyer, C. Wilcox, T. R. Siegler, M. Perryman, A. Andrady, R. Narayan and K. L. Law, *Science (80-. )*., 2015, **347**, 768–771.
- 25 S. A. Miller, *ACS Macro Lett.*, 2013, **2**, 550–554.
- 26 H. Zhao, *J. Chem. Technol. Biotechnol.*, 2018, **93**, 9–19.
- 27 C. Romain and C. K. Williams, *ACS Symp. Ser.*, 2015, **1192**, 135–146.
- 28 A. Duda, P. Kubisa, G. Lapienis and S. Slomkowski, *Polimery/Polymers*, 2014, **59**, 9–23.
- 29 S. Paul, Y. Zhu, C. Romain, R. Brooks, P. K. Saini and C. K. Williams, *Chem. Commun. Chem. Commun*, 2015, **51**, 6459–6479.
- 30 P. Olsén, K. Odelius and A. C. Albertsson, *Biomacromolecules*, 2016, **17**, 699–709.
- 31 X. Zhang, G. O. Jones, J. L. Hedrick and R. M. Waymouth, *Nat. Chem.*, 2016, **8**, 1047–1053.
- 32 B. Lin and R. M. Waymouth, *Macromolecules*, 2018, **51**, 2932–2938.
- 33 K. Schröder, K. Matyjaszewski, K. J. T. Noonan and R. T. Mathers, *Green Chem.*, 2014, **16**, 1673–1686.
- 34 Y. Xia and J. Zhao, *Polymer (Guildf)*., 2018, **143**, 343–361.
- 35 A. Manuel Stephan and K. S. Nahm, *Polymer (Guildf)*., 2006.
- 36 R. C. Agrawal and G. P. Pandey, *J. Phys. D. Appl. Phys.*, , DOI:10.1088/0022-3727/41/22/223001.
- 37 J. M. Chem, 2016, 10038–10069.

- 38 D. T. Hallinan and N. P. Balsara, *Annu. Rev. Mater. Res.*, 2013, **43**, 503–525.
- 39 L. Long, S. Wang, M. Xiao and Y. Meng, *J. Mater. Chem. A*, 2016, **4**, 10038–10039.
- 40 K. P. Barteau, University of California, Santa Barbara, 2015.
- 41 B. K. Wheatle, J. R. Keith, S. Mogurampelly, N. A. Lynd and V. Ganesan, *ACS Macro Lett.*, 2017, **6**, 1362–1367.
- 42 A. M. Alb, P. Enohnyaket, M. F. Drenski, R. Shunmugam, G. N. Tew and W. F. Reed, *Macromolecules*, 2006, **39**, 8283–8292.
- 43 D. Leibig, J. Seiwert, J. C. Liermann and H. Frey, *Macromolecules*, 2016, **49**, 7767.
- 44 J. Herzberger, K. Niederer, H. Pohlitz, J. Seiwert, M. Worm, F. R. Wurm and H. Frey, *Chem. Rev.*, 2016, **116**, 2170.
- 45 J. Herzberger and H. Frey, *Macromolecules*, 2015, **48**, 8144.
- 46 C. Mangold, F. Wurm and H. Frey, *Polym. Chem.*, 2012, **3**, 1714.
- 47 C. Mangold, C. Dingels, B. Obermeier, H. Frey and F. Wurm, *Macromolecules*, 2011, **44**, 6326.
- 48 B. Obermeier, F. Wurm, C. Mangold and H. Frey, *Angew. Chem., Int. Ed.*, 2011, **50**, 7988.
- 49 B. Obermeier and H. Frey, *Bioconjugate Chem.*, 2011, **22**, 436.
- 50 C. Mangold, F. Wurm, B. Obermeier and H. Frey, *Macromolecules*, 2010, **43**, 8511.
- 51 F. Heatley, G.-E. Yu, C. Booth and T. G. Blease, *Eur. Polym. J.*, 1991, **27**, 573.
- 52 X.-H. Zhang, R.-J. Wei, Y. Y. Zhang, B.-Y. Du and Z.-Q. Fan, *Macromolecules*, 2015, **48**, 536.
- 53 B. Han, L. Zhang, S. J. Kyran, B. Liu, Z. Duan and D. J. Darensbourg, *J. Polym. Sci., Part A Polym. Chem.*, 2016, **54**, 1938.
- 54 S. Inoue, H. Koinuma and T. Tsuruta, *J. Polym. Sci. Part B-Polymer Lett.*, 1969, **7**, 287–292.
- 55 S. Inoue, *J. Macromol. Sci., Chem.*, 1979, **13**, 651.

- 56 Y. Tominaga, T. Shimomura and M. Nakamura, *Polymer (Guildf.)*, 2010, **51**, 4295.
- 57 M. H. Chisholm and Z. Zhou, *J. Am. Chem. Soc.*, 2004, **126**, 11030.
- 58 S. Inoue, H. Koinuma and T. Tsuruta, *Makromol. Chem.*, 1969, **130**, 210.
- 59 M. W. Lehenmeier, C. Bruckmeier, S. Klaus, J. E. Dengler, P. Deglmann, A.-K. Ott and B. Rieger, *Chem. - Eur. J.*, 2011, **17**, 8858.
- 60 K. Nakano, S. Hashimoto, M. Nakamura, T. Kamada and K. Nozaki, *Angew. Chem., Int. Ed.*, 2011, **50**, 4868.
- 61 G. Trott, P. K. Saini and C. K. Williams, *Philos. Trans. R. Soc., A*, 2016, **374**, 20150085.
- 62 R. C. Jeske, A. M. DiCiccio and G. W. Coates, *J. Am. Chem. Soc.*, 2007, **129**, 11330.
- 63 R. Baumgartner, Z. Song, Y. Zhang and J. Cheng, *Polym. Chem.*, 2015, **6**, 3586.
- 64 E. Hosseini Nejad, C. G. W. van Melis, T. J. Vermeer, C. E. Koning and R. Duchateau, *Macromolecules*, 2012, **45**, 1770.
- 65 A. M. DiCiccio, J. M. Longo, G. G. Rodríguez-Calero and G. W. Coates, *J. Am. Chem. Soc.*, 2016, jacs.6b03113.
- 66 N. J. Van Zee, M. J. Sanford and G. W. Coates, *J. Am. Chem. Soc.*, 2016, **138**, 2755–2761.
- 67 A. Sudo, Y. Zhang and T. Endo, *J. Polym. Sci., Part A Polym. Chem.*, 2011, **49**, 619.
- 68 A. Tadokoro and T. Takata, *Macromolecules*, 1993, **26**, 4400–4406.
- 69 X. Chen, P. Stephen, A. McCarthy and R. A. Gross, *Macromolecules*, 1997, **30**, 4295.
- 70 L. M. Pitet, S. B. Hait, T. J. Lanyk and D. M. Knauss, *Macromolecules*, 2007, **40**, 2327.
- 71 J. Zhao, D. Pahovnik, Y. Gnanou and N. Hadjichristidis, *Polym. Chem.*, 2014, **5**, 3750.
- 72 J. Raynaud, C. Absalon, Y. Gnanou and D. Taton, *J. Am. Chem. Soc.*, 2009, **131**,

- 3201.
- 73 J. Xu, J. Yang, X. Ye, C. Ma, G. Zhang and S. Pispas, *J. Polym. Sci., Part A Polym. Chem.*, 2015, **53**, 846.
- 74 R. Lindner, M. L. Lejkowski, S. Lavy, P. Deglmann, K. T. Wiss, S. Zarbakhsh, L. Meyer and M. Limbach, *ChemCatChem*, 2014, **6**, 618.
- 75 C. Romain, Y. Zhu, P. Dingwall, S. Paul, H. S. Rzepa, A. Buchard and C. K. Williams, *J. Am. Chem. Soc.*, 2016, **138**, 4120–4131.
- 76 B. F. Lee, M. Wolffs, K. T. Delaney, J. K. Sprafke, F. A. Leibfarth, C. J. Hawker and N. A. Lynd, *Macromolecules*, 2012, **45**, 3722–3731.
- 77 B. S. Beckingham, G. E. Sanoja and N. A. Lynd, *Macromolecules*, 2015, **48**, 6922–6930.
- 78 T. Dudev and C. Lim, *J. Am. Chem. Soc.*, 1998, **120**, 4450.
- 79 D. K. Schneiderman and M. A. Hillmyer, *Macromolecules*, 2016, **49**, 2419.
- 80 D. J. Darensbourg and W.-C. Chung, *Polyhedron*, 2013, **58**, 139.
- 81 H. Liu and J. Zhang, *J. Polym. Sci., Part B Polym. Phys.*, 2011, **49**, 1051.
- 82 E. J. Vandenberg, *J. Polym. Sci. Part A Polym. Chem.*, 1960, **47**, 486–489.
- 83 M.-A. Munoz-Hernandez, T. S. Keizer, P. Wei, S. Parkin and D. A. Atwood, *Inorg. Chem.*, 2001, **40**, 6782–6787.
- 84 D. A. Atwood and B. C. Yearwood, *J. Organomet. Chem.*, 2000, **600**, 186–197.
- 85 M.-A. Munoz-Hernandez, T. S. Keizer, S. Parkin, Y. Zhang and D. A. Atwood, *J. Chem. Crystallogr.*, 2000, **30**, 219–222.
- 86 J. A. Francis, S. G. Bott and A. R. Barron, *J. Chem. Soc., Dalt. Trans.*, 1998, 3305.
- 87 J. A. Francis, C. N. McMahon, S. G. Bott and A. R. Barron, *Organometallics*, 1999, **18**, 4399–4416.
- 88 C. N. McMahon, J. A. Francis, S. G. Bott and A. R. Barron, *J. Chem. Soc., Dalt. Trans.*, 1999, 67.
- 89 C. N. McMahon, S. J. Obrey, A. Keys, S. G. Bott and A. R. Barron, *J. Chem. Soc., Dalt. Trans.*, 2000, 2151.
- 90 B. Wu, C. J. Harlan, R. W. Lenz and A. R. Barron, *Macromolecules*, 1997, **30**,

- 316.
- 91 C. S. Branch, L. G. van Poppel, S. G. Bott and A. R. Barron, *J. Chem. Crystallogr.*, 1999, **29**, 993.
- 92 M. R. Mason, J. M. Smith, S. G. Bott and A. R. Barron, *J. Am. Chem. Soc.*, 1993, **115**, 4971–4984.
- 93 E. J. Vandenberg, *J. Polym. Sci. Part A-1 Polym. Chem.*, 1972, **10**, 329–354.
- 94 K. A. M. Thakur, R. T. Kean, E. S. Hall, J. J. Kolstad, T. A. Lindgren, M. A. Doscotch, J. I. Siepman and E. J. Munson, *Macromolecules*, 1997, **30**, 2422.
- 95 M. I. Childers, J. M. Longo, N. J. Van Zee, A. M. LaPointe and G. W. Coates, *Chem. Rev.*, 2014, **114**, 8129.
- 96 C. H. Tan, A. Ahmad and F. H. Anuar, *Int. J. Polym. Anal. Charact.*, 2016, **21**, 104.
- 97 P. Dimitrov, A. Porjazoska, C. P. Novakov, M. Cvetkovska and C. B. Tsvetanov, *Polymer (Guildf.)*, 2005, **46**, 6820–6828.
- 98 Y. Lemmouchi, M. C. Perry, A. J. Amass, K. Chakraborty and F. Schué, *J. Polym. Sci., Part A Polym. Chem.*, 2007, **45**, 2235.
- 99 N. Y. Choi, S. Kelch and A. Lendlein, *Adv. Eng. Mater.*, 2006, **8**, 439.
- 100 D. Liu and C. W. Bielawski, *Macromol. Rapid Commun.*, 2016, **37**, 1587.
- 101 V. E. Meyer and G. G. Lowry, *J. Polym. Sci. Part A*, 1965, **3**, 2843–2851.
- 102 M. Vayer, M. A. Hillmyer, M. Dirany, G. Thevenin, R. Erre and C. Sinturel, *Thin Solid Films*, 2010, **518**, 3710.
- 103 G. Schwach, J. Coudane, R. Engel and M. Vert, *Biomaterials*, 2002, **23**, 993.
- 104 J. Puls, S. A. Wilson and D. Höfner, *J. Polym. Environ.*, 2011, **19**, 152–165.
- 105 H. Tian, Z. Tang, X. Zhuang, X. Chen and X. Jing, *Prog. Polym. Sci.*, 2012, **37**, 237–280.
- 106 K. R. Kamath and K. Park, *Adv. Drug Deliv. Rev.*, 1993, **11**, 59–84.
- 107 A. Rahimi and J. M. García, *Nat. Rev. Chem.*, 2017, **1**, 0046.
- 108 J. A. Ivar do Sul and M. F. Costa, *Environ. Pollut.*, 2014, **185**, 352–364.
- 109 M. A. Browne, T. Galloway and R. Thompson, *Integr. Environ. Assess. Manag.*,

- 2007, **3**, 559–561.
- 110 F. Nederberg, B. G. G. Lohmeijer, F. Leibfarth, R. C. Pratt, J. Choi, A. P. Dove, R. M. Waymouth and J. L. Hedrick, *Biomacromolecules*, 2007, **8**, 153–160.
- 111 M. Helou, O. Miserque, J.-M. Brusson, J.-F. Carpentier and S. M. Guillaume, *Chem. - A Eur. J.*, 2008, **14**, 8772–8775.
- 112 R. Abdul-Karim, A. Hameed and M. I. Malik, *RSC Adv.*, 2017, **7**, 11786–11795.
- 113 T. J. Deming, *Prog. Polym. Sci.*, 2007, **32**, 858–875.
- 114 T. J. Deming, *Adv. Polym. Sci.*, 2006, **202**, 1–18.
- 115 D. M. Rosenbaum and D. R. Liu, *J. Am. Chem. Soc.*, 2003, **125**, 13924–13925.
- 116 M. E. Fieser, M. J. Sanford, L. A. Mitchell, C. R. Dunbar, M. Mandal, N. J. Van Zee, D. M. Urness, C. J. Cramer, G. W. Coates and W. B. Tolman, , DOI:10.1021/jacs.7b09079.
- 117 I. Cl, D. J. Darensbourg, R. R. Poland and C. Escobedo, , DOI:10.1021/ma2026385.
- 118 A. M. DiCiccio and G. W. Coates, *J. Am. Chem. Soc.*, 2011, **133**, 10724–10727.
- 119 S. Woodward and S. Dagonne, Eds., *Modern Organoaluminum Reagents*, Springer Berlin Heidelberg, Berlin, Heidelberg, 2013, vol. 41.
- 120 P. A. Offit and R. K. Jew, .
- 121 S. Shirodkar, R. L. Hutchinson, D. L. Perry, J. L. White and S. L. Hem, *Pharm. Res. An Off. J. Am. Assoc. Pharm. Sci.*, 1990, **7**, 1282–1288.
- 122 C. G. Rodriguez, R. C. Ferrier, A. Helenic and N. A. Lynd, *Macromolecules*, 2017, **50**, 3121–3130.
- 123 H. Plommer, I. Reim and F. M. Kerton, *Dalt. Trans.*, 2015, **44**, 12098–12102.
- 124 D. J. D. and and D. R. Billodeaux, , DOI:10.1021/IC048508G.
- 125 \* Donald. J. Darensbourg, and Poulomi Ganguly and D. Billodeaux, , DOI:10.1021/MA050666J.
- 126 M. P. F. Pepels, M. Bouyahyi, A. Heise and R. Duchateau, *Macromolecules*, 2013, **46**, 4324–4334.
- 127 E. D. Cross, L. E. N. Allan, A. Decken and M. P. Shaver, *J. Polym. Sci. Part A*

- Polym. Chem.*, 2013, **51**, 1137–1146.
- 128 J. P. MacDonald and M. P. Shaver, 2015, pp. 147–167.
- 129 S. Inoue, *J. Polym. Sci. Part A Polym. Chem.*, 2000, **38**, 2861–2871.
- 130 T. Aida and S. Inoue, *Acc. Chem. Res.*, 1996, **29**, 39–48.
- 131 H. Sugimoto, M. Saika, Y. Hosokawa, T. Aida and S. Inoue, *Macromolecules*, 1996, **29**, 3359–3369.
- 132 X. Sheng, Y. Wang, Y. Qin, X. Wang and F. Wang, *RSC Adv.*, 2014, **4**, 54043–54050.
- 133 T. Aida, Y. Maekawa, S. Asano and S. Inoue, *Macromolecules*, 1988, **21**, 1195–1202.
- 134 S. Inoue, H. Sugimoto, C. Kawamura, M. Kuroki and T. Aida, *Macromolecules*, 1994, **27**, 2013–2018.
- 135 M. Akatsuka, T. Aida and S. Inoue, *Macromolecules*, 1994, **27**, 2820–2825.
- 136 M. Chwatko and N. A. Lynd, *Macromolecules*, 2017, **50**, 2714–2723.
- 137 C. N. McMahon, S. J. Obrey, A. Keys, S. G. Bott and A. R. Barron, *J. Chem. Soc. Dalt. Trans.*, 2000, 2151–2161.
- 138 D. A. Atwood, F. P. Gabbai, J. Lu, M. P. Remington, D. Rutherford and M. P. Sibi, *Organometallics*, 1996, **15**, 2308–2313.
- 139 R. Benn, E. Janssen, H. Lehmkuhl and A. Ruffńska, *J. Organomet. Chem.*, 1987, **333**, 169–180.
- 140 J. Lewiński, P. Horeglad, K. Wójcik and I. Justyniak, *Organometallics*, 2005, **24**, 4588–4593.
- 141 H. Shirahama, K. Akinori and H. Yasuda, *Polym. J.*, 2000, **32**, 280–286.
- 142 W. Guerin, M. Helou, M. Slawinski, J.-M. Brusson, J.-F. Carpentier and S. M. Guillaume, *Polym. Photochem.*, 2015, **6**, 1972–1985.
- 143 S. Agarwal, N. Naumann and X. Xie, *Macromolecules*, 2002, **35**, 7713–7717.
- 144 H. Sun, F. Meng, A. A. Dias, M. Hendriks, J. Feijen and Z. Zhong, *Biomacromolecules*, 2011, **12**, 1937–1955.
- 145 J. C. Middleton and A. J. Tipton, *Biomaterials*, 2000, **21**, 2335–46.

- 146 Y. Ikada and H. Tsuji, *Macromol. Rapid Commun.*, 2000, **21**, 117–132.
- 147 P. K. Saini, C. Romain, Y. Zhu and C. K. Williams, *Polym. Chem.*, 2014, **5**, 6068–6075.
- 148 D.-F. Liu, ab Lu-Qun Zhu, J. Wu and L.-Y. Wu, , DOI:10.1039/c4ra08969c.
- 149 R. C. C. Ferrier, J. Imbrogno, C. G. G. Rodriguez, M. Chwatko, P. W. W. Meyer and N. A. A. Lynd, *Polym. Chem.*, 2017, **8**, 4503–4511.
- 150 R. C. Ferrier, S. Pakhira, S. E. Palmon, C. G. Rodriguez, D. E. Goldfeld, O. O. Iyiola, M. Chwatko, J. L. Mendoza-Cortes and N. A. Lynd, *Macromolecules*, 2018, **51**, 1777–1786.
- 151 J. Imbrogno, R. C. Ferrier, B. K. Wheatle, M. J. Rose and N. A. Lynd, *ACS Catal.*, 2018, **8**, 8796–8803.
- 152 V. Siracusa, P. Rocculi, S. Romani and M. D. Rosa, *Trends Food Sci. Technol.*, 2008.
- 153 V. Siracusa, N. Lotti, A. Munari and M. Dalla Rosa, *Polym. Degrad. Stab.*, , DOI:10.1016/j.polymdegradstab.2015.04.026.
- 154 G. Guidotti, M. Soccio, V. Siracusa, M. Gazzano, E. Salatelli, A. Munari and N. Lotti, *Polymers (Basel)*, 2017, **9**, 1–16.
- 155 J. C. Pech, E. Purgatto, M. Bouzayen and A. Latché, *Plant Horm. Ethyl.*, 2012, **44**, 275–304.
- 156 M. J. L. Tschan, E. Brulé, P. Haquette and C. M. Thomas, *Polym. Chem.*, 2012, **3**, 836–851.
- 157 W. J. Choi, C. Y. Choi, J. A. M. De Bont and C. A. G. M. Weijers, *Appl. Microbiol. Biotechnol.*, 2000, **54**, 641–646.
- 158 L. P. Saunders, M. J. Bowman, J. A. Mertens, N. A. Da Silva and R. E. Hector, *J. Ind. Microbiol. Biotechnol.*, 2015, **42**, 711–721.
- 159 Y. Oda, Y. Yajima, M. Kinoshita and M. Ohnishi, *Food Microbiol.*, 2003, **20**, 371–375.
- 160 G. Q. Chen and X. R. Jiang, *Synth. Syst. Biotechnol.*, 2017, **2**, 192–197.
- 161 P. Suriyamongkol, R. Weselake, S. Narine, M. Moloney and S. Shah, *Biotechnol.*

- Adv.*, 2007, **25**, 148–175.
- 162 R. M. Zelle, E. De Hulster, W. A. Van Winden, P. De Waard, C. Dijkema, A. A. Winkler, J. M. A. Geertman, J. P. Van Dijken, J. T. Pronk and A. J. A. Van Maris, *Appl. Environ. Microbiol.*, 2008, **74**, 2766–2777.
- 163 H. Chang, D. Li, T. Cao, Q. Li, Z. Bu, W. Zhao and T. Lin, *Polym. Adv. Technol.*, 2018, **29**, 1870–1874.
- 164 H. Plommer, I. Reim and F. M. Kerton, *Dalt. Trans.*, 2015, **44**, 12098–12102.
- 165 S. Khatua and Y. Lo Hsieh, *J. Polym. Sci. Part A Polym. Chem.*, 1997, **35**, 3263–3273.
- 166 F. Kawai, *Appl. Microbiol. Biotechnol.*, 2002, **58**, 30–38.
- 167 C. G. Rodriguez, M. Chwatko, C. L. Bentley, N. A. Lynd and B. D. Freeman, *Prep.*
- 168 Y. Wang, A. J. Easteal and X. D. Chen, *Packag. Technol. Sci.*, 1998, **11**, 169–178.
- 169 T. Komatsuka, A. Kusakabe and K. Nagai, *Desalination*, 2008, **234**, 212–220.
- 170 K.-J. Lin, K. Li and J. K. Maranas, , DOI:10.1039/c2ra21644b.
- 171 J. Sun, G. M. Stone, N. P. Balsara and R. N. Zuckermann, *Macromolecules*, 2012, **45**, 5151–5156.
- 172 T. F. Miller, Z. G. Wang, G. W. Coates and N. P. Balsara, *Acc. Chem. Res.*, 2017, **50**, 590–593.
- 173 D. H. C. Wong, J. L. Thelen, Y. Fu, D. Devaux, A. A. Pandya, V. S. Battaglia, N. P. Balsara and J. M. DeSimone, *Proc. Natl. Acad. Sci. U. S. A.*, 2014, **111**, 3327–3331.
- 174 N. P. Young, D. Devaux, R. Khurana, G. W. Coates and N. P. Balsara, *Solid State Ionics*, 2014, **263**, 87–94.
- 175 D. E. Fenton, J. M. Parker and P. V. Wright, *Polymer (Guildf.)*, 1973, **14**, 589.
- 176 A. A. Teran, M. H. Tang, S. A. Mullin and N. P. Balsara, *Solid State Ionics*, 2011, **203**, 18–21.
- 177 M. Petrowsky and R. Frech, *J. Phys. Chem. B*, 2009, **113**, 5996–6000.
- 178 M. Petrowsky and R. Frech, *J. Phys. Chem. B*, 2009, **113**, 16118–16123.

- 179 M. Petrowsky, A. Fleshman and R. Frech, *J. Phys. Chem. B*, 2012, **116**, 5760–5.
- 180 M. Petrowsky, A. Fleshman, D. N. Bopege and R. Frech, *J. Phys. Chem. B*, 2012, **116**, 9303–9.
- 181 M. Petrowsky, A. Fleshman, M. Ismail, D. T. Glatzhofer, D. N. Bopege and R. Frech, *J. Phys. Chem. B*, 2012, **116**, 10098–105.
- 182 M. Petrowsky, M. Ismail, D. T. Glatzhofer and R. Frech, *J. Phys. Chem. B*, 2013, **117**, 5963–70.
- 183 M. Kumar and S. S. Sekhon, *Eur. Polym. J.*, 2002, **38**, 1297–1304.
- 184 U. H. Choi, S. Liang, Q. Chen, J. Runt and R. H. Colby, ,  
DOI:10.1021/acsami.5b10797.
- 185 M. Nakamura and Y. Tominaga, *Electrochim. Acta*, 2011, **57**, 36–39.
- 186 A. A. Aziz and Y. Tominaga, *Polym. J.*, 2019, **51**, 61–67.
- 187 A. Ab Aziz and Y. Tominaga, *Ionics (Kiel)*, 2018, **24**, 3475–3481.
- 188 D. M. Pesko, Y. Jung, A. L. Hasan, M. A. Webb, G. W. Coates, T. F. Miller and N. P. Balsara, *Solid State Ionics*, 2016, **289**, 118–124.
- 189 M. A. Webb, Y. Jung, D. M. Pesko, B. M. Savoie, U. Yamamoto, G. W. Coates, N. P. Balsara, Z. G. Wang and T. F. Miller, *ACS Cent. Sci.*, 2015, **1**, 198–205.
- 190 R. K. Cersonsky, L. L. Foster, T. Ahn, R. J. Hall, H. L. van der Laan and T. F. Scott, *J. Chem. Educ.*, 2017, **94**, 1639–1646.
- 191 W. Qiang, W. Li, X. Li, X. Chen and D. Xu, *Chem. Sci.*, 2014, **5**, 3018–3024.
- 192 M. Liu, G. Zeng, K. Wang, Q. Wan, L. Tao, X. Zhang and Y. Wei, *Nanoscale*, 2016, **8**, 16819–16840.
- 193 J. H. Jiang, L. P. Zhu, X. L. Li, Y. Y. Xu and B. K. Zhu, *J. Memb. Sci.*, 2010, **364**, 194–202.
- 194 D. R. Dreyer, D. J. Miller, B. D. Freeman, D. R. Paul and C. W. Bielawski, *Langmuir*, 2012, **28**, 6428–6435.
- 195 H. Lee, S. M. Dellatore, W. M. Miller and P. B. Messersmith, *Science (80-. )*, 2007, **318**, 426–430.
- 196 J. H. Waite, *Nat. Mater.*, 2008, **7**, 8–9.

- 197 M. d'Ischia, A. Napolitano, V. Ball, C.-T. Chen and M. J. Buehler, *Acc. Chem. Res.*, 2014, **47**, 3541–3550.
- 198 J. Liebscher, R. Mrówczyński, H. a Scheidt, C. Filip, N. D. Hādade, R. Turcu, A. Bende and S. Beck, *Langmuir*, 2013, **29**, 10539–48.
- 199 J. Yang, M. A. Cohen Stuart and M. Kamperman, *Chem. Soc. Rev.*, 2014, **43**, 8271–8298.
- 200 H.-C. Yang, J. Luo, Y. Lv, P. Shen and Z.-K. Xu, *J. Memb. Sci.*, 2015, **483**, 42–59.
- 201 V. Ball, D. Del Frari, V. Toniazzo and D. Ruch, *J. Colloid Interface Sci.*, 2012, **386**, 366–372.
- 202 Q. Wei, F. L. Zhang, J. Li, B. J. Li and C. S. Zhao, *Polym. Chem.*, 2010, **1**, 1430.
- 203 J. V. Crivello and W. -G Kim, *J. Polym. Sci. Part A Polym. Chem.*, 1994, **32**, 1639–1648.
- 204 B. F. Lee, M. J. Kade, J. A. Chute, N. Gupta, L. M. Campos, G. H. Fredrickson, E. J. Kramer, N. A. Lynd and C. J. Hawker, *J. Polym. Sci. Part A Polym. Chem.*, 2011, **49**, 4498–4504.
- 205 A.-L. Brocas, G. Cendejas, S. Caillol, A. Deffieux and S. Carlotti, *J. Polym. Sci. Part A Polym. Chem.*, 2011, **49**, 2677–2684.